AD-A039 522 PENNSYLVANIA STATE UNIV UNIVERSITY PARK APPLIED RESE--ETC F/G 20/3
FLUXOID PINNING BY VANADIUM CARBIDE PRECIPITATES IN SUPERCONDUC--ETC(U)
MAR 77 A J MARKER

UNCLASSIFIED TM-77-81 NL

1 OF 2
AD
A039 522



AD A039522

(12)
B.S.

FLUXOID PINNING BY VANADIUM CARBIDE PRECIPITATES IN SUPERCONDUCTING VANADIUM

Alexander J. Marker, III

DDC
MAY 16 1977
C

Technical Memorandum
File No. 77-81
March 30, 1977
Contract No. N00017-73-C-1418

Copy No. 5

The Pennsylvania State University
Institute for Science and Engineering
APPLIED RESEARCH LABORATORY
Post Office Box 30
State College, PA 16801

APPROVED FOR PUBLIC RELEASE
DISTRIBUTION UNLIMITED

NAVY DEPARTMENT

NAVAL SEA SYSTEMS COMMAND

AD No.
DDC FILE COPY

REPORT DOCUMENTATION PAGE

READ INSTRUCTIONS BEFORE COMPLETING FORM

1. REPORT NUMBER: TM 77-81	2. GOVT ACCESSION NO.
3. RECIPIENT'S CATALOG NUMBER	
4. TITLE (and Subtitle): FLUXOID PINNING BY VANADIUM CARBIDE PRECIPITATES IN SUPERCONDUCTING VANADIUM	5. TYPE OF REPORT & PERIOD COVERED: PhD Thesis, Physics, May 1977
	6. PERFORMING ORG. REPORT NUMBER: TM-77-81
7. AUTHOR(s): Alexander J. Marker, III	8. CONTRACT OR GRANT NUMBER(s): N00017-73-C-1418
9. PERFORMING ORGANIZATION NAME AND ADDRESS: The Pennsylvania State University, Applied Research Laboratory, P. O. Box 30, State College, PA 16801	10. PROGRAM ELEMENT, PROJECT, TASK AREA & WORK UNIT NUMBERS
11. CONTROLLING OFFICE NAME AND ADDRESS: Naval Sea Systems Command, Department of the Navy, Washington, D. C. 20362	12. REPORT DATE: March 30, 1977
	13. NUMBER OF PAGES: 131 pages & figures
14. MONITORING AGENCY NAME & ADDRESS (if different from Controlling Office)	15. SECURITY CLASS. (of this report): Unclassified, Unlimited
	15a. DECLASSIFICATION/DOWNGRADING SCHEDULE

16. DISTRIBUTION STATEMENT (of this Report)

Approved for public release, distribution unlimited, per NSSC (Naval Sea Systems Command) 4/25/77

DDC
RECEIVED
MAY 16 1977
C

17. DISTRIBUTION STATEMENT (of the abstract entered in Block 20, if different from Report)

18. SUPPLEMENTARY NOTES

391 007

19. KEY WORDS (Continue on reverse side if necessary and identify by block number)

20. ABSTRACT (Continue on reverse side if necessary and identify by block number)

The purpose of this investigation is to study fluxoid pinning in a Type II superconductor. Vanadium was chosen as the superconductor to study because it is obtainable in high purity and its microstructure can be readily controlled. The pinning centers are formed by introducing carbon into the vanadium matrix forming vanadium carbide precipitates. The vanadium carbide precipitates are disc-shaped particles whose thickness is only a few atomic layers. The precipitates are likely to be superconducting when H = 0 by reason of the

DD FORM 1 JAN 73 1473 EDITION OF 1 NOV 65 IS OBSOLETE

UNCLASSIFIED

SECURITY CLASSIFICATION OF THIS PAGE (When Data Entered)

20. ABSTRACT (continued)

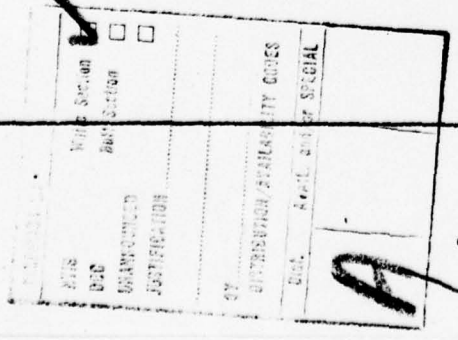
proximity effect. The vanadium carbide precipitates on the {310} habit planes. According to studies with the transmission electron microscope, the particles are uniformly distributed throughout the specimen. The particle size and number density is changed by aging the specimens for fixed amount of time at 350° C.

The present results are based on the study of thirty specimens. A 99.95% pure annealed vanadium specimen was used as a control. The other vanadium specimens contain 0.1 atomic percent to 0.6 atomic percent carbon. As a result of metallurgical analysis, the mean diameters of the particles range from less than 100 Å to 2613 Å and the number density of the pinning centers range from 3.3×10^{15} particles/cm^3 to 4.2×10^{17} particles/cm^3. The measurement of the superconducting properties lead to values of the macroscopic pinning force density ranging from 3.34×10^{9} dynes/cm$^3_{cc}$ to 3.17×10^{6} dynes/cm$^3_{cc}$ for T - 0 K.

The macroscopic pinning force density is calculated from the Lorentz force equation. The value of $\bar{B}$ is numerically equal to $\bar{H}$ for the geometry used in this investigation. The value of the critical current density is determined by a four probe technique. $\bar{J}_c$ is the value of the current density at a voltage just large enough to be deemed above the noise level of the signal; in all cases, this voltage is less than or equal to 50 nV. Attempts were made to correlate the present results with existing fluxoid pinning theories. None of the theories tried were compatible with the present work. Therefore, a calculation of the macroscopic pinning force density based on the concept of an activation volume is performed. This calculation leads to the proper temperature dependence for F_p. However, the reduced magnetic field dependence of the size of the activation volume cannot be directly calculated. Hence, the calculated F_p cannot be completely compared to the experimental results. From the method of investigation used in this study, the reduced magnetic field dependence of the activation volume cannot be tested.

Vanadium is a low K Type II superconductor and as a result of this investigation, it is found that the macroscopic pinning force density obeys a scaling law of the form $F_p = C_p H_{c2}^{3/2}(T)\, h(1-h)^{\frac{1}{2}}$. The $H_{c2}(T)$ term contains all the temperature dependence of the macroscopic pinning force density. The constant C_p depends on the size and number density of the pinning centers. If the number of pinning centers whose diameters a is greater than $2\xi(T)$ is above some critical number, the specimen will obey the scaling law. Here, $2\xi(T)$ is the diameter of the fluxoid core at the temperature T which is the temperature at which the specimen begins to obey the scaling law. The form factor in the scaling law equation is then only a function of reduced magnetic field. If the number of pinning centers whose diameters are greater than $2\xi(T)$ is below the critical number for a given temperature, the specimen does not obey the scaling law and the form factor is a function of temperature as well as h. If all the particle diameters is less than $2\xi(0)$, then the specimen will not obey the scaling law at any temperature no matter what the number of pinning centers.

* 3.3 x 10 to the 15th power particles/cc to 4.2 x 10 to the 17th power particles/cc.



ABSTRACT

The purpose of this investigation is to study fluxoid pinning in a Type II superconductor. Vanadium was chosen as the superconductor to study because it is obtainable in high purity and its microstructure can be readily controlled. The pinning centers are formed by introducing carbon into the vanadium matrix forming vanadium carbide precipitates. The vanadium carbide precipitates are disc shaped particles whose thickness is only a few atomic layers. The precipitates are likely to be superconducting when H = 0 by reason of the proximity effect. The vanadium carbide precipitates on the {310} habit planes. According to studies with the transmission electron microscope the particles are uniformly distributed throughout the specimen. The particle size and number density is changed by aging the specimens for fixed amounts of time at 350°C.

The present results are based on the study of thirty specimens. A 99.95% pure annealed vanadium specimen was used as a control. The other vanadium specimens contain 0.1 atomic percent to 0.6 atomic percent carbon. As a result of metallurgical analysis the mean diameters of the particles range from less than 100 Å to 2613 Å and the number density of the pinning centers range from 3.3×10^{15} particles/cm^3 to 4.2×10^{17} particles/cm^3. The measurement of the superconducting properties lead to values of the macroscopic pinning force density ranging from 3.34×10^4 dynes/cm^3 to 3.17×10^6 dynes/cm^3 for T = 0 K.

The macroscopic pinning force density is calculated from the Lorentz force equation. The value of $\vec{B}$ is numerically equal to $\vec{H}$ for the geometry used in this investigation. The value of the critical current density is determined by a four probe technique, $\vec{J}_c$ is the value of the current density at a voltage just large enough to be deemed above the noise level of the signal, in all cases this voltage is less than or equal to 50 nV. Attempts were made to correlate the present results with existing fluxoid pinning theories. None of the theories tried were compatible with the present work. Therefore, a calculation of the macroscopic pinning force density based on the concept of an activation volume is performed. This calculation leads to the proper temperature dependence for F_p. However, the reduced magnetic field dependence of the size of the activation volume can not be directly calculated. Hence, the calculated F_p can not be completely compared to the experimental results. From the method of investigation used in this study the reduced magnetic field dependence of the activation volume can not be tested.

Vanadium is a low κ Type II superconductor and as a result of this investigation it is found that the macroscopic pinning force density obeys a scaling law of the form

$$F_p = C_p H_{c2}^{\frac{3}{2}}(T)\, h(1-h)^{\frac{1}{2}}.$$

The $H_{c2}(T)$ term contains all the temperature dependence of the macroscopic pinning force density of the pinning centers. If the number of

pinning centers/cm length of fluxoid, whose diameters, a, is greater than $2\xi(T_s)$, is above some critical number, the specimen will obey the scaling law. Here $2\xi(T_s)$ is the diameter of the fluxoid core at the temperature T_s, which is the temperature at which the specimen begins to obey the scaling law. The form factor in the scaling law equation is, then, only a function of reduced magnetic field. If the number of pinning centers, whose diameters are greater than $2\xi(T_s)$, is below the critical number/cm length of fluxoid ($\sim 10^6$ pinning center/cm) for a given temperature the specimen does not obey the scaling law and the form factor is a function of temperature as well as h. If all the particle diameters are less than $2\xi(0)$ then the specimen will not obey the scaling law at any temperature no matter what the number of pinning centers.

ACKNOWLEDGMENTS

The author wishes to thank Professors Robert W. Reed and F. G. Brickwedde for suggesting this project. Special thanks is due Professor Reed for his aid in solving the many technical problems associated with this study. Also, his encouragement and many stimulating discussions of technical problems and experimental results are greatly appreciated. Professor Brickwedde's interest in this undertaking is reflected in his continual encouragement during the past four years. The author wishes to thank him for this encouragement and his many hours of discussion on particular points of interest.

The author wishes to thank Professor William R. Bitler of the Metallurgical Section of the Department of Material Sciences of The Pennsylvania State University for his supervising of the fabrication and characterization of the specimens used in this investigation. The author appreciates the many conversations with Professor Bitler concerning the metallurgy involved with this study and superconductivity in general.

The support of the Applied Research Laboratory of The Pennsylvania State University under contract with the Naval Sea Systems Command is also acknowledged.

TABLE OF CONTENTS

	Page
ACKNOWLEDGMENTS	ii
LIST OF TABLES	iv
LIST OF FIGURES	v
LIST OF SYMBOLS	vii
I. INTRODUCTION	1
II. THEORY	4
A. Historical Background	4
B. Magnetization Considerations	19
C. Nature of the Driving Force	20
D. Fluxoid Pinning	24
III. EXPERIMENTAL PROCEDURES	44
A. Specimens	44
B. Specimen Holder	47
C. Temperature Measurement	52
D. Determination of the Transition Temperature	53
E. Determination of the Critical Current Density	53
F. Determination of the Upper Critical Magnetic Field.	60
IV. EXPERIMENTAL RESULTS	63
A. Introduction	63
B. Important Superconducting Parameters	63
C. Transition Temperature	70
D. Fluxoid Pinning	74
V. CONCLUDING REMARKS	102
A. Summary	102
B. Comments on Further Work	103
APPENDICES	106
A. Temperature Regulation of the Vacuum Can	106
B. Magnet Systems and Calibration	111
BIBLIOGRAPHY	113

LIST OF TABLES

Table		Page
I.	Important superconducting parameters	69
II.	More superconducting parameters	71
III.	Important specimen parameters	73
IV.	Parameters relevant to the scaling law equation	83
V.	Metallurgical microstructure parameters	86
VI.	Critical parameters associated with specimens which obey the scaling law	100
VII.	Values of a and b appearing in Equation (B.1)	112

LIST OF FIGURES

Figure		Page
1.	Magnetic induction, $\vec{B}$, as a function of the applied magnetic field, $\vec{H}$, for an ideal Type I superconductor	6
2.	Temperature dependence of the critical magnetic field, H_c	8
3.	Magnetic induction, $\vec{B}$, as a function of the applied magnetic field, $\vec{H}$, for an ideal Type II superconductor . . .	18
4.	Schematic representation of the flux creep experiment . .	21
5.	Schematic model for flux creep	26
6.	Schematic diagram of fluxoid pinning	27
7.	The electric field, $\vec{E}$, as a function of the transport current density, $\vec{J}$, through a specimen	29
8.	Schematic representation of the specimen holder	48
9.	Diagram of the specimen block used to determine J_c and T_c	51
10.	Block diagram for T_c determination	54
11.	V_L as a function of the recording thermometer voltage for the 0.4 atomic percent carbon specimen, aged zero hours. .	55
12.	Block diagram of the equipment used to measure the critical current density	56
13.	a) Current control unit. b) Schematic diagram of the complete transport current circuit	57
14.	V_L - I for the 0.4 atomic percent carbon specimen, aged zero hours	59
15.	Normalized pinning force density vs. applied magnetic field for the 0.4 atomic percent carbon specimen, aged zero hours	62
16.	The upper critical magnetic field as a function of reduced temperature for the 0.4 atomic percent carbon specimen, aged zero hours	64

LIST OF FIGURES (cont.)

Figure		Page
17.	Transition temperature as a function of ρ_r^{-1}	72
18.	Macroscopic pinning force density as a function of reduced magnetic field	75
19.	J_c vs. h for a pure, annealed specimen	76
20.	J_c vs. h for the 0.3 atomic percent carbon specimen, aged one hour	77
21.	J_c vs. h for the 0.4 atomic percent carbon specimen, aged zero hours	78
22.	Normalized pinning force density, F_p/F_{pmax}, vs. reduced magnetic field, h, for the 0.3 atomic percent carbon specimen, aged one hour	80
23.	F_{pmax} vs. H_{c2} for the 0.3 atomic percent carbon specimen, aged one hour	82
24.	F_{pmax} vs. T for the 0.1 atomic percent carbon specimen, aged one hour	87
25.	F_p as a function of $h(1-h)^{\frac{1}{2}}$ for the 0.3 atomic percent carbon specimen, aged one hour	88
26.	K vs. $H_{c2}^{\frac{3}{2}}$ for the 0.3 atomic percent carbon specimen, aged one hour	92
27.	Normalized pinning force density vs. reduced magnetic field for the 0.3 atomic percent carbon specimen, aged zero hours	93
28.	Histogram showing the distribution of particle diameters	96
29.	Histogram showing the distribution of particle diameters	97
30.	Histogram showing the distribution of particle diameters	98
31.	Block diagram of the temperature regulation circuit	107
32.	Temperature control circuit	108

LIST OF SYMBOLS

$\vec{A}$	vector potential
a	geometrical width of the pinning center parallel to the fluxoid
$\vec{B}$,B	magnetic induction
c	speed of light
C_1	constant
C_p	constant in the scaling law equation
D	demagnetizing factor
d	fluxoid lattice parameter = $(\phi_0/B)^{\frac{1}{2}}$
2Δ	superconducting gap energy
ΔT_c	half width of the resistive transition in the determination of T_c
$\vec{E}$,E	electric field
E_F	Fermi energy
e	electronic charge in esu
E_d	electric field corresponding to the predetermined voltage cut off
ε	interaction energy between a single fluxoid and a single pinning center
$\vec{F}_p$,F_p	macroscopic pinning force density
F_{pmax}	maximum value of F_p for a given temperature
$\vec{F}_L$,F_L	Lorentz force per unit volume
f(h)	form factor
F	Helmholtz free energy per unit volume
$\vec{F}_D$,F_D	driving force on the fluxoids per unit volume
f_p	interaction force between a pinning center and a fluxoid

LIST OF SYMBOLS (cont.)

f	relative order parameter = ψ/ψ_0
G_T	activation energy
G	Gibbs free energy per unit volume
$\vec{H}, H$	applied magnetic field
H_{c1}	lower critical magnetic field
H_{c2}	upper critical magnetic field
H_{c3}	critical magnetic field above which surface superconductivity is destroyed
h	reduced magnetic field = H/H_{c2}
$\vec{h}$	local microscopic magnetic field
H_c	critical magnetic field
I	current
$\vec{J}, J$	current density
$\vec{J}_c, J_c$	critical current density
$\vec{J}_s, J_s$	supercurrent density
$\vec{J}_f, J_f$	threshold current density
$\vec{J}_d, J_d$	current density in the non-linear dynamic region
κ	Ginzburg-Landau parameter
κ_1	first Maki parameter
k	distance between effective pinning centers
k_B	Boltzmann's constant
$\lambda, \lambda(T)$	penetration depth
Λ	London's phenomenological parameter
λ_L	London penetration depth
ℓ	normal state electronic mean free path
ℓ^*	critical distance between pinning centers

LIST OF SYMBOLS (cont.)

m	exponent in the scaling law equation, or electronic mass
$\vec{M}, M$	magnetization per unit volume
M_T	total magnetization of the specimen
n_s	number density of superconducting electrons
N_p	number of pinning centers/cm length of fluxoid
n_p	number density of pinning centers
n_{p2}	number density of particles with diameters greater than $2\xi(T_s)$
n^*	critical number density of pinning centers
$\vec{p}, p$	momentum
$\psi(\vec{r}), \psi$	complex order parameter
ϕ_0	flux quantum = $hc/2e = 2.07 \times 10^{-7}$ gauss-cm^2
R	rate of fluxoid jumps
R_N	net rate of fluxoid notion
R_{295}	resistance of the specimen at room temperature
$R_{5.45}$	resistance of the specimen at 5.45 K
ρ_0	residual resistivity
$\rho_{5.45}$	resistivity of the specimen at 5.45 K
ρ_r	resistance ratio
ρ_n	normal state resistivity
ρ_d	dynamic resistivity at the value of J_d
ρ_f	flux flow resistivity
T	temperature
T_c	transition temperature
T_{co}	intrinsic transition temperature, the transition temperature for infinite electronic mean free path

LIST OF SYMBOLS (cont.)

t	reduced temperature = T/T_c, or time
T_s	temperature at which the specimen first obeys the scaling law
U_p	maximum value of the interaction energy
$\vec{v}, v$	velocity
v_F	Fermi velocity
$\vec{v}_L, v_L$	velocity of the fluxoid lattice
V_p	activation volume
V_d	cut off voltage
V_L	longitudinal voltage along the specimen
$\xi(T)$	temperature dependent coherence length
ξ	coherence length in the presence of scattering
ξ_0	Pippard or BCS coherence length
x_p	effective width or range of the pinning center

I. INTRODUCTION

The purpose of this investigation is to study pinning centers in a Type II superconductor. If one considers a thin rectangular slab of ideal Type II superconductor placed in an applied magnetic field, such that the applied magnetic field is perpendicular to the broad surface of the specimen, the applied magnetic field will cause magnetic flux to enter into the superconductor. In a Type II superconductor, the magnetic flux will exist in quantized bundles called fluxoids. Consider now passing a transport current through the specimen in such a manner that the transport current is perpencidular to the applied magnetic field and parallel to the broad surface of the specimen. A driving force, which is equal to the Lorentz force, will then act upon the fluxoids and the fluxoids may begin to move. The fluxoid motion is impeded by a viscous force. Thus, a pure defect free Type II superconductor cannot sustain a lossless current. There is energy dissipation, since work is being done in moving the fluxoids. In order to make a Type II superconductor capable of supporting high transport currents, the motion of the fluxoids must be impeded. This is accomplished by introducing pinning centers into the Type II superconductor.

Pinning centers may be produced in the superconductor by one or more common methods, such as cold working the specimen (1,2,3) or ion irradiation of the specimen to produce voids (4). Many methods of producing pinning centers lead to an end product which is quite useful technologically, but as yet not well understood in terms of a fundamental interpretation of the basic mechanisms involved.

The purpose of this work is to study fluxoid pinning in a well defined and controlled superconducting system. Vanadium was chosen as the superconductor to study because it is obtainable in high purity and its microstructure can be readily controlled. Vanadium also happens to be one of the two known elemental intrinsic Type II superconductors, niobium being the other. The pinning centers are formed by introducing carbon into the vanadium matrix forming vanadium carbide precipitates. The vanadium carbide precipitate provides a well behaved pinning center: first, the precipitate can be made coherent with the vanadium lattice, and second, the particle size and number density can be controlled by appropriate heat treatment.

Measurements of the superconducting properties and metallurgical microstructure were carried out on vanadium specimens containing 0.1 atomic percent to 0.6 atomic percent carbon. The upper critical magnetic fields ranged from 4.1 kOe to 5.8 kOe. The macroscopic pinning force density, extrapolated to T = 0 K, varied from 3.34×10^4 dynes/cm^3 3.17×10^6 dynes/cm^3. The mean precipitate diameters varied from less than 100 Å to 2613 Å, and the number density of the pinning centers ranged from 3.3×10^{15} particles/cm^3 to 4.2×10^{17} particles/cm^3.

The current carrying capability of the superconductor is directly dependent on the effectiveness of the pinning centers. The pinning centers provide a macroscopic pinning force density, $\vec{F}_p$, which counteracts the Lorentz force, $\vec{F}_L = \vec{J} \times \vec{B}/c$, on the fluxoids. According to Bean (5) and Kim et al. (6), when the pinning force exactly balances the Lorentz force, the specimen is in the critical state, which is given by

$$\vec{F}_p = - \vec{J}_c \times \vec{B}/c \quad . \tag{1.1}$$

If the critical current density, $\vec{J}_c$, and the magnetic induction, $\vec{B}$, are known, the pinning force per unit volume can be calculated. The pinning force is a macroscopic quantity which must be related to the microstructure of the specimen (7,8).

Another objective of this study to to see if low κ Type II superconductors obey a scaling law (9) of the form

$$F_p = \text{const.}\ H_{c2}^{m}(T)\ f(h), \tag{1.2}$$

where H_{c2} is the upper critical magnetic field and the reduced magnetic field, h, is defined as H/H_{c2}. As a result of this investigation, the form factor, f(h), is found to be given by

$$f(h) = h(1-h)^{\frac{1}{2}}\ , \tag{1.3}$$

and the exponent in the scaling law, m, is approximately $\frac{3}{2}$. The scaling law becomes

$$F_p = \text{const.}\ H_{c2}^{\frac{3}{2}}(T)\ h(1-h)^{\frac{1}{2}} \quad . \tag{1.4}$$

The conditions under which Equation (1.4) is valid are discussed.

II. THEORY

A. Historical Background

A brief historical discussion is presented in order to introduce the reader to terms and concepts basic to the understanding of fluxoid pinning in Type II superconductors. Many excellent books have been written on superconductivity and may be consulted for further details. On a phenomenological level, Lynton (10) and Kuper (11) give excellent accounts of superconductivity. In a more theoretical vein, books such as de Genes (12), Saint-James et al. (13), and Tinkham (14) may be consulted. Many of the terms and concepts basic to the understanding of Type II superconductivity are extended from definitions and concepts first applied to Type I superconductors, since these were studied first. Thus, the discussion begins with Type I superconductors.

Superconductivity was first observed by Kamerlingh Onnes in 1911 while studying the electrical conductivity of metals at low temperatures. Kamerlingh Onnes (15,16,17,18) observed that the electrical resistance of such metals as mercury, lead, and tin went to zero at very well defined temperatures. The temperature at which the electrical resistance goes to zero is called the critical temperature, T_c , below which the metal is in the superconducting state. In the superconducting state, the specimen shows perfect conductivity.

Meissner and Ochsenfeld (19) observed that the superconducting state possesses perfect diamagnetism. Perfect diamagnetism cannot be explained by the assumption that the specimen is a perfect conductor, for if the specimen is placed in a magnetic field, then cooled

below T_c , the magnetic flux is expelled from the bulk of the superconductor. This is contrary to what one would predict in the limit of perfect conductivity. On a microscopic scale, however, the magnetic field penetrates into the superconductor a distance λ , the penetration depth. The magnetic field decays exponentially in this region from H at the surface to zero in the bulk of the specimen. The superconducting state can be destroyed by increasing the magnetic field above some critical value, see Figure 1.

The critical magnetic field, H_c , as a function of temperature is given approximately by

$$H_c(T) = H_c(0) \left[1 - (T/T_c)^2\right] \quad . \tag{2.1}$$

The critical magnetic field is related to the free energy difference between the normal state and the superconducting state in zero applied magnetic field (20). The Gibbs free energy per unit volume is

$$G(H,T) = F(T) - \frac{1}{4\pi} \int_0^H B(H)dH \quad . \tag{2.2}$$

F(T) is the Helmholtz free energy of the system in zero magnetic field. For a bulk superconductor with $H < H_c$ and $B = 0$,

$$G_s(H,T) = F_s(T) \quad . \tag{2.3}$$

In the normal state, assuming that the magnetic susceptibility is negligible.

$$G_n(H,T) = F_n(T) - H^2/8\pi \quad . \tag{2.4}$$

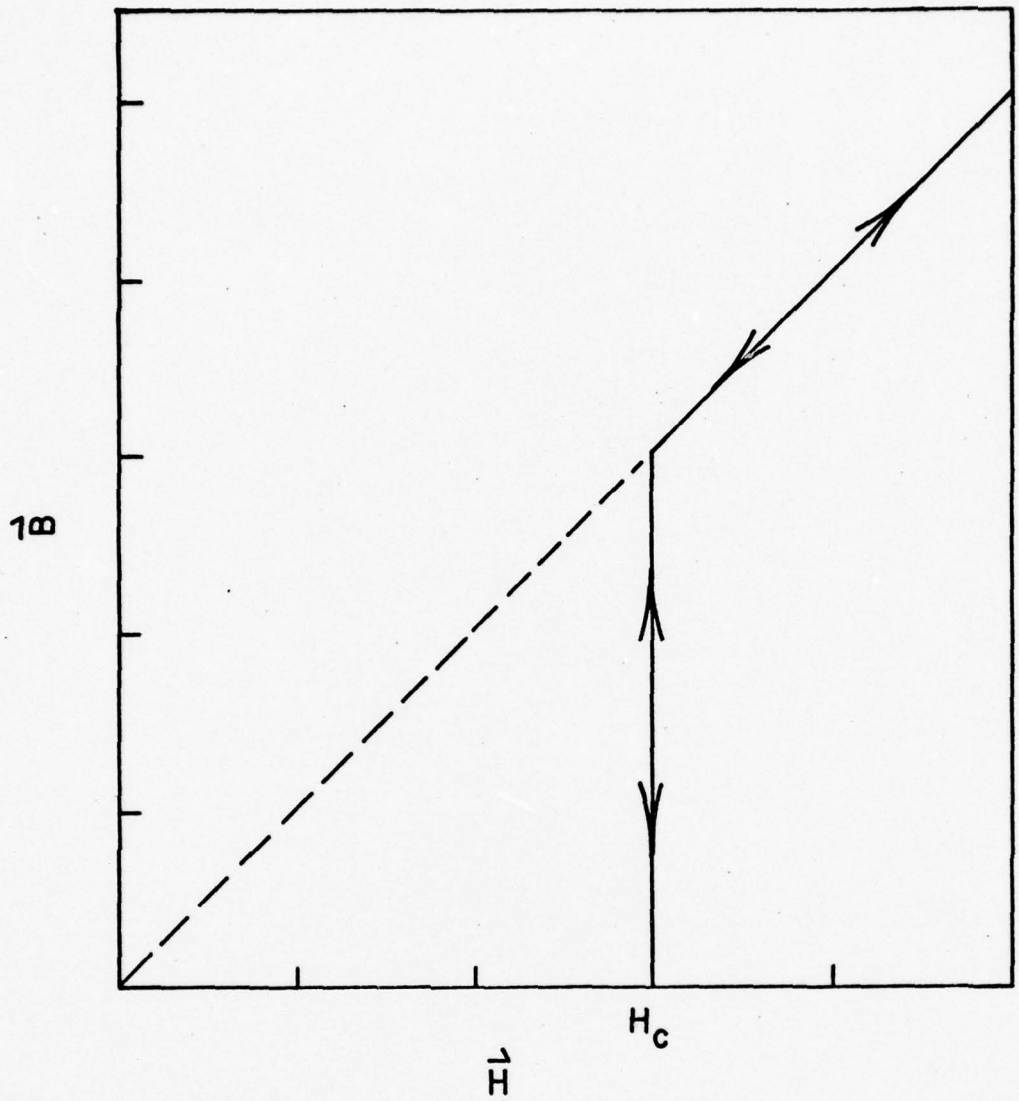


Figure 1. Magnetic induction, $\vec{B}$, as a function of the applied magnetic field, $\vec{H}$, for an ideal Type I superconductor.

The critical magnetic field as a function of temperature represents a thermodynamic phase boundary, see Figure 2. On the boundary $G_s(H_c,T) = G_n(H_c,T)$, thus,

$$F_n(T) - F_s(T) = H_c^2(T)/8\pi \quad . \tag{2.5}$$

where $H_c^2(T)/8\pi$ is the energy density associated with the magnetic field. The difference in the free energy between the normal state and the superconducting state is called the condensation energy. The condensation energy is of the order $\sim (k_B T_c)^2/E_F$, where E_F is the Fermi energy.

In order to treat the electromagnetic properties of superconductors, London and London (21) proposed that

$$\vec{E} = \Lambda \partial \vec{J}_s/\partial t \quad , \tag{2.6}$$

which describes perfect conductivity, and

$$\vec{h} = -c\Lambda\vec{\nabla} \times \vec{J}_s \tag{2.7}$$

be added to the Maxwell equations. Here, $\Lambda = m/n_s e^2$ is a phenomenological parameter, $\vec{E}$ is the electric field, $\vec{J}_s$ is the supercurrent density, and $\vec{h}$ is the value of the local magnetic field on a microscopic scale. The magnetic induction, $\vec{B}$, is the value of the magnetic induction on a macroscopic and scale is given by $\langle\vec{h}\rangle$.

London (22) gave a quantum explanation of the London Equation (2.6) using the vector potential, $\vec{A}$. In the absence of an applied magnetic field, the ground state would have zero net momentum, $\langle\vec{p}\rangle = 0$. If the wavefunction of the superconducting electron is "rigid" and

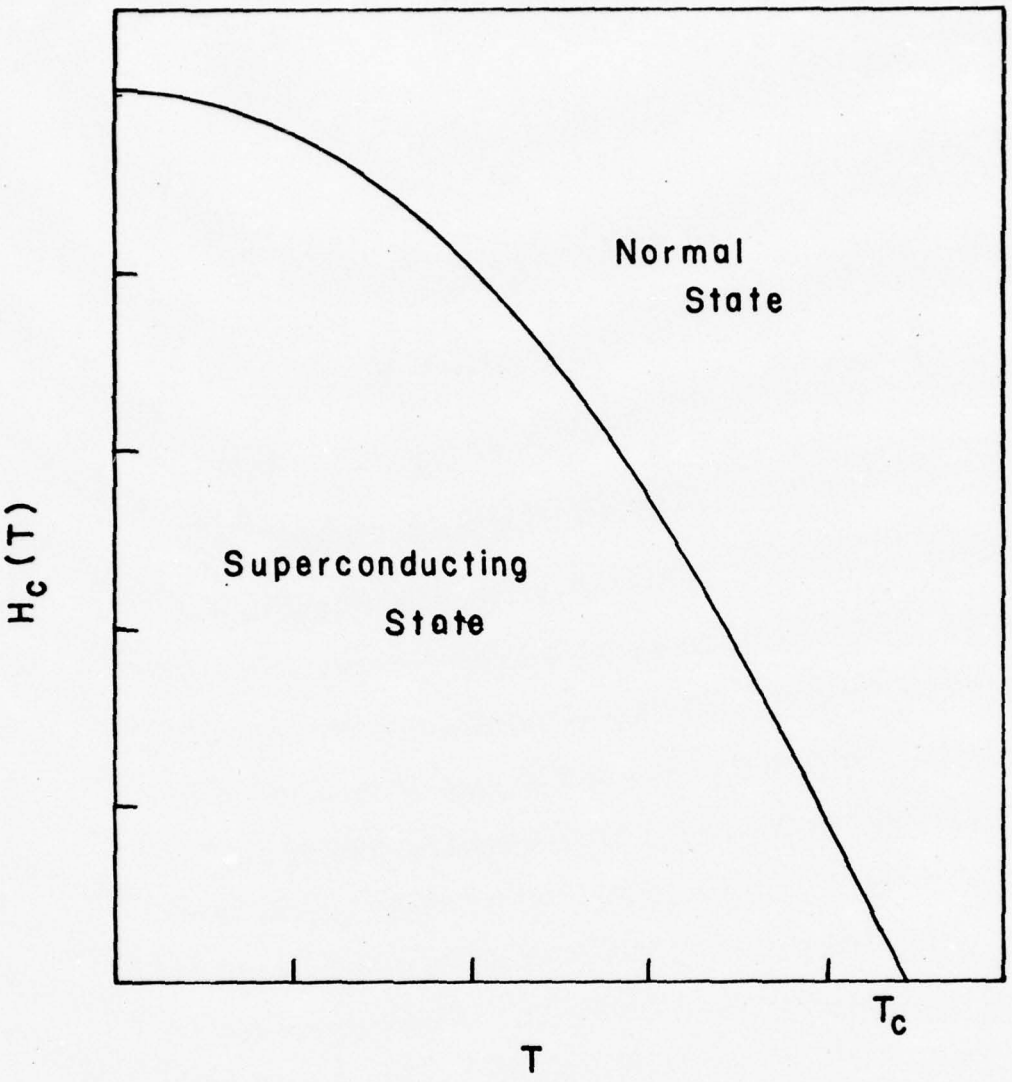


Figure 2. Temperature dependence of the critical magnetic field, H_c.

retains the ground state form even with a magnetic field present, then the conjugate momentum is given by

$$\langle \vec{p} \rangle = \langle m\vec{v} \rangle - e\vec{A}/c = 0 \quad . \tag{2.8}$$

Equation (2.8) reduces to

$$\langle \vec{v}_s \rangle = - e\vec{A}/mc \quad . \tag{2.9}$$

The supercurrent is then

$$\vec{J}_s = n_s e \langle \vec{v}_s \rangle = - n_s e^2 \vec{A}/mc \quad , \tag{2.10}$$

where n_s is the number of superconducting electrons per unit volume. Now, taking the time derivative of Equation (2.10) yields

$$\frac{\partial \vec{J}_s}{\partial t} = - \frac{n_s e^2}{mc} \frac{\partial \vec{A}}{\partial t} \quad . \tag{2.11}$$

Recall that

$$\vec{E} = - \vec{\nabla}\phi - \frac{1}{c} \frac{\partial \vec{A}}{\partial t} \quad .$$

In the London gauge, ϕ is constant, thus

$$\vec{E} = - \frac{1}{c} \frac{\partial \vec{A}}{\partial t} \quad . \tag{2.12}$$

Using Equation (2.12) in Equation (2.11), one obtains

$$\frac{\partial \vec{J}_s}{\partial t} = \frac{n_s e^2 \vec{E}}{m}$$

or

$$\vec{E} = \frac{m}{n_s e^2} \frac{\partial \vec{J}_s}{\partial t} = \Lambda \frac{\partial \vec{J}_s}{\partial t} \quad .$$

This is just Equation (2.6).

Returning to Equation (2.10) and taking the curl of both sides, one obtains

$$\vec{\nabla} \times \vec{J}_s = - \frac{n_s e^2}{mc} \vec{\nabla} \times \vec{A} \quad . \tag{2.13}$$

Making use of the fact that $\vec{h} = \vec{\nabla} \times \vec{A}$, Equation (2.13) reduces to

$$\vec{h} = - \frac{mc}{n_s e^2} \vec{\nabla} \times \vec{J}_s$$

which is just Equation (2.7) above. Now, taking the curl of both sides of the Maxwell relation $\vec{\nabla} \times \vec{h} = (4\pi/c)\vec{J}$ leads to

$$\vec{\nabla} \times \vec{\nabla} \times \vec{h} = \frac{4\pi}{c} \vec{\nabla} \times \vec{J}_s \quad . \tag{2.14}$$

Using the vector identity $\vec{\nabla} \times \vec{\nabla} \times \vec{h} = \vec{\nabla}(\vec{\nabla} \cdot \vec{h}) - \nabla^2 \vec{h}$, the Maxwell relation $\vec{\nabla} \cdot \vec{h} = 0$, and Equation (2.7), Equation (2.14) becomes

$$\nabla^2 \vec{h} = \vec{h}/\lambda_L^2 \quad , \tag{2.15}$$

where $\lambda_L = (mc^2/4\pi n_s e^2)^{\frac{1}{2}}$ is called the London penetration depth. For a semi-infinite slab of superconductor, it can easily be shown that

$$h(x) = h(0) \exp(-x/\lambda_L) \quad . \tag{2.16}$$

Thus, Equation (2.7) leads to the Meissner state for a bulk specimen.

The superconductors discussed so far are Type I superconductors. The measured penetration depth for a Type I superconductor is found, experimentally, to be greater than λ_L predicted by the London theory. This along with work on the magnetic field dependence of the penetration depth and experiments on the inductive and the resistive components of the surface impedance of tin at microwave frequences led Pippard (23) to propose replacing the local London theory by a non-local theory where the supercurrents are given by

$$\vec{J}_s(\vec{r}) = -\frac{3c}{16\pi^2\xi_0\lambda_L^2}\int \frac{\vec{R}[\vec{R}\cdot\vec{A}(\vec{r}')]e^{-R/\xi}}{R^4}\,d\vec{r}' \quad , \tag{2.17}$$

where $\vec{R} = \vec{r} - \vec{r}'$ and ξ_0 is a coherence length which may be estimated from an uncertainty principle argument (24). The coherence length, ξ, in the presence of scattering has the form

$$\frac{1}{\xi} = \frac{1}{\xi_0} + \frac{1}{\ell} \quad . \tag{2.18}$$

Here, ℓ, is the normal state electronic mean free path.

Another approach to generalize and extend the concepts of the London theory was developed by Ginzburg and Landau (25). They introduced a complex order parameter $\psi(\vec{r})$. $|\psi(\vec{r})|^2$ represents the local density of superconducting electrons $n_s(r)$. This theory takes into account the spatial variation of n_s and also nonlinear effects due to magnetic fields strong enough to change the order parameter. The Ginzburg-Landau theory is limited to small values of ψ and slow variations in space. The Gibbs free energy density, G_s, can be expanded as

$$G_s = G_{no} + \alpha|\psi|^2 + \frac{1}{2}\beta|\psi|^4 + \frac{1}{2m}\left|\left(-i\hbar\vec{\nabla} - \frac{2e\vec{A}}{c}\right)\psi\right|^2 + |\vec{h}|^2/8\pi \quad . \qquad (2.19)$$

G_s is the Gibbs free energy in the superconducting state, G_{no} is the free energy in the normal state in zero applied magnetic field, $\vec{A}$ is the vector potential, such that $\vec{h} = \vec{\nabla} \times \vec{A}$, and $|\vec{h}|^2/8\pi$ is the magnetic field energy density.

If the free energy is minimized with respect to the order parameter and the vector potential, Equation (2.19) reduces to two differential equations:

$$\frac{1}{2m}\left(-i\hbar\vec{\nabla} - \frac{2e\vec{A}}{c}\right)^2 \psi + \beta|\psi|^2\psi = -\alpha(T)\,\psi \qquad (2.20)$$

and

$$J_s = \frac{e\hbar}{im}(\psi^*\vec{\nabla}\psi - \psi\vec{\nabla}\psi^*) - \frac{4e^2}{mc}|\psi|^2\vec{A} \quad . \qquad (2.21)$$

In the absence of an applied magnetic field and gradients, the free energy, Equation (2.19), reduces to

$$G_s - G_{no} = \alpha|\psi|^2 + \frac{1}{2}\beta|\psi|^4 \quad . \qquad (2.22)$$

For this to be an absolute minimum,

$$\psi_0^2 = -\alpha/\beta \quad . \qquad (2.23)$$

Thus, Equation (2.22) becomes

$$G_s - G_{no} = -\alpha^2/2\beta \quad . \qquad (2.24)$$

Now, using Equation (2.5), one obtains

$$\frac{\alpha^2}{2\beta} = \frac{H_c^2}{8\pi} \quad . \tag{2.25}$$

In the perfect Meissner state, $\vec{A} = 0$. The solution of the free energy for this state is

$$\psi = \psi_0 = (-\alpha/\beta)^{\frac{1}{2}} \quad . \tag{2.26}$$

α is a negative quantity for $T < T_c$ and vanishes at $T = T_c$; however, the slope $d\alpha/dT$ remains finite at $T = T_c$.

For very weak magnetic fields, the order parameter varies very slowly with distance. The variation of the order parameter can be found from Equation (2.20) by setting $\vec{A} = 0$ and introducing a new function, the relative order parameter,

$$f = \psi/\psi_0 \quad . \tag{2.27}$$

Equation (2.20) becomes

$$- \frac{\hbar^2}{2m\alpha(T)} \nabla^2 f - f^3 + f = 0 \quad . \tag{2.28}$$

Now if a new characteristic length called the temperature dependent coherence length is defined as

$$\xi^2(T) = \hbar^2/2m\alpha(T) \quad , \tag{2.29}$$

Equation (2.28) becomes

$$- \xi^2(T)\nabla^2 f - f^3 + f = 0 \quad .$$

The temperature dependent coherence length is the range over which f varies from 0 to 1.

Consider the current Equation (2.21). $|\psi|^2$ can be replaced by ψ_0^2 for weak magnetic fields and, to first order in $\vec{h}$, Equation (2.21) becomes

$$\vec{J}_s = \frac{eh}{im} (\psi^* \vec{\nabla} \psi - \psi \vec{\nabla} \psi^*) - \frac{4e^2}{mc} \psi_0^2 \vec{A} \quad . \tag{2.30}$$

Taking the curl of Equation (2.30) leads to

$$\vec{\nabla} \times \vec{J}_s = - \frac{4e^2}{mc} \psi_0^2 \vec{h} \quad .$$

This is equivalent to the London Equation (2.7) with a penetration depth given by

$$\lambda(T) = \left[\frac{mc^2}{16\pi e^2 \psi_0^2} \right]^{\frac{1}{2}} \quad . \tag{2.31}$$

If the number of superconducting electrons, n_s , is equal to $4\psi_0^2$, Equation (2.31) reduces to the London penetration depth $\lambda_L(0)$. This temperature dependent penetration depth $\lambda(T)$, determines the distance over which the magnetic field, h, varies from its maximum value to 1/e of its maximum value.

The Ginzburg-Landau equations are valid only near the transition temperature where $\xi(T) >> \xi_0$. Also this theory yields a local relation between the current and the vector potential. For constant $|\psi|$ and a small value of $\vec{h}$, the current depends on the vector potential over a distance $|\vec{r} - \vec{r}'| \sim \xi_0$ in a pure superconductor. The local approximation is valid if $\vec{h}$ and $\vec{A}$ are slowly varying functions over distances of the order ξ_0 . For this to be true $\lambda(T) >> \xi_0$.

The ratio of the penetration depth, $\lambda(T)$, to the temperature dependent coherence length, $\xi(T)$, defines the Ginzburg-Landau parameter

$$\kappa = \frac{\lambda(T)}{\xi(T)} \quad . \tag{2.32}$$

This parameter is rather temperature insensitive since, as T_c is approached, both $\lambda(T)$ and $\xi(T)$ diverge in the same way.

Type I superconductors have values of κ less than $1/\sqrt{2}$. Type I superconductors show an intermediate state that is geometry dependent (26). Consider a sphere of Type I superconducting material placed in an external magnetic field much less than the critical magnetic field, H_c. The magnetic field will be expelled from the bulk of the specimen and the specimen will be in the Meissner state. Now, if the applied magnetic field is increased to $(1-D)H_c$, where D is the demagnetizing factor, the magnetic flux expelled from the bulk of the specimen will cause the local magnetic field at the equator to be greater than H_c . When this occurs, the specimen enters into the intermediate state. The intermediate state is the coexistence of regions in the Meissner state and of regions in the normal state which carry the magnetic flux. There is a positive surface energy associated with the boundary between the normal state and the Meissner state. Physically, a positive energy per unit area, $\sim \xi H_c^2/8\pi$, is associated with the variation of the order parameter, while there is a negative energy per unit area, $\sim \lambda H_c^2/8\pi$, associated with reducing the diamagnetic energy (27). Therefore, as long as $\kappa < 1/\sqrt{2}$, there is a total positive energy associated with the normal-superconducting interface.

Bardeen, Cooper and Schrieffer (28) developed a microscopic theory of superconductivity based on the pairing of electrons through a phonon mediated interaction. These paired electrons, called Cooper pairs, have a spatial extension of ξ_0 ; this is the same ξ_0 as used in the Pippard non-local theory. The formation of the pairs of electrons in the condensed state is related to the existence of a gap in the low energy excitation spectrum for a superconductor. The gap energy, 2Δ , is related to the energy, ε_{eh} , needed to create an electron-hole pair close to the Fermi surface, i.e.,

$$\varepsilon_{eh} \geq 2\Delta \quad .$$

The coherence length, ξ_0 , is related to the energy gap. Because an electron-hole pair is created, certain values of the momenta are forbidden. The forbidden values of the momenta are related to the energy condition

$$E_F - \Delta \leq \frac{\hbar p^2}{2m} \leq E_F + \Delta \quad . \tag{2.33}$$

The coherence length is related to the uncertainty in the momenta by

$$\xi_0 \, \delta p \sim \hbar \quad ,$$

thus,

$$\xi_0 = \hbar/\delta p \quad ,$$

where $\delta p \simeq p_F \, \Delta/E_F$. Then,

$$\xi_0 = \frac{\hbar v_F}{\pi \Delta} \quad . \tag{2.34}$$

The factor $1/\pi$ is arbitrary and is chosen for convenience. v_F is the Fermi velocity.

Gor'kov (29) showed that the Ginzburg-Landau phenomenological approach is a limiting form of the BCS microscopic theory.

In a 1957 paper, Abrikosov (30), who was extending the work of Ginzburg and Landau, developed the theory of Type II superconductors. Ginzburg and Landau anticipated a laminar structure for the intermediate state of a superconductor with low values of κ , i.e., Type I superconductors. This is because the gain in the free energy due to the penetration of the magnetic field, $H > H_c$, must be balanced against the positive surface energy which is a result of creating a normal-superconducting interface. For values of $\kappa > 1/\sqrt{2}$, the surface energy is negative. $\kappa = 1/\sqrt{2}$ is the value of κ which separates Type I superconductors from Type II superconductors. As long as $\kappa > 1/\sqrt{2}$, negative surface energy causes the maximum amount of surface area between superconducting and normal regions to be created. The subdivision into small regions of normal material carrying the magnetic flux is limited by the quantum nature of the magnetic flux. Each fluxoid containing one quantum of magnetic flux has a normal core, the diameter of which extends over a distance of twice the temperature dependent coherence length, $\xi(T)$. The flux quantum, ϕ_0 , is equal to $hc/2e$ or 2.07×10^{-7} gauss-cm^2 .

In the case of a zero demagnetizing factor, the external magnetic field is expelled from the Type II superconductor for applied magnetic fields lower than some critical value, H_{c1} , see Figure 3. Above H_{c1} , the magnetic field begins to penetrate into the superconductor in

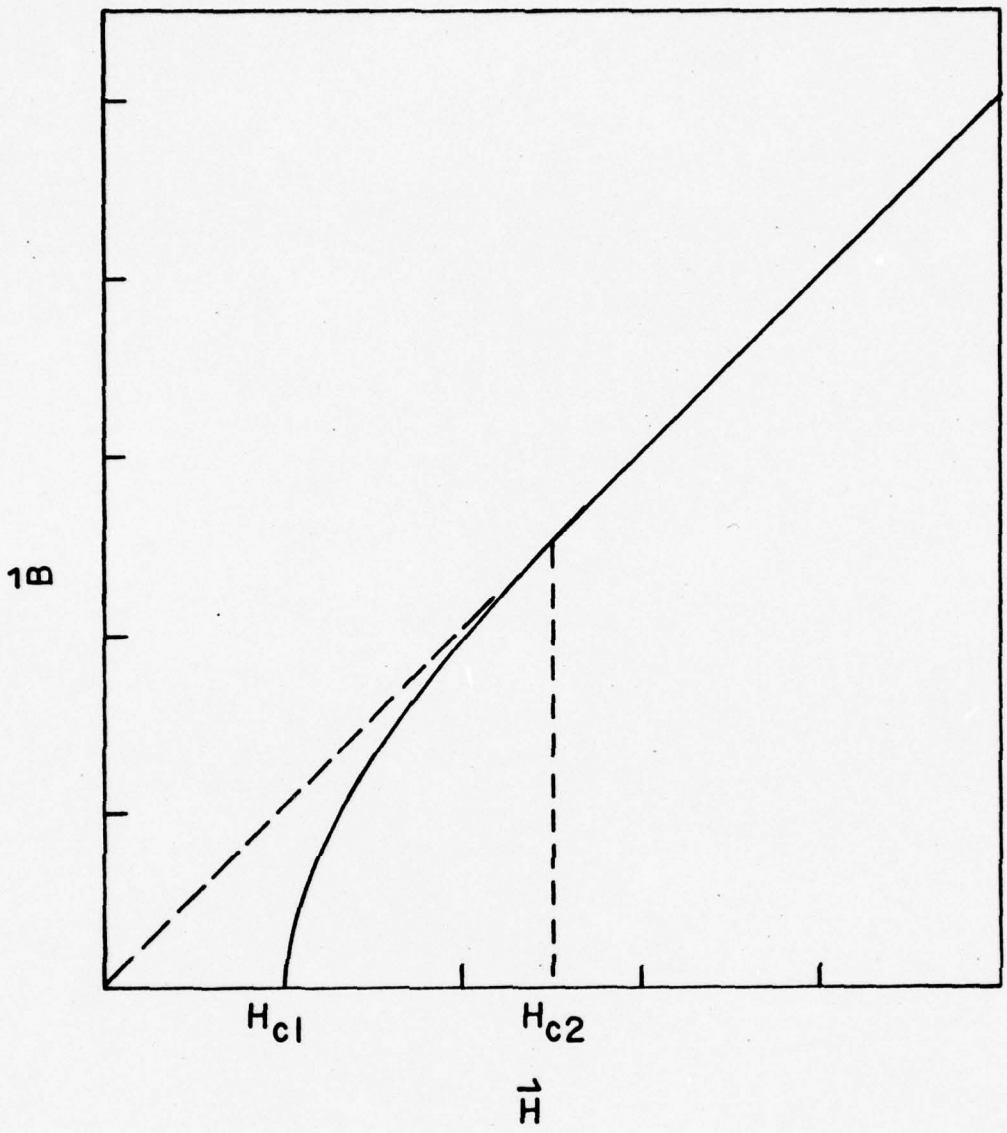


Figure 3. Magnetic induction, $\vec{B}$, as a function of the applied magnetic field, $\vec{H}$, for an ideal Type II superconductor.

quantized units of magnetic flux. In this mixed state, the fluxoids establish a fluxoid lattice (30,31,32,33,34,35). This fluxoid lattice compresses as the external magnetic field is increased until the normal cores of the fluxoids are 2.5 $\xi(T)$ apart. This defines the upper critical magnetic field, H_{c2} . For applied magnetic fields greater than H_{c2} , the specimen is in the normal state.

B. Magnetization Considerations

An important question arises as to whether the applied magnetic field, $\vec{H}$, is numerically equal to the magnetic induction, $\vec{B}$, in the calculation of the macroscopic pinning force density. When a magnetic field is applied to a Type II superconductor with a demagnetizing factor, $D \neq 0$, the magnetic field penetrates into the superconductor if the applied magnetic field exceeds $(1-D)H_{c1}$. In a Type II superconductor with $\kappa >> 1$ and $D > 0$, the Ginzburg-Landau theory predicts a mixed state if $H > (1-D)H_{c1}$ and the magnetic flux is dispersed throughout the superconductor in the smallest units possible, consistent with the quantum nature of the flux (26,36,37).

For the geometry of the specimens used in this investigation, the demagnetizing factor is approximately one (38). This leads to magnetic flux penetration into the specimen for any value of the applied magnetic field. The magnetic induction, in Gaussian units, is given by

$$\vec{B} = \vec{H} + (1-D)4\pi\vec{M} \quad . \tag{2.33}$$

Here $\vec{M}$ is the magnetization and $D \approx 1$; thus Equation (2.33) becomes (39,40)

$$\vec{B}(\text{gauss}) \approx \vec{H}(\text{oersted}) \quad .$$

C. Nature of the Driving Force

One can show, using thermodynamic arguments, that the driving force on the fluxoid is equal to the Lorentz force (41,42,12). Consider a superconducting specimen in an applied magnetic field, $\vec{H}$, as in Figure 4. The applied magnetic field produces a fluxoid lattice inside the superconductor. If a transport current is passed through the superconductor, the current will cause a gradient in the magnetic field across the specimen. The fluxoids will tend to move in the direction opposite the gradient in the magnetic induction, $\vec{B}$.

The pressure may be calculated by considering n fluxoids intersecting a surface, A, in the x-y plane. The Gibbs free energy per unit thickness (12)

$$G = AG \quad , \tag{2.34}$$

where $G = F - BH/4\pi$. The free energy, F, contains the interactions and self energies of the fluxoids. The Helmholtz free energy is

$$F = U - TS + H^2/8\pi \quad .$$

The differential internal energy for a magnetic system is given by

$$dU = TdS - PdV + HdM \quad ,$$

where M is the magnetization of the specimen. Hence the differential Helmholtz free energy becomes

$$dF = - SdT - PdV + HdM + HdH/4\pi \tag{2.35}$$

Since $B = H + 4\pi M$, and $dM = (dB - dH)/4\pi$, Equation (2.35) becomes

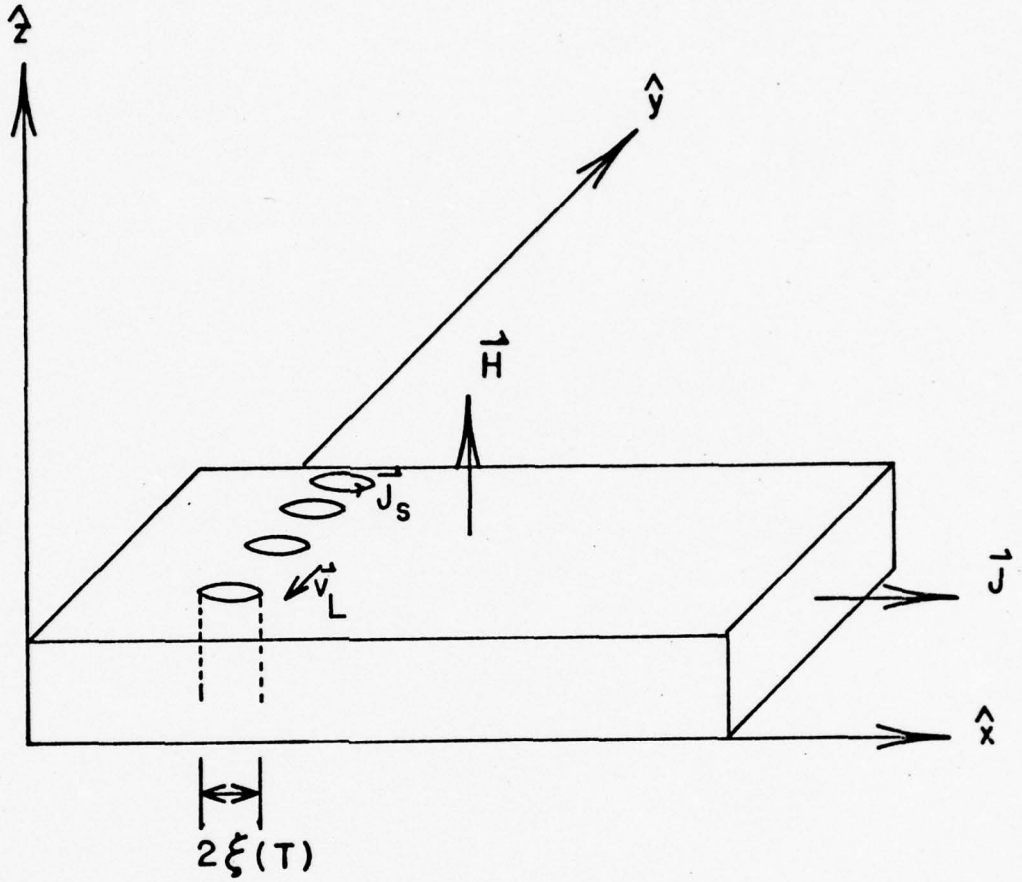


Figure 4. Schematic representation of the flux creep experiment.

$$dF = - SdT - PdV + HdB/4\pi \quad . \tag{2.36}$$

Thus, the differential of the Gibbs function is

$$dG = - SdT - PdV - BdH/4\pi \quad . \tag{2.37}$$

The pressure is given by (12)

$$P = - \left(\frac{\partial G}{\partial V}\right)_{T,H} \quad . \tag{2.38}$$

If the fluxoids are locked to the pinning sites and the number of fluxoids is constant, then changing the density of fluxoids is equivalent to mechanical work and one may talk about a pressure. Making use of Equation (2.34), Equation (2.38) becomes

$$P_{mag} = - \left(\frac{\partial G}{\partial A}\right) = - G - \frac{A\ \partial G}{\partial A} \quad . \tag{2.39}$$

The Gibbs energy is a function of T, A, and H. If the number of fluxoids is fixed, one can make a transformation which takes

$$G(T,A,H) \Rightarrow G'(T,B,H) \quad .$$

The constraint is $n = BA/\phi_0$. Then, the derivative with respect to A in Equation (2.39) can be replaced by a derivative with respect to B, i.e.,

$$\frac{A\ \partial G(T,A,H)}{\partial A} = \frac{A\ \partial B}{\partial A}\ \frac{\partial G'(T,B,H)}{\partial B} \quad . \tag{2.40}$$

Making use of the constraint, $n = BA/\phi_0$,

$$\frac{\partial B}{\partial A} = - \frac{n\phi_0}{A^2} = - \frac{B}{A} \quad .$$

Substituting this back in Equation (2.40), one obtains

$$\frac{A\ \partial G(T,A,H)}{\partial A} = -\frac{B\ \partial G'(T,B,H)}{\partial B} \quad .$$

Thus, Equation (2.39) with P as a function of T, B, and H becomes

$$P' = -G' + \frac{B\ \partial G'}{\partial B} \quad .$$

The equilibrium value of B is obtained from the condition $\partial G'/\partial B = 0$; therefore

$$\frac{\partial G'}{\partial B} = 0 = \frac{\partial F(B)}{\partial B} - \frac{H}{4\pi}$$

or

$$\frac{\partial F(B)}{\partial B} = \frac{H}{4\pi} \quad . \tag{2.41}$$

The *pressure gradient* can be written as (12)

$$\frac{\partial P'}{\partial y} = -\frac{\partial G'}{\partial y} + \frac{\partial B}{\partial y}\frac{\partial G'}{\partial B} + \frac{B\partial^2 G'}{\partial B^2}\frac{\partial B}{\partial y} \quad ,$$

which reduces to

$$\frac{\partial P'}{\partial y} = \frac{B\partial^2 G'}{\partial B^2}\frac{\partial B}{\partial y} \quad .$$

Since $\partial^2 G'/\partial B^2 = \partial^2 F/\partial B^2$, the pressure gradient can be written as

$$\frac{\partial P'}{\partial y} = \frac{B\ \partial(\partial F/\partial B)}{\partial y} \quad . \tag{2.42}$$

Making use of Equation (2.41), Equation (2.42) becomes

$$\frac{\partial P'}{\partial y} = \frac{B}{4\pi}\frac{\partial H}{\partial y} \quad .$$

The driving force per unit volume, $\vec{F}_D$, is equal to the pressure gradient but in the opposite direction. Using the Maxwell relation $\vec{\nabla} \times \vec{H} = (4\pi/c)\vec{J}$, the driving force per unit volume is equal to the Lorentz force per unit volume, i.e.,

$$\vec{F}_D = \frac{\vec{J} \times \vec{B}}{c} = \vec{F}_L \quad . \tag{2.43}$$

D. Fluxoid Pinning

In the case of static pinning, the defining criterion for the critical current density, $\vec{J}_c$, is that the Lorentz force, or driving force, on the fluxoids, per unit volume of specimen, equals the macroscopic pinning force density, $\vec{F}_p$, i.e.,

$$\vec{F}_p = - \vec{F}_L = - \frac{\vec{J}_c \times \vec{B}}{c} \quad . \tag{2.44}$$

In the present investigation, the applied magnetic field is perpendicular to the broad surface of the superconducting specimen. A transport current is passed through the superconductor in such a way that the current is perpendicular to the applied magnetic field and parallel to the broad surface of the superconductor, as shown in Figure 4. The fluxoids will move in a transverse direction under the influence of a driving force equal to $\vec{F}_L$. The fluxoids moving across the superconductor generate a longitudinal voltage proportional to the average creep velocity. This is analogous to the flux flow situation treated by Kim et al. (6,43,44,45,46) and Bardeen and Stephen (47).

Anderson (48) and Anderson and Kim (49) assumed that flux creep occurred by bundles of fluxoids jumping between adjacent pinning centers. G_T is the activation energy which is the increase in the energy of the

system when the fluxoid bundle is at a saddle point between two positions where the energy is at a local minimum. In the absence of any gradient in the magnetic induction, the fluxoid is just as likely to jump in one direction as another. There is no net creep velocity, see Figure 5a.

When an external magnetic field is applied perpendicular to the specimen's broad surface, a fluxoid lattice is formed. If a transport current is passed through the specimen, a gradient in the magnetic induction is created; thus, a fluxoid will have a tendency to jump in the direction of decreasing fluxoid density. The change in the energy barrier height is equal to the work done by the driving force, $\vec{F}_L$ acting through a distance equal to the width of the barrier, see Figure 5b.

A general pinning center is described in terms of an interaction potential with a maximum energy, U_p , and an effective width or range, X_p . This leads to an interaction force, f_p , between the fluxoid and the pinning center. The interaction force is given by

$$f_p = U_p/X_p \quad . \tag{2.45}$$

Schematically, fluxoid pinning can be represented as in Figure 6. The spatial variation of the order parameter $|\psi_0|^2$, which is directly related to the number density of superconducting electrons, is zero at the center of each fluxoid. The pinning center either enhances or inhibits the formation of the Cooper pairs. If the Cooper pair formation is inhibited by the pinning center, the fluxoid core, which already has a lower density of Cooper pairs, is attracted to the pinning center.

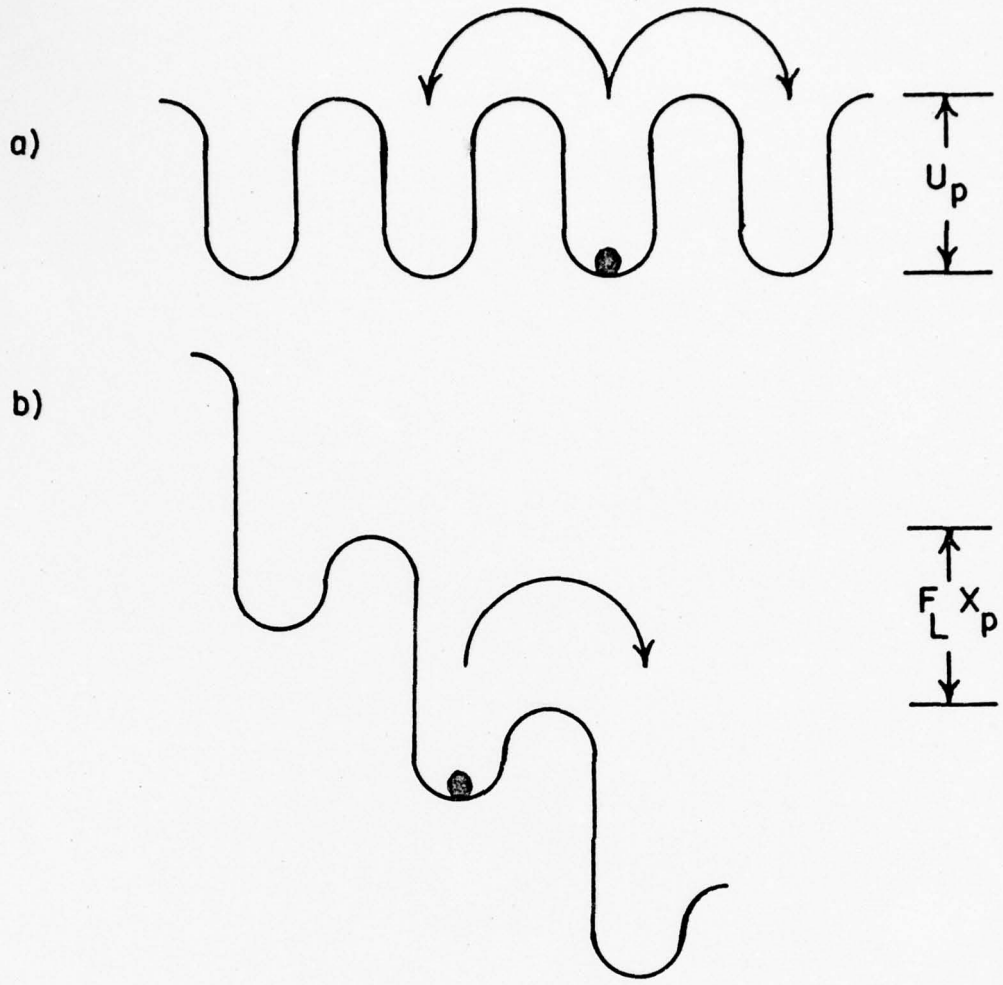


Figure 5. Schematic model for flux creep. a) U_p, the barrier height, b) the Lorentz force on the fluxoids will result in the tilting of the energy barrier.

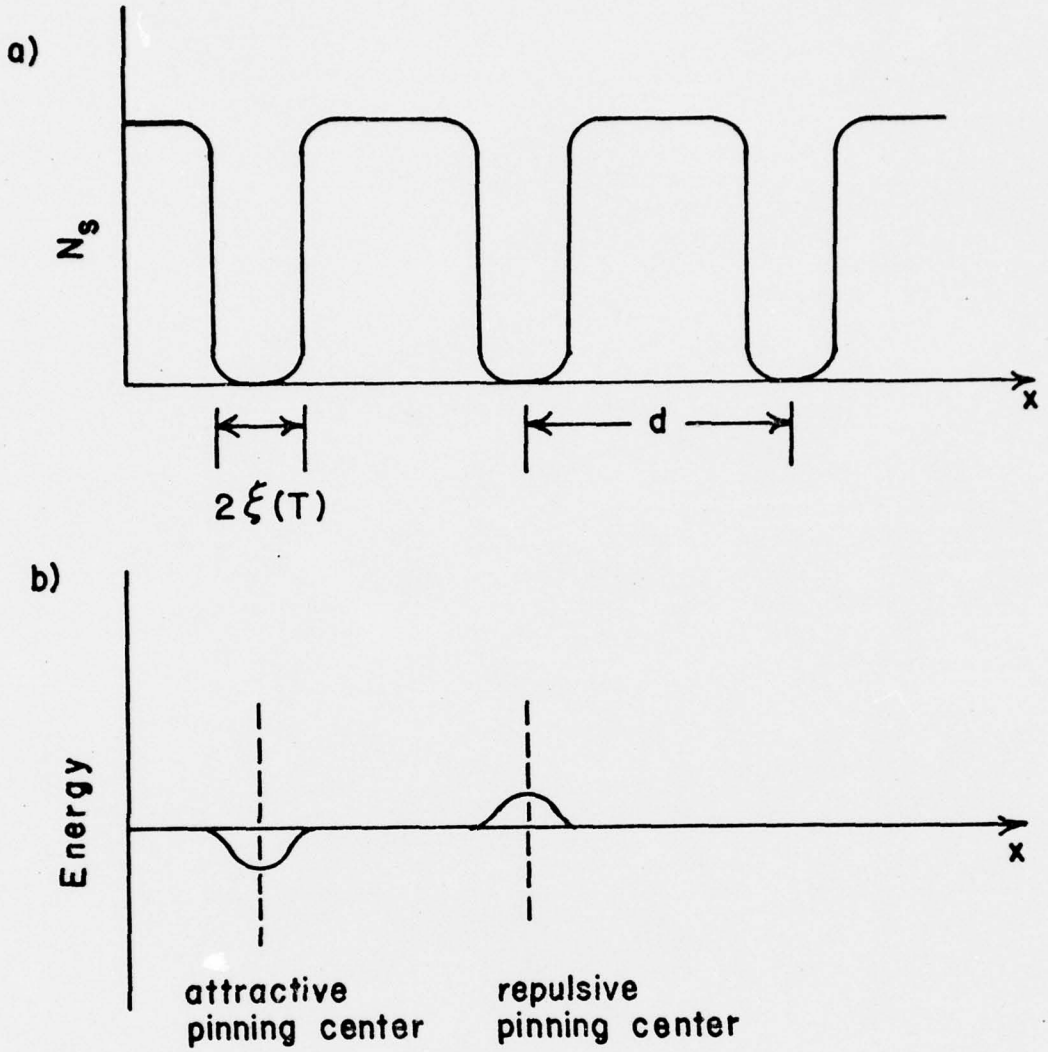


Figure 6. Schematic diagram of fluxoid pinning.

If, on the other hand, Cooper pair formation is enhanced by the presence of the pinning center, the fluxoid will be repelled from the pinning center.

The fluxoid motion involves activated jumps at a rate given by (8)

$$R = R_0 \exp(-G_T/k_B T) \quad . \tag{2.46}$$

The activation energy, G_T, is not equal to the pinning energy in the presence of a transport current, but is reduced by the action of the Lorentz force: thus,

$$G_T = U_p - JBV_p X_p/c \quad , \tag{2.47}$$

where V_p can be identified as the activation volume. The activation volume is the region where the Lorentz force per unit volume, $\vec{J} \times \vec{B}/c$, is transferred to the activation barrier so that the force $V_p \vec{J} \times \vec{B}/c$ is acting on the barrier during the activation event. X_p is the effective width of the pinning energy potential.

The electric field associated with the fluxoid motion is given by (46)

$$\vec{E} = \vec{v}_L \times \vec{H}/c \quad . \tag{2.48}$$

The difference between the flux creep region, considered here, and the flux flow region is the magnitude of the electric field involved. In the flux flow region, $E \sim 10^{-3}$ V/cm, whereas in the flux creep region, the electric field may be orders of magnitude smaller.

Flux creep dominates in the nonlinear region of the I-V traces. A typical I-V trace is shown in Figure 7. In the flux flow region,

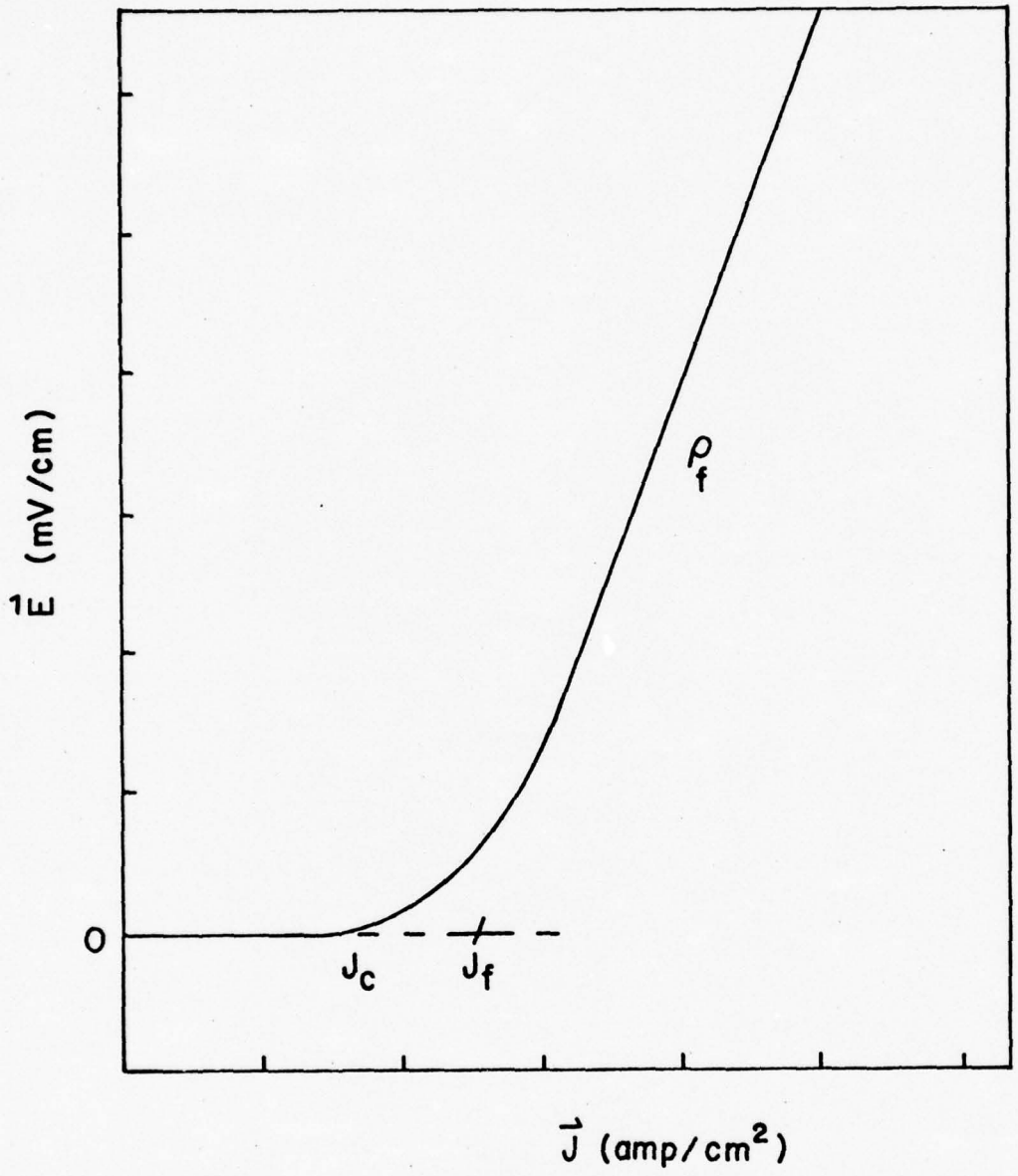


Figure 7. The electric field, $\vec{E}$, as a function of the transport current density, $\vec{J}$, through a specimen.

$\vec{v}_L$ and $\vec{E}$ are determined by a viscous drag force due to quasiparticle currents in the fluxoid cores. In this region, the velocity of the fluxoid lattice is so high that the flow is independent of pinning (39). The viscous force is proportional to $\vec{v}_L$ and leads to a flow electric field of the form

$$\vec{E} = \rho_f(\vec{J} - \vec{J}_f) \quad , \tag{2.49}$$

where $\vec{J}_f$ is a threshold current density and ρ_f is the flow resistivity which is given by

$$\rho_f = \rho_n B/H_{c2}(T) \quad , \tag{2.50}$$

where ρ_n is the normal state resistivity (50). Yamafugi and Irie (7), and Willis et al. (51) discuss the dissipation due to pinning in the flux flow region. The pinning forces are responsible for the threshold current density and dominate the fluxoid motion for small values of the electric fields.

Most experiments on fluxoid pinning are performed in the dynamic region, which includes both the flux creep and the flux flow regions, because the experiments require voltage measurements by electronic instruments which are sensitive to finite voltages. The minimum detectable voltage levels may be small, in which case one is investigating the flux creep region but not the static region. The critical state models of fluxoid pinning, however, are derived for the static pinning case, where there is no net fluxoid motion and where the Lorentz force is balanced by the pinning forces until the condition that $\vec{F}_L = -\vec{F}_p$ is just reached. Once $\vec{F}_L$ exceeds $\vec{F}_p$, the system goes

from the static regime to the dynamic regime. The question of whether one can use the condition

$$\vec{F}_p = - \frac{\vec{J}_c \times \vec{B}}{c}$$

in the dynamic regime will now be addressed. The argument presented here is different than the standard ones presented in the literature.

Consider Equation (2.46), i.e., the rate at which the fluxoids jump from one pinning site to another pinning site. In the case of static pinning, the rate of fluxoid jumps is given by

$$R = R_0 \exp (-U_p/k_B T) \quad . \tag{2.51}$$

If a transport current is passed through the specimen and $F_L < F_p$, then the net rate, R_N, is given as

$$R_N = R_0 \exp \left\{ - \frac{1}{k_B T} (U_p - JBV_p X_p/c) \right\} \quad , \tag{2.52}$$

with $U_p > JBV_p X_p/c$. The critical state is reached when the Lorentz force exactly balances the pinning force. When this condition is fulfilled, the rate is given by

$$R_N = R_0 \quad . \tag{2.53}$$

In the linear flux flow region, the rate is given by

$$R_N = R_0 \exp \left\{ - \frac{1}{k_B T} (U_p - JBV_p X_p/c) \right\} \quad , \tag{2.54}$$

with $U_p < JBV_p X_p/c$. In the nonlinear region at a point $\vec{J}_d$ where an electric field, $\vec{E}_d$, is just sufficiently large to be observed, a

dymamic resistivity, the tangent to the curve, can be defined. This observable electric field is measured in practice as a "cut off voltage," V_d . In this case, it follows that

$$\vec{E} = \rho_d(\vec{J} - \vec{J}_d) \quad . \tag{2.55}$$

The rate is given as

$$R_N = R_0 \exp\left\{-\frac{1}{k_B T}\,(U_p - J_d B V_p X_p/c)\right\} \quad , \tag{2.56}$$

with $U_p < J_d B V_p X_p/c$ since $J_c < J_d$. Rewriting J_d , the rate can be written as

$$R_N = R_0 \exp\left\{-\frac{1}{k_B T}\left[U_p - (J - E/\rho_d)\,\frac{B V_p X_p}{c}\right]\right\} \quad . \tag{2.57}$$

At the cut off voltage, Equation (2.57) becomes

$$R_N = R_0 \exp\left\{-\frac{1}{k_B T}\left[U_p - (J - E_d/\rho_d)\,\frac{B V_p X_p}{c}\right]\right\} \quad . \tag{2.58}$$

As E_d goes to zero, Equation (2.58) has to reduce to the rate equation for the static pinning case in the critical state, i.e., Equation (2.53). For this to be true, the argument of the exponent of Equation (2.58) must go to zero, i.e.,

$$U_p - (J - E_d/\rho_d)\, B V_p X_p/c = 0 \quad . \tag{2.59}$$

The pinning force is given by

$$F_p = \frac{U_p}{V_p X_p} = \frac{JB}{c} - \frac{E_d B}{c\rho_d} \quad . \tag{2.60}$$

As E_d goes to zero and J goes to J_c , then,

$$F_p = J_c B/c \quad ,$$

which is the pinning force density in the static case. However, from Equation (2.60), one can see that for a finite cut off voltage, the pinning force is

$$F_p = \frac{J_d B}{c} - \frac{E_d B}{c\rho_d} \quad . \tag{2.61}$$

In the dynamic pinning case, J_d in the above equation is the value of the critical current at some predetermined voltage cut off. J_d is actually larger than J_c of the static pinning case. E_d is the electric field corresponding to the predetermined cut off voltage and ρ_d is the dynamic resistivity at the value of J_d .

In a complete fluxoid pinning theory, the parameters of the pinning model must be related to the parameters of the dynamic pinning case discussed above. The important parameters associated with the pinning centers are the interaction energy between a single pinning center and a single fluxoid, ε , the geometrical width of the pinning center parallel to the fluxoid, a , and the number density of the pinning centers, n_p . These parameters must be related to the dynamic pinning parameters: U_p , the maximum energy of the interaction potential; X_p , the energy barrier width; and V_p , the activation volume.

Beasley et al. (52) present a good discussion of the energy barrier width. If the geometrical width of the pinning center is larger than the coherence length, $\xi(T)$, but smaller than the fluxoid lattice parameter, d, then,

$$x_p = a \quad . \tag{2.62}$$

If the geometrical width of the pinning center is larger than the fluxoid lattice parameter, then,

$$x_p = d \quad , \tag{2.63}$$

because of the periodicity of the fluxoid lattice. Finally, if the geometrical width of the pinning center is smaller than the temperature dependent coherence length, then

$$x_p = \xi(T) \quad . \tag{2.64}$$

This follows because the range of the interaction between a fluxoid and a pinning center cannot be smaller than the coherence length, which is the lower range of any interaction.

Certain pinning mechanisms can be eliminated from the discussion. The vanadium carbide precipitates used as pinning centers in this experiment are disc shaped particles whose thickness is less than the superconducting coherence length for the vanadium: thus, the precipitate will very likely be superconducting for B = 0 because of the proximity effect (10). For high values of the reduced magnetic field, $h = H/H_{c2}(T)$, the precipitate will act like a surface pinning center, since the vanadium carbide precipitate is disc shaped with a diameter greater than the fluxoid lattice parameter, d. The important parameter is the surface area of the precipitate perpendicular to the Lorentz force (53). In the low reduced magnetic field region, the diameter of the precipitate, a, is less than d and the precipitate may act like a point pinning center (54).

For superconductors approaching the London limit, $\kappa \to \infty$, the pinning is usually attributed to magnetic interactions or core interactions. The selection of which interaction applies is determined by the size and the spacing of the pinning centers in relation to the penetration depth, λ . The magnetic interaction is due to the change in the magnetic energy upon crossing the boundary separating the superconducting and pinning materials. The regions on either side of the boundary must be large enough to define a value of B and an equilibrium magnetization. If the regions on either side of the boundary are too small to define a value of B and an equilibrium magnetization, then one uses the core interaction. The free energy of the fluxoids in the superconducting matrix is different than the free energy of the fluxoids with their cores passing through the pinning center. This difference in the energy leads to the core interaction (55,42). Because vanadium is a low κ superconductor, the concepts of core interaction and magnetic interaction as derived in the literature for high κ superconductors are not applicable and one must use the Ginzburg-Landau expression for the free energy (42).

Upon careful examination of the transmission electron micrographs of the superconducting specimens no evidence of long-range strain fields associated with the vanadium carbide precipitates is observed (56). Therefore, elastic interactions can be excluded as the main cause of pinning (57).

The main question in the understanding of fluxoid pinning is how does one sum over the individual pinning centers and fluxoids to obtain the macroscopic pinning force density. The summation problem has met with limited success, and is far from being understood completely.

If the fluxoids were straight and the fluxoid lattice were completely rigid, for a high density array of identical pinning centers no pinning would result. Statistically, the interaction forces tending to cause the fluxoid to move to the right are balanced by the forces tending to cause the fluxoids to move to the left. Thus, the net force on the fluxoid is zero. However, pinning does occur and, according to Labusch (58,59), localized pinning forces cause inhomogeneous deformation of the fluxoid lattice. These inhomogeneous deformations of the fluxoid lattice allows the pinning (60). In a dilute system of pinning centers, the interaction between a single fluxoid and a single pinning center can be calculated. Using the statistical approach of Labusch, the macroscopic pinning force density is given by (57)

$$F_p = \frac{n_p a f_p^2}{8\sqrt{\pi}} \left(\frac{B}{\phi_0}\right)^{\frac{3}{2}} \frac{1}{(C_{44}C_{66})^{\frac{1}{2}}} \quad . \tag{2.65}$$

The modulus, C_{44} , for a deformation that tilts the fluxoid lattice away from the z-direction while leaving its cross-section in the x-y plane constant is given by (59)

$$C_{44} = \frac{BH}{4\pi} \quad . \tag{2.66}$$

The shear modulus, C_{66} , in the x-y plane is given by (59)

$$C_{66} = \frac{0.48(1-h)^2 H_{c2}^2}{8\pi(2\kappa^2 - 1)\beta_a^2} \quad , \tag{2.67}$$

where β_a is a geometrical factor which is equal to 1.16 (13).

Since the fluxoid lattice has a certain amount of rigidity, all the pinning centers present in the superconductor will not be equally effective. Thus, in a dense system of pinning centers, the interaction between a single fluxoid and a single pinning center cannot be calculated and the pinning is provided for by effective pinning centers. Campbell and Evetts (42) give the condition for a system of pinning centers to be considered dilute. If the number density of pinning centers is greater than some critical value, n*, the system is no longer dilute. n* is given by (42)

$$n^* = (10^4 \, X_p^2 d)^{-1} \quad , \tag{2.68}$$

where X_p is the energy barrier width. To calculate the largest n* consistent with a dilute array of pinning centers, consider the system at T = 0, and $X_p = d$. The smallest value of d is near H_{c2} where $d \approx \xi(0)$: thus Equation (2.68) becomes

$$n^* = [10^4 \, \xi^3(0)]^{-1} \sim 6 \times 10^{12} \text{ particles/cm}^3 \quad . \tag{2.69}$$

For Labusch's theory of point pinning centers to be applicable, the density of pinning centers must be less than the number given by Equation (2.69).

If the number of pinning centers in the specimen is greater than n*, one may be able to apply Kramer's line pinning theory (61,62). In this model, the strain field in the fluxoid lattice due to the individual pinning centers overlap if the distance between the pinning centers is less than some critical length (61)

$$\ell^* = \left[\frac{C_{44}\ \phi_0}{C_{66}B}\right]^{\frac{1}{2}} \quad . \tag{2.70}$$

In the low reduced magnetic field region, the pinning interaction is overcome by the Lorentz force. The pinning force density is given by (62)

$$F_p(h) = \frac{K_p h^{\frac{1}{2}}}{(1-h)^2} \quad , \tag{2.71}$$

with

$$K_p = \frac{5 \times 10^6\ \rho P w^4\ \beta^4\ H_{c2}^{\frac{5}{2}}}{\phi_0^{\frac{1}{2}}\ \kappa^2}\ \text{dynes/cm}^3 \quad , \tag{2.72}$$

where ρ is the density of initially strong line pinning centers per cm^2, w is the net number of pinning centers of strength, f_p, per unit length of fluxoid. β and P are constants. In the high reduced magnetic field region, $h > h_p$, the fluxoid lattice shears around pinning centers whose interactions are too strong to be broken. h_p is the value of the reduced magnetic field at the peak in the pinning force density curve. The pinning force density is given as (62)

$$F_s(h) = K_s h^{\frac{1}{2}} (1-h)^2 \quad , \tag{2.73}$$

with

$$K_s = 2C_s H_{c2}^{\frac{1}{2}} H_c^2\ \text{dynes/cm}^3 \quad , \tag{2.74}$$

where C_s is a number which varies from 0.14 to 0.56 depending on the density of the pinning centers. According to this theory, the

macroscopic pinning force density for low values of the reduced magnetic field is given as (62)

$$F_p(h) \propto H_{c2}^{\frac{5}{2}} h^{\frac{1}{2}} (1-h)^{-2} \quad h < h_p \quad , \tag{2.75}$$

while for high values of reduced magnetic field,

$$F_s(h) \propto H_{c2}^{\frac{1}{2}} H_c^2 h^{\frac{1}{2}} (1-h)^2 \quad h > h_p \quad . \tag{2.76}$$

In both cases, the macroscopic pinning force density is derived from the elastic energy stored in the fluxoid lattice.

Experimentally, Fietz and Webb (9) have found that the macroscopic pinning force density for a large number of superconductors obey a scaling law of the form given by

$$F_p = \text{Const.}\ H_{c2}^m(T)\ f(h) \quad . \tag{2.77}$$

The constant depends on the size distribution and the number density of the pinning centers. $H_{c2}^m(T)$ contains the temperature dependence of the macroscopic pinning force density. The exponent, m, is obtained from a plot of the $\ln(F_{pmax})$ as a function of $\ln(H_{c2})$. The form factor, f(h), depends only on the reduced magnetic field, h. Labusch's and Kramer's summation methods do not yield the form factor observed in this investigation. In order to obtain the observed value of m, a summation procedure is developed. First, an expression for the microscopic pinning force is obtained.

According to Campbell and Evetts (42) and Khanha (63), for low κ superconductors, the Ginzburg-Landau expression for the free energy must be used to calculate the interaction energy. In this study, the

thickness of the precipitates is less than the temperature dependent coherence length: thus, the proximity effect ensures that the order parameter does not change very much and perturbation theory may be used. The change in the Ginzburg-Landau free energy per unit volume is given by (62)

$$\delta G(H,T) = \frac{H_c}{4}\left[-\frac{\delta H_{c2}}{H_{c2}} f^2 + \frac{1}{2}\frac{\delta\kappa^2}{\kappa^2} f^4\right] \quad , \tag{2.78}$$

where f is the unperturbed relative order parameter and δH_{c2} is the upper critical magnetic field of the superconductor minus the upper critical magnetic field of the pinning center. For reduced magnetic fields high enough that $f^2 >> f^4$, the first term in the square brackets dominates, and

$$\delta G(H,T) = -\frac{H_c^2}{4\pi}\frac{\delta H_{c2}}{H_{c2}} f^2 \quad . \tag{2.79}$$

The mean value of the relative order parameter is given by (42)

$$f^2 = -\frac{8\pi\kappa^2 M}{H_{c2}} \quad . \tag{2.80}$$

Upon substitution for the magnetization, M, this equation yields

$$f^2 = -\frac{2\kappa^2}{H_{c2}}\left[\frac{H_{c2} - B}{1 + \beta_a (2\kappa^2 - 1)}\right] \quad . \tag{2.81}$$

The largest change in δH_{c2} would be to let $\delta H_{c2} = H_{c2}$. Then Equation (2.79) becomes

$$\delta G(H,T) = \frac{2\kappa^2 H_c^2 (1 - h)}{4\pi[1 + \beta_a (2\kappa^2 - 1)]} \quad . \tag{2.82}$$

Since $H_{c2} = \sqrt{2}\,\kappa H_c$, Equation (2.82) reduces to

$$\delta G(H,T) = \frac{H_{c2}^2 (1 - h)}{4\pi[1 + \beta_a (2\kappa^2 - 1)]} \quad . \tag{2.83}$$

The interaction energy is the energy difference between the energy of the fluxoid when it passes through the superconductor without passing through a pinning center, and the energy of the fluxoid when its core passes through a pinning center. The interaction energy is given by

$$\varepsilon \approx \frac{\xi^2(T)\ a\ H_{c2}^2 (1 - h)}{4\pi[1 + \beta_a (2\kappa^2 - 1)]} \quad . \tag{2.84}$$

where a is the diameter of the precipitate parallel to the fluxoid.

The microscopic pinning force, f_p, can be obtained from

$$f_p = \frac{d\varepsilon}{dx} \approx \frac{\varepsilon}{X_p} \tag{2.85}$$

Substituting Equation (2.84) into Equation (2.85) and letting X_p = a (64), one obtains

$$f_p = \frac{\xi^2(T)\ H_{c2}^2\ (1 - h)}{4\pi[1 + \beta_a (2\kappa^2 - 1)]} \quad . \tag{2.86}$$

Ordinarily one would expect to compute the pinning force density by calculating a summation of all the contributions to F_p by all the pinning centers involved. No completely satisfactory method of accomplishing this summation in a direct way has been found. Hence instead of using a direct summation, the concept of an activation volume is used.

This volume is the effective volume of an effective pinning center for each fluxoid which would accomplish the same pinning as the sum of all the real individual pinning centers. The fluxoid interacts with the pinning centers in this volume in such a manner that the interaction is between the fluxoid and an effective pinning center. The macroscopic pinning force density is given by

$$F_p = f_p/V_p \quad . \tag{2.87}$$

The activation volume, V_p, is given by (57)

$$V_p = X_p kd \quad . \tag{2.88}$$

where k is the distance between effective pinning centers. This is likely to depend on the magnetic field. The fluxoid lattice parameter, d, is given by $(\phi_0/B)^{\frac{1}{2}}$ (13), and letting $X_p = a$ (64), Equation (2.88) becomes

$$V_p = kad \quad . \tag{2.89}$$

Substituting this and Equation (2.86) into Equation (2.87) one obtains

$$F_p = \frac{\phi_0^{\frac{1}{2}} H_{c2}^{\frac{3}{2}} h^{\frac{1}{2}} (1 - h)}{8\pi a[1 + \beta_a (2\kappa^2 - 1)] k} \quad . \tag{2.90}$$

The macroscopic pinning force density for the specimens used in this investigation is given by

$$F_p = C_p H_{c2}^{\frac{3}{2}}(T) h(1 - h)^{\frac{1}{2}} \quad . \tag{2.91}$$

By equating Equation (2.91) with Equation (2.90), one obtains the distance between effective pinning centers, i.e.,

$$k = \frac{\phi_0^{\frac{1}{2}}}{8\pi a[1 + \beta_a (2\kappa^2 - 1)]C_p} \frac{(1 - h)^{\frac{1}{2}}}{h^{\frac{1}{2}}} \tag{2.92}$$

where C_p is a number which depends on the size and/or the number density of the pinning centers.

The scaling law observed by Fietz and Webb (9)

$$F_p = \text{Const.}\ H_{c2}^m(T)\ f(h)$$

is adjusted to the particular superconductor in question through the experimentally determined values of $H_{c2}(T)$, m, f(h), and the constant. The summation problem, if solved correctly, starts with the microstructure of the pinning centers and the basic interaction between a pinning center and a fluxoid and arrives at the form of the macroscopic pinning force density given by the scaling law equation.

III. EXPERIMENTAL PROCEDURES

A. Specimens

The superconducting specimens were prepared and characterized under the supervision of Professor William R. Bitler of the Metallurgy Section of the Department of Material Sciences of The Pennsylvania State University. For details concerning the preparation and characterization of the specimens, one may consult Schuyler (56). The vanadium was obtained from the Materials Research Corporation, Orangeberg, New York. The original material was in the form of a foil 2.54 cm wide by 2.5×10^{-2} cm thick. The control specimen is a well annealed, 99.95% pure vanadium specimen with a residual resistance ratio of 25. The other specimens contained 0.1 atomic percent to 0.6 atomic percent carbon in vanadium. The resistance ratios of the carbon containing specimens range from 10 to 22.

The carbon containing specimens start as a 99.95% pure vanadium specimen which is then annealed at 1500°C for one-half hour, just as is the control specimen. The annealing process is carried out in a vacuum chamber, typically, the vacuum was in the 10^{-4} torr range, with a magnesium getter to reduce the oxygen and nitrogen partial pressures. After the specimen is annealed, the carbon, in the form of methane, is introduced into the bell jar while the specimen is still at an elevated temperature, approximately 1500°C. The proper amount of methane is mixed with a hydrogen gas carrier. The mixture is then introduced into the bell jar. The methane breaks down and the carbon goes into solid solution in the vanadium. After two minutes, the hydrogen is pumped

out of the bell jar and the specimen is allowed to cool to room temperature in vacuum. This procedure results in the formation of vanadium carbide precipitates in the vanadium matrix. If the vanadium carbide precipitates are to comprise the main type of pinning center in the specimens, a low lattice dislocation density is required. This is why all the specimens used in this investigation are annealed first. The annealing process results in the specimens having large grain size (65). Also, studies with the transmission electron microscope confirm the fact that the specimens have very low lattice dislocation densities.

The final specimens are polycrystalline with grain sizes of approximately 2 mm. Transmission electron micrographs show that the surfaces of the grains are near to {001} planes and the precipitates are platelet or disc shaped with a thickness of only a few atomic layers. The vanadium carbide precipitates on the {310} habit planes. Thus, if one looks along the [010] direction, the planes of the disc shaped vanadium carbide precipitates would be at angles of 90°, 71.6°, and 18.4° to this direction. The precipitates are coherent with the vanadium lattice. A coherent particle is one in which the lattice planes in the precipitate are continuous with the lattice planes of the matrix. If the diameter of the solute atoms differ from the diameter of the solvent atoms, the lattice of the matrix will be strained by the presence of the precipitate. The strain associated with the precipitate will enlarge until the lattice of the precipitate breaks away from the lattice of the matrix. When this occurs, an incoherent grain boundary is formed between the precipitate and the matrix (66).

The cross-sectional dimension of the specimen is chosen in order that a high current density at a low total current flows through the specimen. The specimens are electrochemically cut to shape. A typical specimen has dimensions of 1.3×10^{-2} cm by 0.32 cm by 3.8 cm. The specimens are electropolished from the original foil thickness of 2.5×10^{-2} cm down to the final thickness, approximately 1.3×10^{-2} cm, in order to remove any surface contamination and thermally created dislocations on the surface which often lead to enhanced surface layer superconductivity.

The electrochemical cutting and the electropolishing of the specimens are carried out with the same apparatus. The specimen is mounted in a metal holder which is placed in a solution of 20% H_2SO_4 and 80% methanol. On each side of the specimen, approximately one centimeter away from the specimen, is a pointed stainless steel electrode. The specimen is connected to the positive terminal of a dc power supply while the stainless steel electrodes are connected to the negative terminal. When the specimen is being electrochemically cut to shape, the specimen is coated with "Miccrostop stop-off lacquer". A templet of the desired shape is placed on a lacquer coated specimen and a razor blade is used to cut a small channel through the lacquer, about one millimeter wide, around the templet. The templet is removed and the specimen is placed in the electrolyte. The dc power supply is connected and maintains seven volts across the system. The cutting operation takes 2 to 5 hours to complete. Once the specimen is cut to shape, the lacquer is removed and the specimen is remounted in its holder. The specimen is placed in the electrolyte and the dc power supply is

connected. To electropolish the specimen the voltage is maintained at 12 volts for approximately one-half hour. The electrolyte is maintained at a constant temperature by means of a cooling coil that is connected to cold running water. The electrolyte is constantly stirred by means of a magnetic stirrer to reduce the anodic layer which tends to form (67).

B. Specimen Holder

The specimen holder is used to suspend the specimen in the center of a superconducting magnet. The specimen holder is placed in a finger dewar which is connected to a vacuum pumping system. By adjusting the pumping speed using a manostat and a system of values, the temperature of the liquid helium bath surrounding the specimen holder may be adjusted. Temperatures down to 1.2 K are obtainable.

A schematic representation of the specimen holder is shown in Figure 8. On the top of the specimen holder is an aluminum electronic chassis which supports and electrically shields the voltage terminal and the recording thermometer connector. Also, on the top of the specimen holder is a terminal board which contains the helium bath level resistor terminals, the current terminals, the specimen block heater terminals, and the regulating thermometer connector for the temperature control circuit. On the top flange is a pumping port used to evacuate the vacuum can and a thermalcouple gauge used to monitor the vacuum can pressure.

The vacuum can is supported on the bottom of the specimen holder by a single 3/8-inch diameter stainless steel vacuum line. The voltage

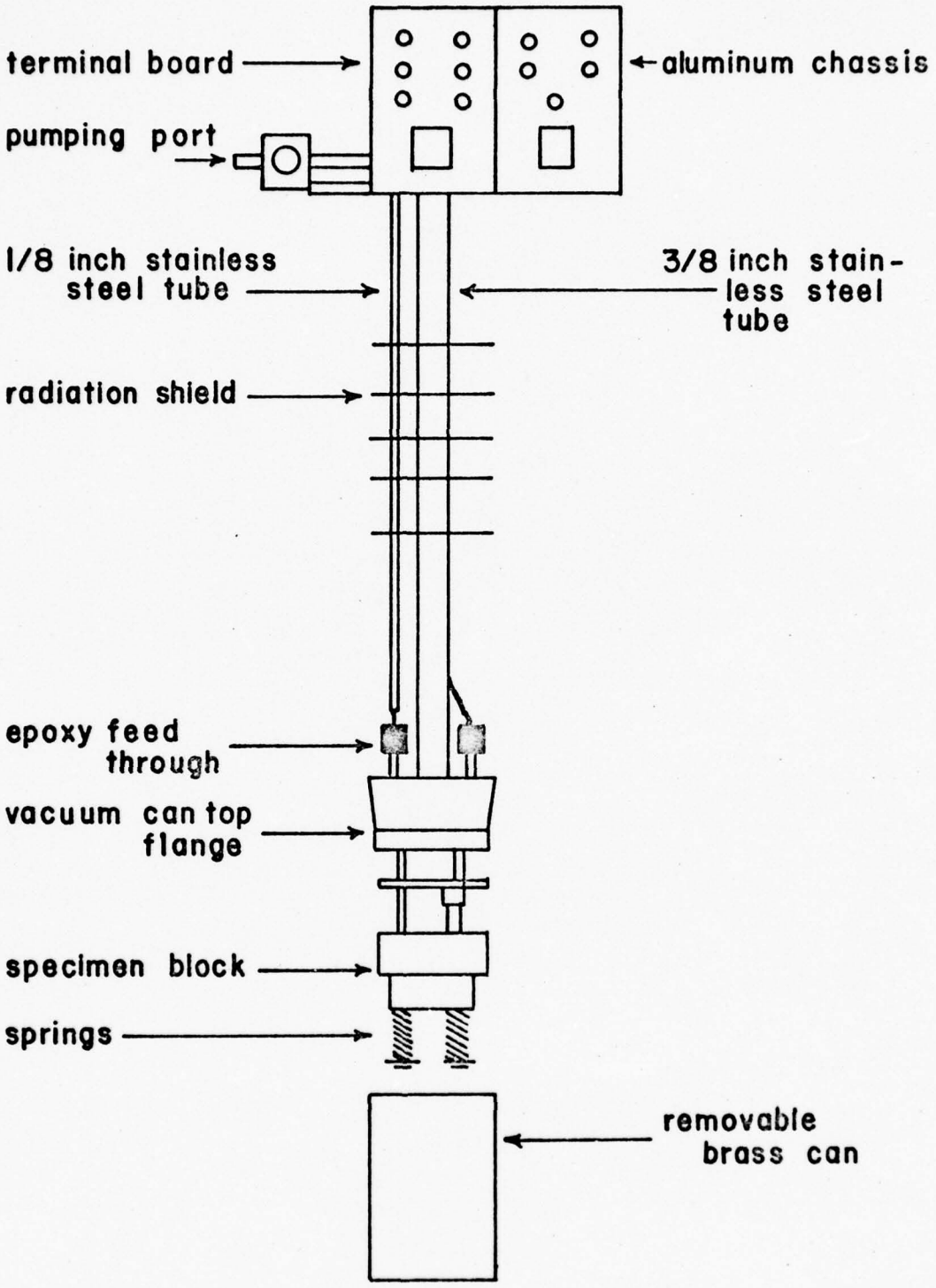


Figure 8. Schematic representation of the specimen holder.

leads and the recording thermometer leads are shielded by a 1/8-inch diameter stainless steel tube which extends down to the epoxy feed through. All the leads running to the vacuum can pass through the liquid helium bath. This insures that there is no appreciable heat leak down the leads to the specimen block. The leads pass through epoxy feed throughs into the vacuum can. Stycast epoxy #2850 with catalyst #9 is used to make the epoxy feed throughs. The feed throughs proved to be recyclable (68).

The vacuum can has a brass top flange with a four degree taper. A removable brass cylindrical can has a matching four degree taper. The vacuum seal is made with Dow Corning 200 fluid, viscosity 60,000 centistokes. After the vacuum seal is made, the specimen holder is connected to a vacuum pump and the vacuum can is evacuated at room temperature. This allows the cylindrical can and the top flange to press toegther and squeeze out the excess Dow Corning 200 fluid. The excess Dow Corning 200 fluid is wiped off the cylindrical can and the specimen holder is placed in a dewar. As the vacuum can is continuously pumped, liquid nitrogen is transferred into the dewar. Once the vacuum can comes to liquid nitrogen temperature, the vacuum can is sealed off and the vacuum pump is disconnected from the specimen holder. The vacuum can is then backfilled with helium gas to approximately atmospheric pressure. The helium gas acts as a transfer gas to help cool down the specimen block to liquid nitrogen temperature. Once the specimen block is at liquid nitrogen temperature, most of the helium gas is pumped out of the vacuum can. About 1000 microns of helium gas

is left in the vacuum can. The specimen holder is again removed from the vacuum pump and is placed in liquid helium. At liquid helium temperature, there will be approximately 150 microns of transfer gas in the vacuum can. The vacuum seal is leak tight to liquid helium II.

The specimen block, Figure 9, is constructed from copper. All the leads are epoxied to the specimen block to minimize direct heat exchange between the liquid helium bath and the superconducting specimen itself. The leads are thermally attached to the specimen block by wrapping half a meter of leads around the specimen block. The leads are then coated with epoxy to hold them in place. The specimen block contains the heater, which is a 40 Ω piece of Nicrome wire; the recording thermometer, which is a germanium resistance thermometer; the regulating thermometer, which is a 56 Ω carbon resistor; and fixed position spring loaded voltage probes. The superconducting current leads are fastened to the specimen via indium coated pressure clamps. Superconducting leads are used to carry the current to the specimen since currents up to 13.5 amperes must be provided and there must be no Joule heating. Any heat produced in the current leads would be transferred to the specimen and this would drastically affect the measured values of the parameters. The indium coated pressure clamps are recoated each time the specimen is changed. Because indium is very soft, the pressure clamps produce a large area of contact between the specimen and the current lead. This lowers the contact resistance. The specimen is electrically insulated from the copper blocks by teflon sheets 0.011 cm thick.

The specimen holder, as constructed, allows for the possibility of making ultrasonic attenuation measurements on the specimen. At first,

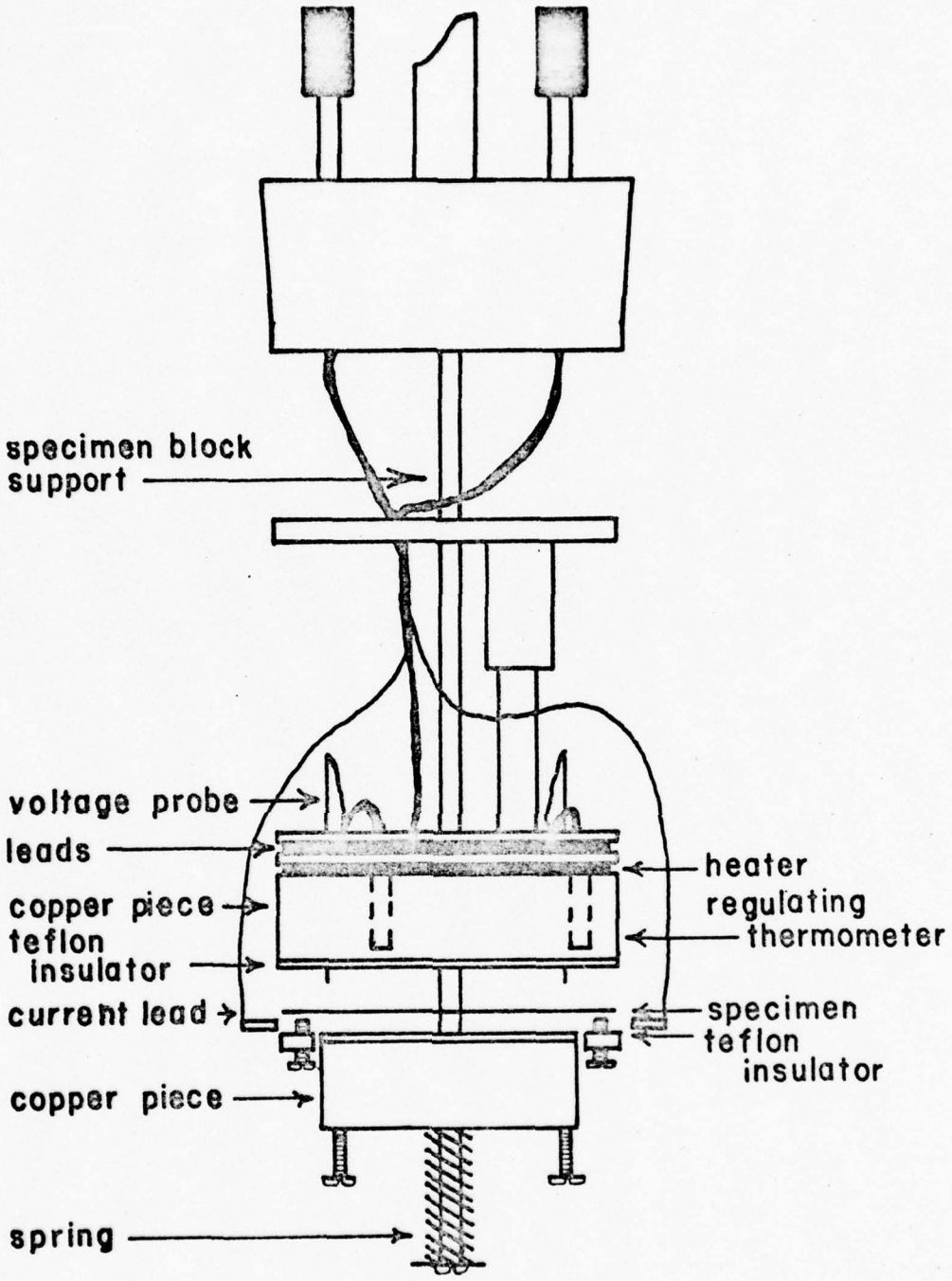


Figure 9. Diagram of the specimen block used to determine J_c and T_c.

it was hoped that ultrasonic attenuation measurements could be used as an independent means of determining H_{c2} and T_c of the specimens. However, all attempts to use ultrasonic attenuation measurements were unsuccessful.

C. Temperature Measurement

A Cryo Cal, Inc. #3759 germanium resistance thermometer is used as the recording thermometer. The recording thermometer has a resistance of 1 kΩ at 4.2 K. The thermometer is a four terminal device. A constant current of 1.1908 μA is driven through the thermometer and the voltage is measured. The voltage from the thermometer is amplified by a Hewlett-Packard model 740B Standard/Differential Voltmeter. The amplified voltage is observed on a four place Digitec model 275A millivoltmeter. The resistance of the thermometer is calculated from the voltage and the constant current. The temperature is obtained from a calibration plot of the recording thermometer's resistance as a function of temperature.

The recording thermometer was calibrated in a vacuum can against two standard thermometers. The first is a Lake Shore Cryotronic, Inc. #1676 germanium resistance thermometer. This thermometer is calibrated for temperatures from 0.8 K to 4.2 K. The second thermometer is a Cryo Cal, Inc. #2290 germanium resistance thermometer. This thermometer is calibrated for the temperature range 1.5 K to 100 K. The recording thermometer is calibrated for the temperature range from 1.2 K to 55 K.

D. Determination of the Transition Temperature

The transition temperature, T_c, is determined from a plot of the voltage along the specimen, V_L, against the voltage across the recording thermometer which is proportional to the temperature, see Figure 10. A four probe technique is used. A transport current, large enough to produce a 1 μV reading on the Keithley 148 Nanovoltmeter when the specimen is in the normal state, is passed through the specimen. The transition temperature is taken as the midpoint of the resistive transition from the superconducting state to the normal state (69), see Figure 11. The transition temperature of the specimen is an average value determined from three increasing temperature plots.

The thermal emfs in the recording thermometer are corrected for by reversing the direction of the current through the recording thermometer. The voltage difference between the forward and the reverse direction of the current through the recording thermometer is typically less than 0.12%.

E. Determination of the Critical Current Density

Figure 12 is a block diagram of the experimental apparatus used to measure the critical current, I_c. The specimen is maintained at a predetermined temperature by the temperature control circuit, see Appendix A. The transverse magnetic field is provided by the superconducting magnet, see Appendix B. An electronic integrator provides a sweep signal which drives the current control unit, see Figure 13. The current passes through a Leeds and Northrup model #4360 (0.1 ± 0.044)

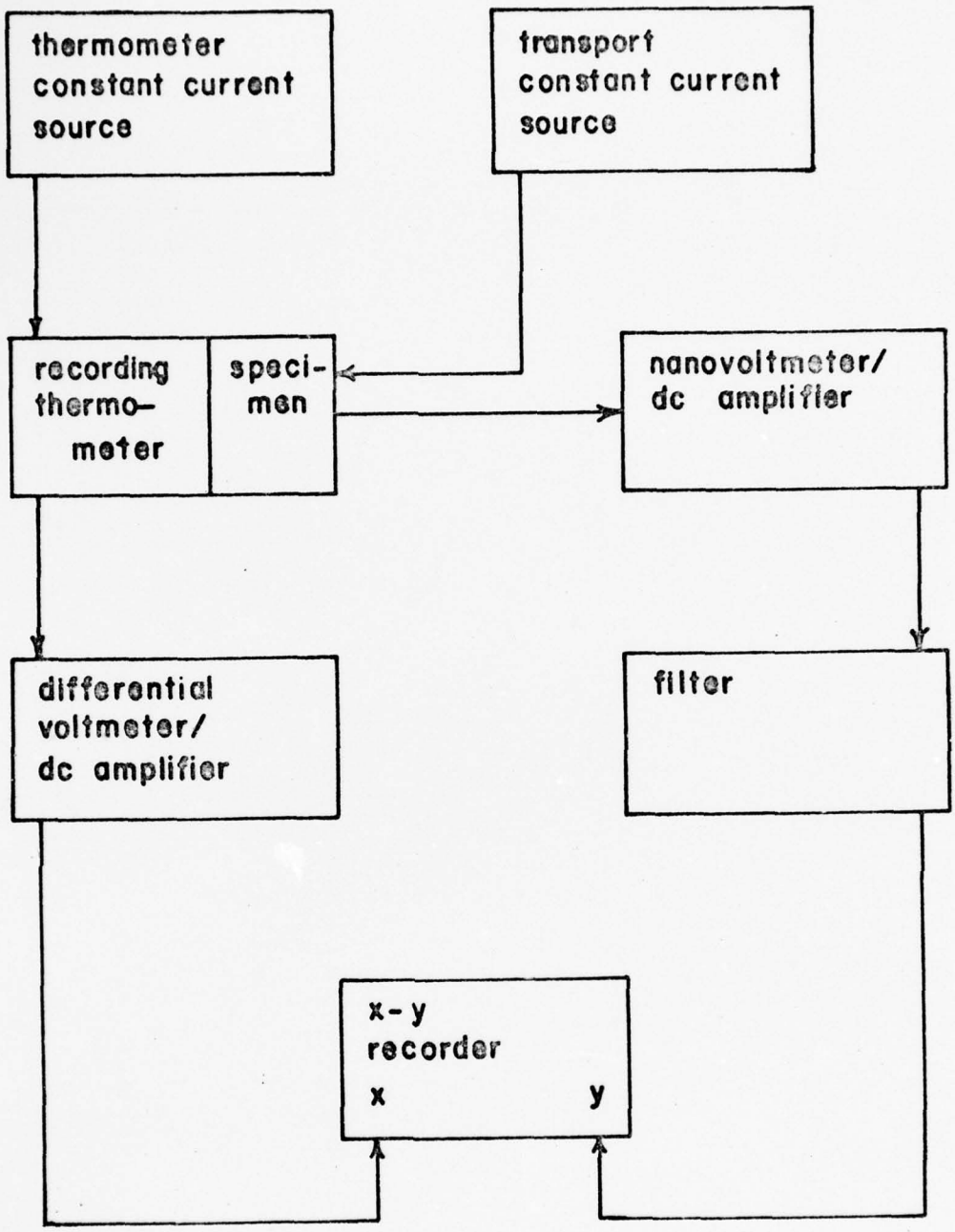


Figure 10. Block diagram for T_c determination.

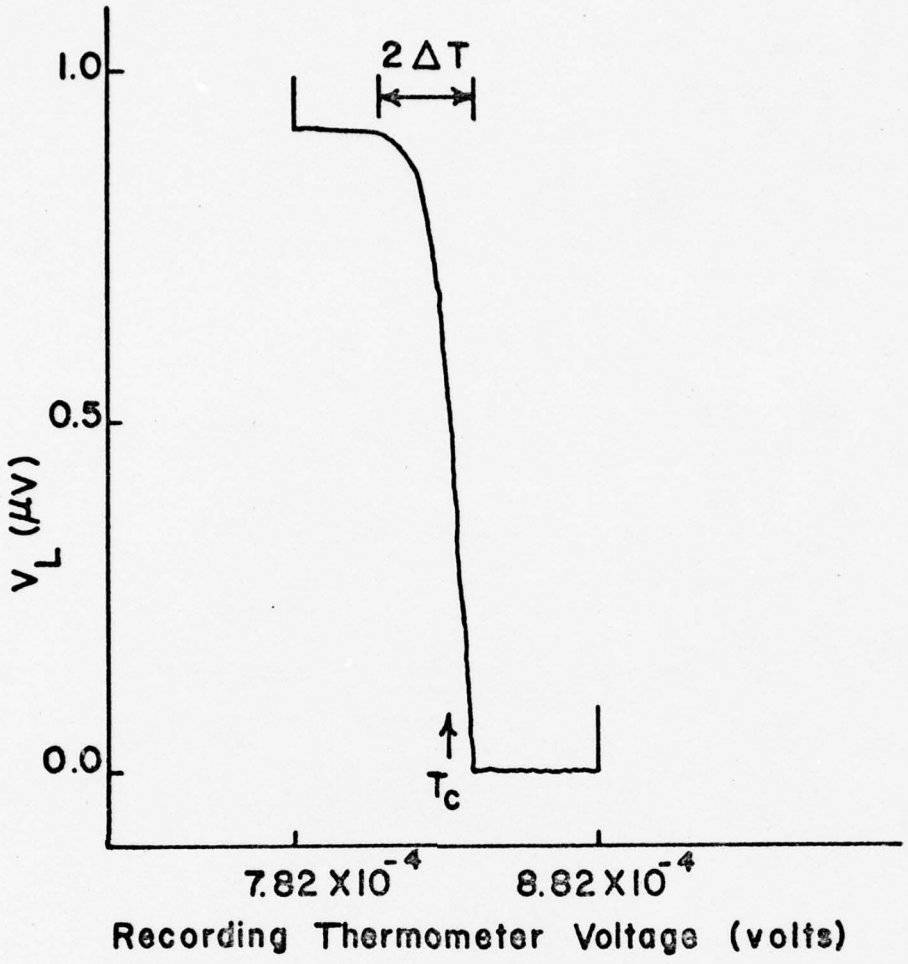


Figure 11. V_L as a function of the recording thermometer voltage for the 0.4 atomic percent carbon specimen, aged zero hours.

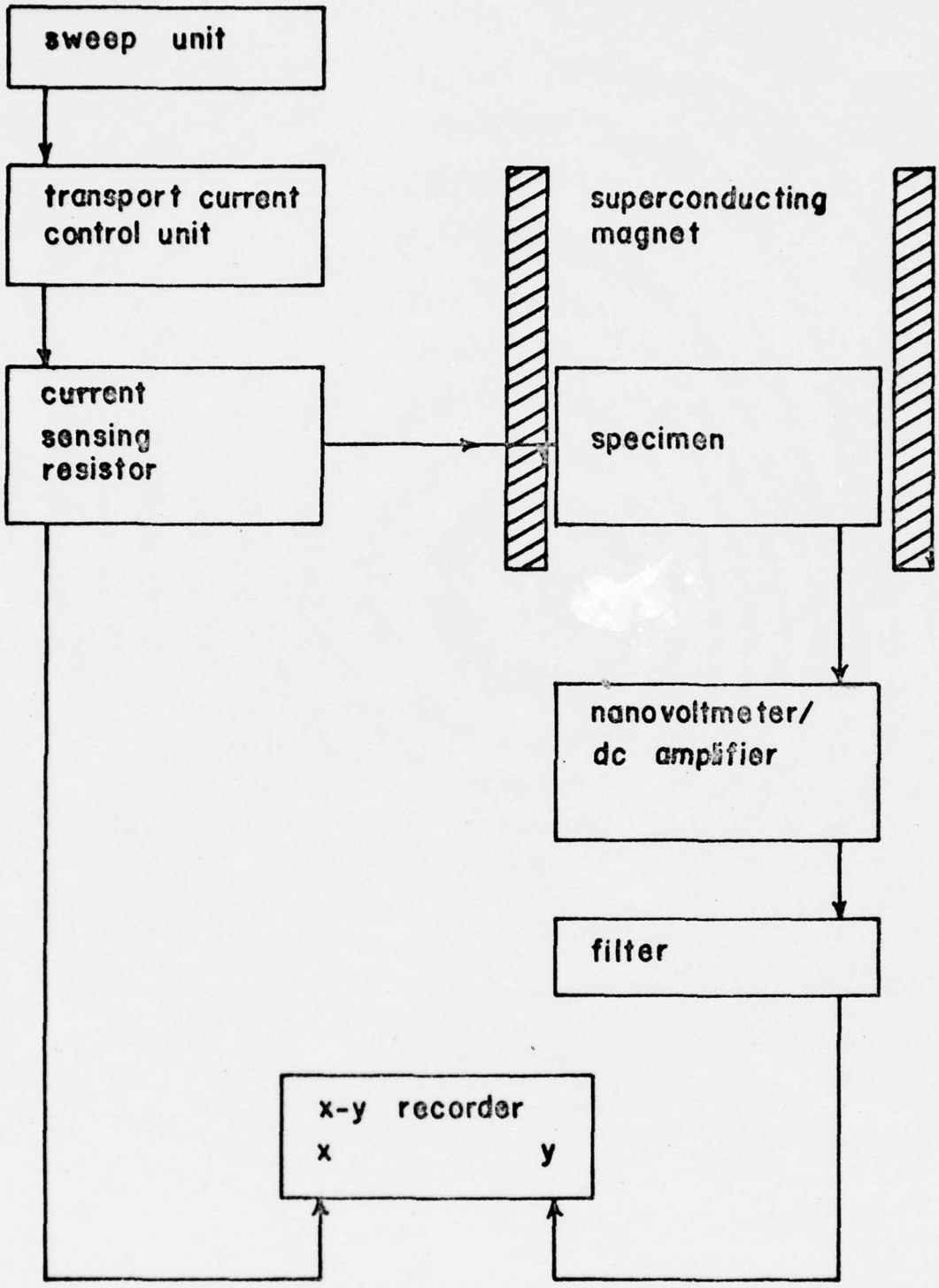


Figure 12. Block diagram of the equipment used to measure the critical current density.

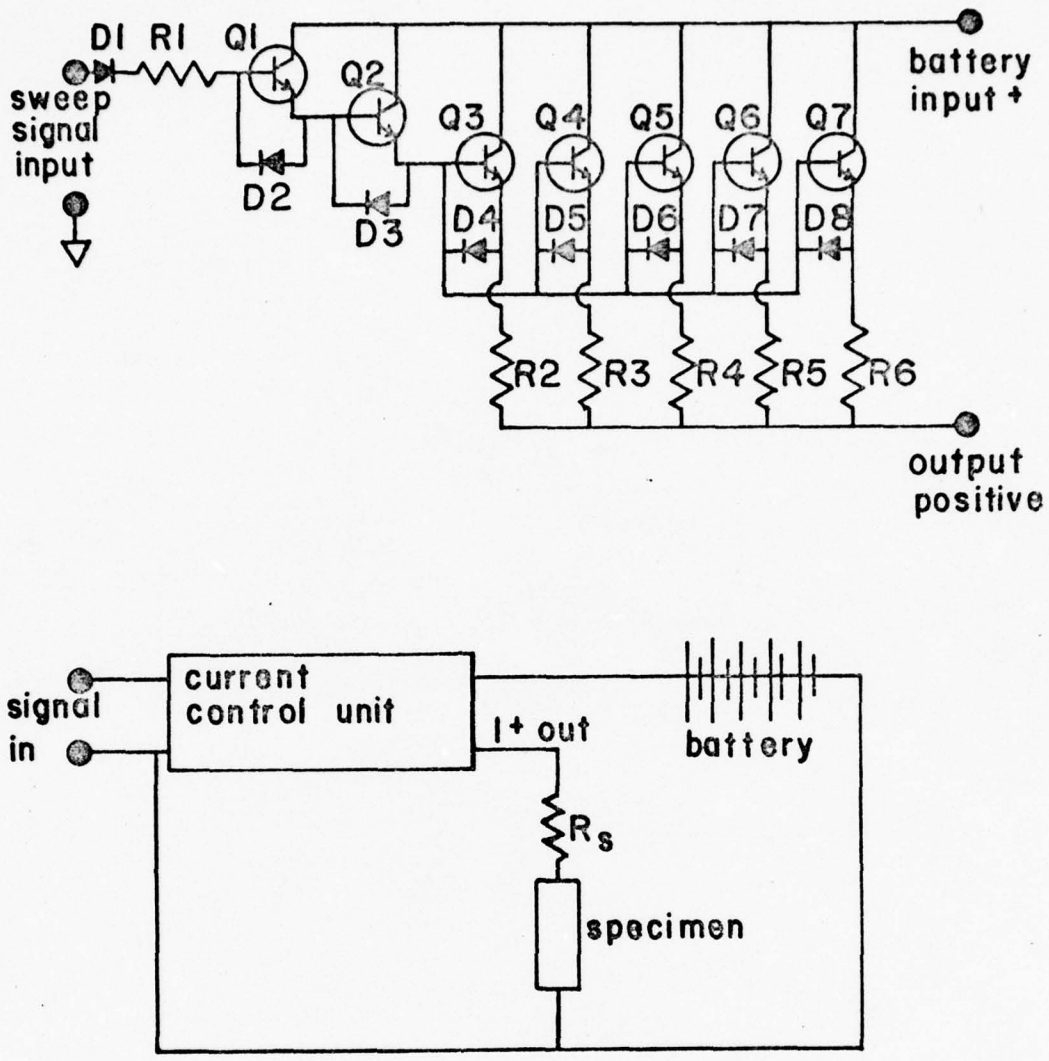


Figure 13. a) Current control unit. Q1-2N2270, Q2 to Q7-2N1487, D1-PTC2050, D2-1N3193, D3 to D8-1N4723, R1-1k Ω, and R2 to R6-0.1 Ω. b) Schematic diagram of the complete transport current sweep circuit.

Ω sense resistor in series with the specimen. The voltage across the sense resistor, which is proportional to the current, is plotted on the x-axis of a Moseley Autograf model 7001AM x-y recorder. The voltage along the specimen, V_L, is amplified and measured by a Keithley model 148 Nanovoltmeter. In earlier investigations, the signal from the nanovoltmeter was low pass filtered by a Krohn-Heite model 3342 filter in order to remove the 8 Hz signal produced by the chopper in the nanovoltmeter. The upper cut off frequency for the filter was 1 Hz. In later experiments, the Krohn-Heite filter was replaced by a passive RC filter designed to alleviate the 8 Hz problem. The amplifier signal from the nanovoltmeter is recorded on the y-axis of the x-y recorder.

An increasing current is driven through the specimen, which is in a fixed transverse magnetic field, as the longitudinal voltage is recorded across the specimen. The critical depinning current, I_c, is designated as that transport current at which the voltage across the length of the specimen, the cut off voltage, is deemed to be above the noise level on that portion of the curve where the voltage level is zero. This cut off voltage is always less than 50 nV. The critical current is obtained using a standard four probe technique. A plot of the longitudinal voltage, V_L, as a function of the voltage across the sense resistor, which is proportional to the current, is shown in Figure 14. The critical current density is calculated from the critical current by assuming the transport current is carried by the full cross-sectional area of the specimen (70,71,36,13,72); thus,

$$J_c = \frac{I_c}{\text{cross-sectional area}} \quad . \tag{3.1}$$

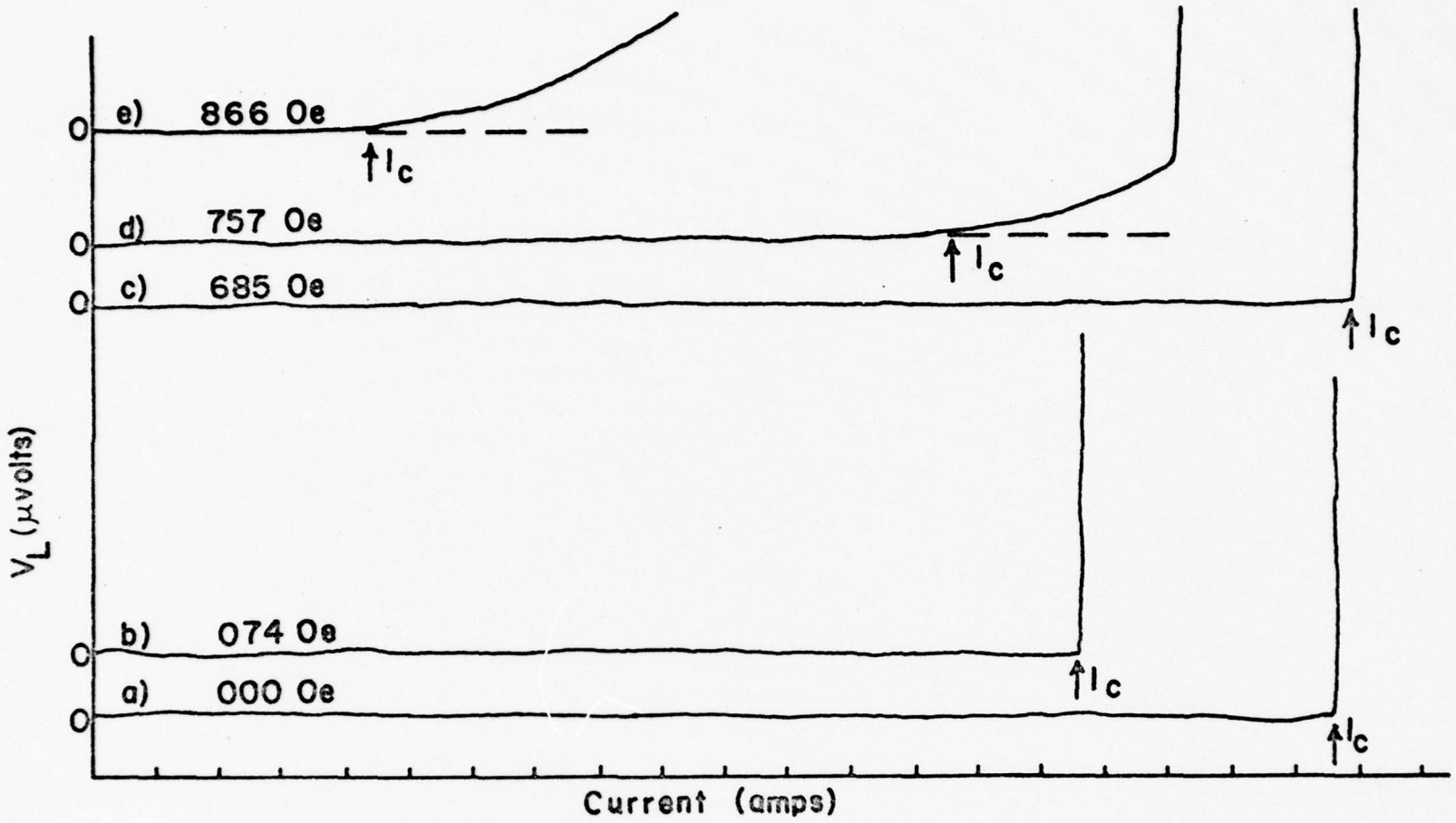


Figure 14. V_L-I for the 0.4 atomic percent carbon specimen, aged zero hours. The temperature at which the data is taken is 4.50 K. For curves a) and b) the current is 0.5 A/div; for c) and d) the current is 0.25 A/div; and for e) the current is 0.05 A/div.

Since each data point should be taken with the same initial conditions (73), the desired magnetic field is applied at zero transport current. The specimen is heated above its transition temperature and then cooled through T_c in the applied magnetic field. This procedure produces an unstrained fluxoid lattice (74). Once the temperature of the specimen returns to the predetermined temperature, the current is swept and the longitudinal voltage measured across the specimen. The process is repeated at new applied magnetic field values until the upper critical magnetic field, H_{c2}, is reached.

F. Determination of the Upper Critical Magnetic Field

The upper critical magnetic field, H_{c2}, is an important parameter. At the outset of this investigation ultrasonic attenuation techniques were tried in order to determine H_{c2}. The advantage of using ultrasonic attenuation techniques is that the upper critical magnetic field would be independent of any transport current phenomena. However, attempts to this end were unsuccessful because reliable acoustic bonds were never achieved. Other common possibilities for determining H_{c2} have not been completely satisfactory. The method of extrapolating $J_c^{\frac{1}{2}}$ versus H, as Montgomery and Sampson (75) did for Nb-Sn specimens, leads to H_{c2} values which are much too high. Also, the method of using the normalized resistance versus H to determine H_{c2} has led to inconsistent values of H_{c2}. The difficulty is two-fold; the flux flow region makes the transition at H_{c2} difficult to observe and, second, the surface superconductivity survives up to H_{c3} (76), thus making a long tail on

the J_c versus H plots. H_{c3} is a critical magnetic field above which even the surface superconductivity is destroyed.

The method of finding H_{c2} which was finally used is as follows: The upper critical magnetic field is determined from a plot of the normalized pinning force density, F_p/F_{pmax}, as a function of the applied magnetic field, see Figure 15. H_{c2} is the value of the magnetic field at which the rapid decrease in F_p/F_{pmax} extrapolates to zero. F_{pmax} is the maximum value of F_p for a given temperature.

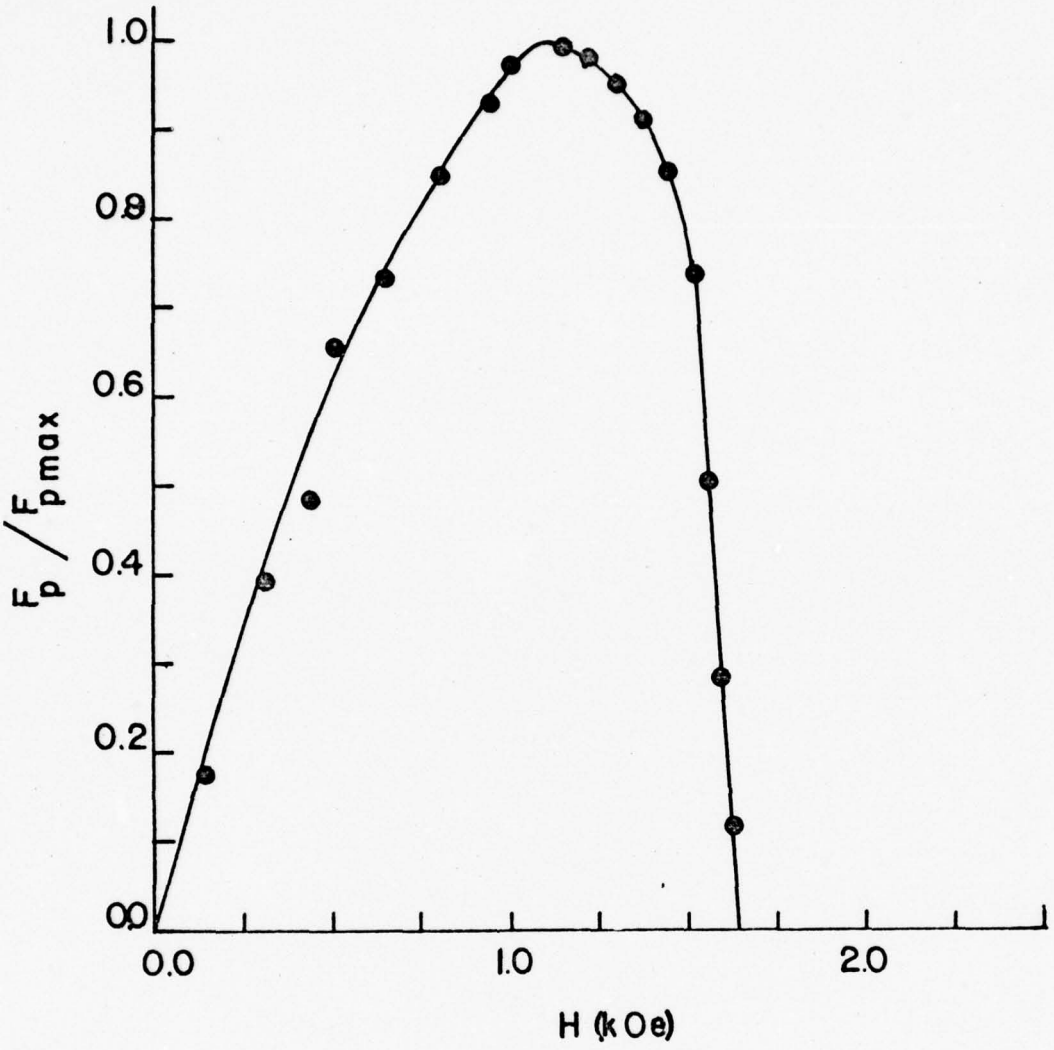


Figure 15. Normalized pinning force vs. applied magnetic field for the 0.4 atomic percent carbon specimen, aged zero hours. The temperature is 4.00 K.

IV. EXPERIMENTAL RESULTS

A. Introduction

Because of the large number of specimens investigated during the course of this investigation, the experimental results will be presented in tabular form with accompanying graphs being representative of the data. The first two sections of this chapter deal with important superconducting parameters. The final section is a presentation of the macroscopic pinning force data and its relation to the metallurgical parameters of the specimen microstructures.

B. Important Superconducting Parameters

One of the most important parameters is $H_{c2}(T)$ since this quantity is used to scale the magnetic fields. The upper critical magnetic field is extrapolated to zero temperature using a least-mean-squares fit to the equation

$$H_{c2}(t) = \frac{H_{c2}(0)(1 - t^2)}{(1 + \eta t^2)} \tag{4.1}$$

as given by Waynert et al. (77). $H_{c2}(0)$ and η are the free parameters which are fit to the data. Figure 16 is a plot of the upper critical magnetic field as a function of reduced temperature, $t = T/T_c$. The precision in determining the upper critical magnetic field, $H_{c2}(0)$, is about five percent.

The Ginzburg-Landau parameter, κ, is defined experimentally as $\kappa = \kappa_1(T = T_c)$, where $\kappa_1(t)$ is given by

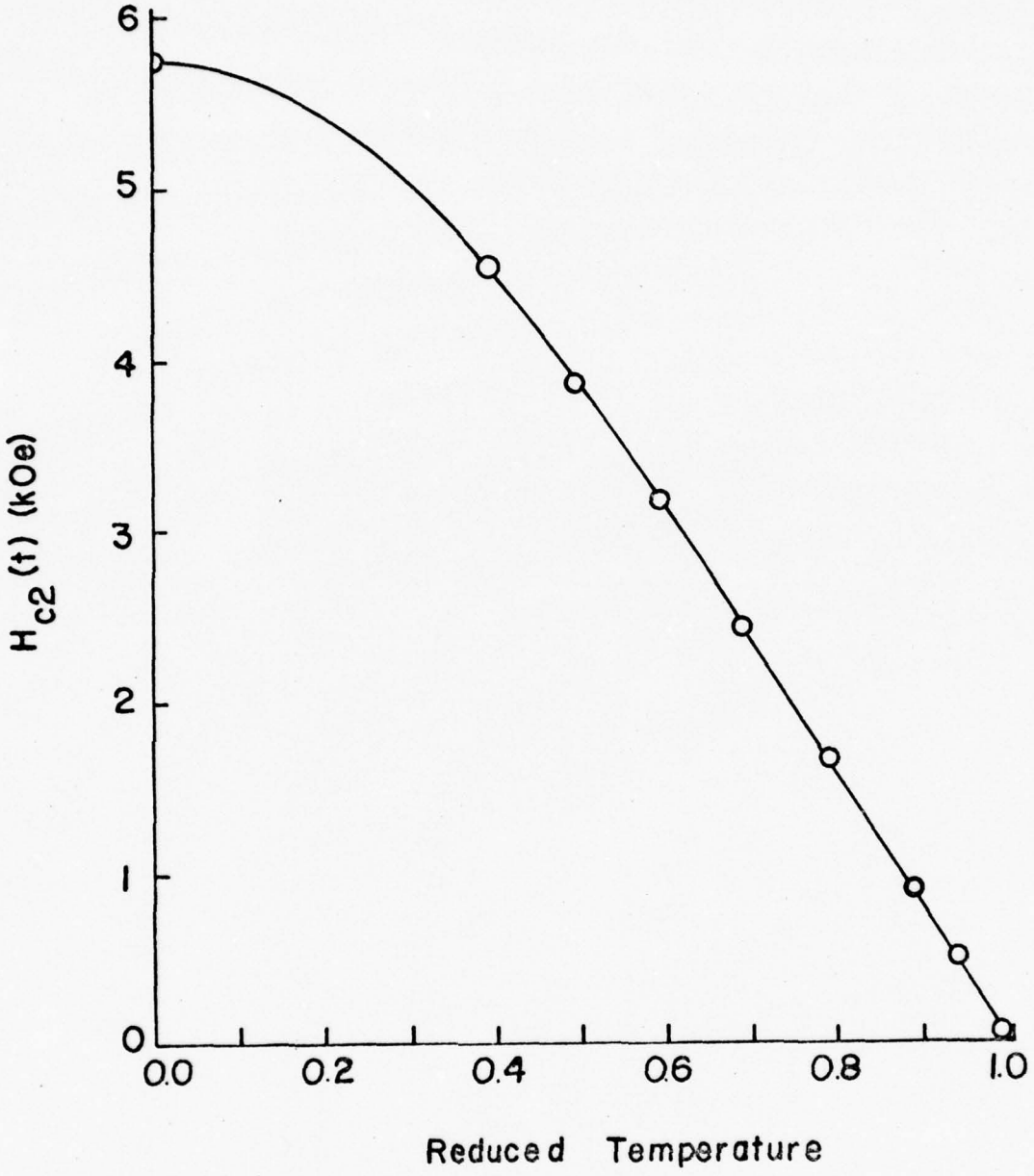


Figure 16. The upper critical magnetic field as a function of reduced temperature for the 0.4 atomic percent carbon specimen, aged zero hours. The curve is given by equation (4-1) with $H_{c2}(0) = 5.8$ kOe and $\eta = 0.527$.

$$\kappa_1(t) = \frac{H_{c2}(t)}{\sqrt{2}\, H_c(t)} \quad . \tag{4.2}$$

Since, both $H_{c2}(t)$ and $H_c(t)$ are zero at $T = T_c$ a limiting process must be used as T_c is approached (78)

$$\kappa = \kappa_1(t = 1) = \lim_{T \to T_c} \frac{1}{\sqrt{2}} \left(\frac{dH_{c2}}{dT}\right)_{T_c} \Bigg/ \left(\frac{dH_c}{dT}\right)_{T_c} \quad . \tag{4.3}$$

Now, using Equation (4.1) and assuming the normal temperature dependence of the thermodynamic critical magnetic field, H_c, Equation (2.1), Equation (4.3) becomes

$$\kappa_1(T_c) = \kappa = \frac{H_{c2}(0)}{\sqrt{2}\, H_c(0)(1 + \eta)} \quad . \tag{4.4}$$

The thermodynamic critical magnetic field is given by

$$H_c(0) = \frac{H_{c2}(0)}{\sqrt{2}\,(1 + \eta)} \quad . \tag{4.5}$$

According to Goodman (79), κ may be expressed as

$$\kappa = \kappa_0 + \kappa_\ell \quad , \tag{4.6}$$

where κ_ℓ depends on the electronic mean free path. In terms of measurable quantities,

$$\kappa_\ell = 7.5 \times 10^3\, \gamma^{\frac{1}{2}}\, \rho_0 \quad , \tag{4.7}$$

where γ, the electronic specific heat coefficient, is 1.179×10^{4} erg cm^{-3} deg^{-2} according to Radebaugh and Keesom (80), and ρ_0 is the normal state residual resistivity in Ω-cm. The residual resistivity is given by

$$\rho_0 \sim \rho_{5.45} \quad , \tag{4.8}$$

since the resistance ratios of the specimens involved in this study are low. $\rho_{5.45}$ is determined from

$$\rho_{5.45} = \rho_r^{-1} \rho_{295}$$

ρ_{295} is the mean value of the room temperature resistivity of all the specimens used in this investigation. The mean value of the resistivity is used since there is a large uncertainty in the determination of the cross-sectional area of any particular specimen. The mean value of ρ_{295} is 2.19×10^{-5} Ω-cm with a standard deviation of 0.27×10^{-5} Ω-cm. This value of the resistivity is in the range of values quoted in the literature (81,82). The resistance ratio ρ_r, is defined by

$$\rho_r = R_{295}/R_{5.45} \quad , \tag{4.9}$$

where R_{295} is the room temperature resistance of the specimen and $R_{5.45}$ is the resistance of the specimen at 5.45 K. The temperature 5.45 K is a little larger than the intrinsic transition temperature of vanadium, thus making the resistance measurements at this temperature, instead of at 4.2 K, alleviates using an applied magnetic field to drive the specimen normal. Any magnetic field effects are thereby eliminated.

κ_0 depends only on the electronic structure of the metal independently of electronic scattering, and is given by (78)

$$\kappa_0 = 0.96\ \lambda_L(0)/\xi_0 \quad . \tag{4.10}$$

$\lambda_L(0)$ is the London penetration depth given by (78)

$$\lambda_L(0) = \frac{(3h\ \gamma^{\frac{1}{2}}\ \pi^{\frac{1}{2}}c)}{(ek_B S)} \quad . \tag{4.11}$$

Here, S is the area of the Fermi surface in k-space excluding zone boundaries, h is Plank's constant, k_B is Boltzmann's constant, γ is the electronic specific heat coefficient in ergs cm^{-3} deg^{-2}. Using the values Radebaugh and Keesom (78) give for the different parameters, one obtains

$$\lambda_L(0) = 398\ \text{Å} \quad . \tag{4.12}$$

Now ξ_0 is the BCS or Pippard coherence length which is given by (78)

$$\xi_0 = \frac{(0.18\ k_B S)}{12\ T_{c0}\ \gamma} \quad , \tag{4.13}$$

where T_{c0} is the intrinsic transition temperature. Once again using values of the parameters given by Radebaugh and Keesom (78) and $T_{c0} = 5.40$ K, one obtains

$$\xi_0 = 445\ \text{Å} \quad . \tag{4.14}$$

Returning to Equation (4.10) and using Equations (4.12) and (4.14), one obtains

$$\kappa_0 = 0.859 \quad . \tag{4.15}$$

The values of $H_{c2}(0)$, η, κ, and ρ_0 are listed in Table I for all the specimens used in this investigation.

The temperature dependence of the parameter $\kappa_1(t)$ is given by

$$\kappa_1(t) = \kappa_1(0)\ [1 + \eta t^2]^{-1} \quad , \tag{4.16}$$

where

$$\kappa_1(0) = \frac{H_{c2}(0)}{\sqrt{2}\ H_c(0)} \quad .$$

The temperature dependent coherence length, $\xi(T)$ of Equation (2.23), in terms of experimentally determined parameters, is given by

$$\xi(T) = \sqrt{\frac{\phi_0}{2\pi\ H_{c2}(T)}} \quad . \tag{4.17}$$

Once $\kappa_1(T)$ and $\xi(T)$ are known, one can calculate the penetration depth $\lambda(T)$ from Equation (2.26). Solving Equation (2.26) for $\lambda(T)$, one obtains

$$\lambda(T) = \kappa_1(T)\ \ \xi(T) \quad . \tag{4.18}$$

There remains only two other parameters of interest; one is the Pippard coherence length in the presence of electronic scattering which is given by Equation (2.18),

$$\frac{1}{\xi} = \frac{1}{\xi_0} + \frac{1}{\ell} \quad .$$

Table I. Important superconducting parameters.

Specimen Number	Aging Time Hours	$H_{c2}(0)$ kOe	η	$H_c(0)$ kOe	κ	$\kappa_1(0)$	ρ_0 $\times 10^{-6}$ Ω-cm
			pure V				
66	0	4.2	0.460	1.3	1.56	2.28	0.861
			0.1 atomic percent carbon				
97	0	4.7	0.483	1.2	1.90	2.77	1.28
98	1	4.6	0.503	1.2	1.83	2.71	1.19
100	5	4.6	0.480	1.2	1.75	2.71	1.09
103	10	4.6	0.499	1.2	1.75	2.71	1.10
			0.2 atomic percent carbon				
107	0	4.7	0.384	1.3	1.80	2.56	1.15
105	2	4.2	0.407	1.2	1.70	2.47	1.03
108	5	4.1	0.451	1.2	1.65	2.42	0.970
113	10	4.5	0.409	1.2	1.84	2.65	1.20
			0.3 atomic percent carbon				
57	0	5.0	0.564	1.1	2.04	3.21	1.45
94	1/4	5.1	0.698	1.1	1.94	3.28	1.33
43	1/2	4.9	0.543	1.1	2.05	3.15	1.46
92	3/4	5.0	0.504	1.1	2.05	3.21	1.46
45	1	5.2	0.548	1.1	2.07	3.34	1.49
46	2	4.8	0.461	1.2	1.97	3.08	1.36
64	5	4.3	0.508	1.1	1.84	2.76	1.20
			0.4 atomic percent carbon				
115	0	5.8	0.527	1.2	2.24	3.42	1.70
125	1/4	4.6	0.608	1.1	1.82	2.96	1.18
124	1/2	4.5	0.536	1.1	1.81	2.89	1.17
123	3/4	5.2	0.660	1.1	2.01	3.34	1.41
135	1	4.8	0.510	1.2	1.91	2.83	1.29
118	2	5.0	0.569	1.2	1.92	2.95	1.30
			0.5 atomic percent carbon				
116	0	5.6	0.543	1.2	2.19	3.30	1.63
131	1/4	4.9	0.485	1.2	2.00	2.89	1.40
127	1/2	5.1	0.527	1.2	1.98	3.00	1.37
134	3/4	4.8	0.444	1.2	1.97	3.08	1.36
129	1	5.3	0.439	1.2	2.23	3.12	1.68
119	2	5.0	0.759	1.2	1.64	2.95	0.966
			0.6 atomic percent carbon				
117	0	5.2	0.642	1.2	1.92	3.06	1.30
120	2	4.7	0.576	1.2	1.79	2.77	1.14

The other quantity of interest is the electronic mean free path, ℓ. The electronic mean free path is given as (78)

$$\ell = \frac{6\pi^2}{he^2 \rho_0 S} \quad .$$

Using parameters given by Radebaugh and Keesom (78) this reduces to

$$\ell = \frac{3.50 \times 10^{-4} \text{ Å}}{\rho_0} \quad . \tag{4.19}$$

The values of ℓ, ξ, $\xi(0)$, and $\lambda(0)$ are listed in Table II. The values of $\kappa_1(0)$ are listed in Table I.

C. Transition Temperature

A measure of the purity of a specimen is given by ρ_r. The intrinsic transition temperature, which is the transition temperature for infinite electronic mean free path, is determined from a least-mean-squares fit to the equation (78)

$$T_c(\rho_r) = q\rho_r^{-1} - T_{c0} \quad , \tag{4.20}$$

where T_{c0} is the intrinsic transition temperature and q is equal to -3.77 K. A plot of T_c versus ρ_r^{-1} extrapolated to zero yields a value of (5.40 ± 0.04) K for the intrinsic transition temperature of the specimens used in this investigation, see Figure 17. The decrease of T_c with impurity concentration arises because of the scattering of the electrons. In Table III are listed the values of ρ_r, $R_{5.45}$, and T_c for the specimens used in this investigation.

Table II. More superconducting parameters.

Specimen Number	ℓ Å	ξ Å	$\xi(0)$ Å	$\lambda(0)$ Å
		pure V		
66	406	213	275	627
		0.1 atomic percent carbon		
97	273	170	260	720
98	294	177	263	713
100	321	187	263	713
103	318	186	263	713
		0.2 atomic percent carbon		
107	304	181	260	666
105	340	193	275	679
108	361	200	279	675
113	292	176	266	705
		0.3 atomic percent carbon		
57	241	157	252	809
94	263	166	250	820
43	240	156	255	803
92	240	156	252	809
45	235	154	247	825
46	257	163	258	795
64	292	176	272	751
		0.4 atomic percent carbon		
115	206	141	234	800
125	297	178	263	778
124	299	179	266	769
123	248	160	247	825
135	271	169	258	780
118	269	168	252	743
		0.5 atomic percent carbon		
116	215	145	238	785
131	250	160	255	737
127	255	163	250	750
134	257	163	258	795
129	208	142	245	764
119	362	200	252	743
		0.6 atomic percent carbon		
117	269	168	247	756
120	307	182	260	720

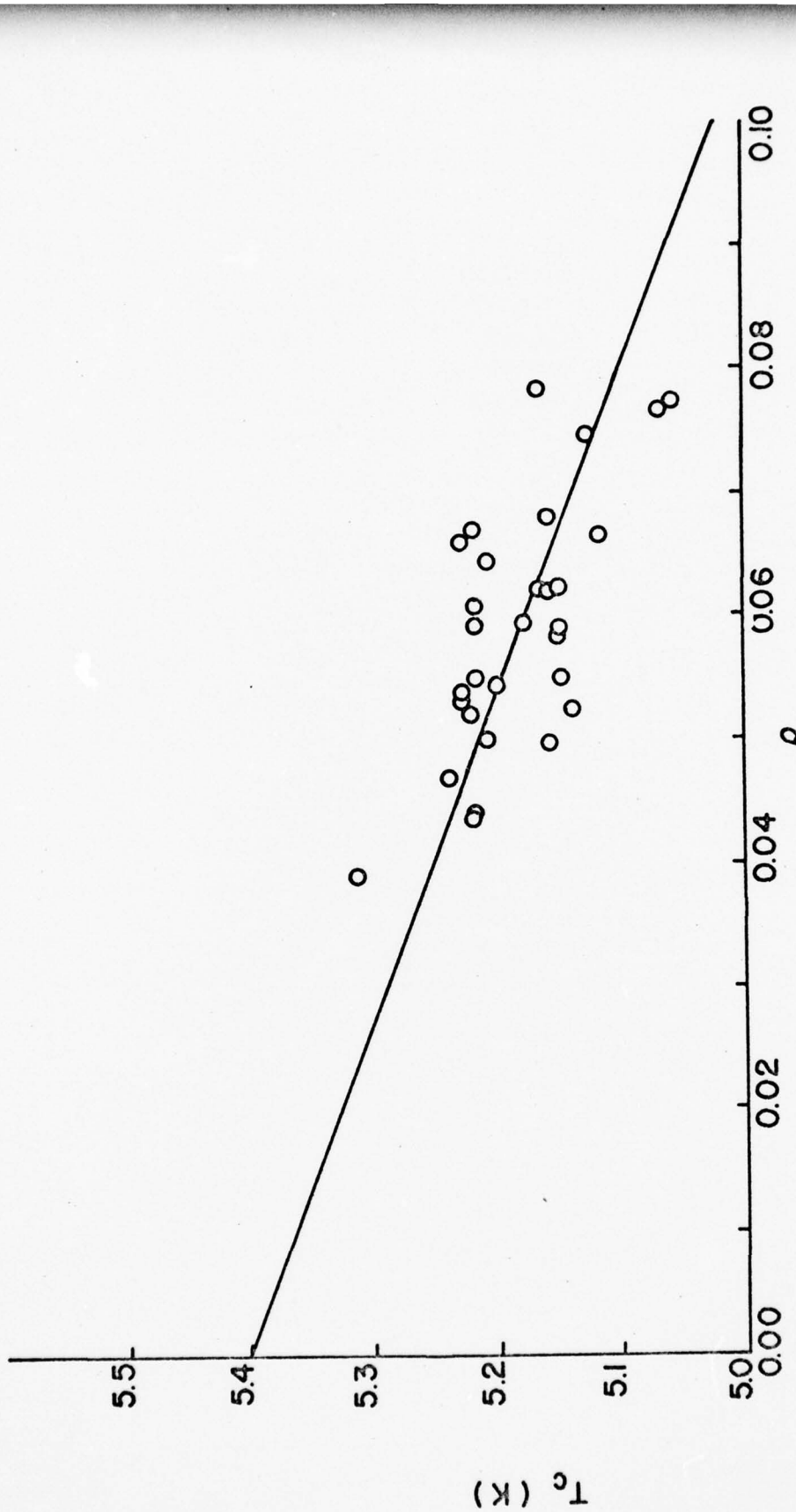


Figure 17. Transition temperature as a function of ρ_r^{-1}.

Table III. Important specimen parameters.

Specimen Number	ρ_r	$R_{5.45}$	T_c	ΔT_c
		mΩ	K	K
		pure V		
66	25.43	0.460	5.28	0.08
		0.1 atomic percent carbon		
97	17.12	0.563	5.15	0.06
98	18.40	0.580	5.20	0.05
100	20.08	0.433	5.16	0.07
103	20.00	0.500	5.21	0.06
		0.2 atomic percent carbon		
107	19.04	0.608	5.14	0.06
105	21.27	0.487	5.24	0.07
108	22.57	0.443	5.22	0.06
113	18.20	0.632	5.20	0.06
		0.3 atomic percent carbon		
57	15.13	0.469	5.23	0.10
94	16.43	0.560	5.22	0.09
43	14.99	0.907	5.22	0.06
92	15.05	0.567	5.12	0.07
45	14.65	0.760	5.16	0.05
46	16.06	0.747	5.17	0.08
64	18.18	1.113	5.22	0.06
		0.4 atomic percent carbon		
115	12.92	2.194	5.06	0.06
125	18.56	0.688	5.23	0.06
124	18.73	0.736	5.23	0.04
123	15.48	0.615	5.21	0.08
135	16.99	0.788	5.15	0.05
118	16.88	0.756	5.18	0.07
		0.5 atomic percent carbon		
116	13.43	0.896	5.13	0.07
131	15.69	0.614	5.17	0.07
127	16.03	0.954	5.15	0.07
134	16.11	0.788	5.16	0.06
129	13.05	1.046	5.07	0.05
119	22.68	0.594	5.22	0.06
		0.6 atomic percent carbon		
117	16.91	0.754	5.22	0.06
120	19.26	0.708	5.22	0.04

The half width, ΔT_c of the resistive transition used to calculate the transition temperature is related to the uniformity of composition of the superconductor. If the superconductor is of uniform composition, the transition half width is narrow; for example, see Figure 11. Specimens which were contaminated and of non-uniform composition showed very broad transition half widths. A few specimens had half widths of 1 K to 2 K. The half width becomes a useful parameter in deciding which specimens are of uniform composition and should be studied further and which specimens should be discarded. Specimens with ΔT_c values in excess of 0.1 K were not used in the present study.

D. Fluxoid Pinning

The pure, annealed vanadium specimen shows very low values of the macroscopic pinning force density, F_p, as can be seen in Figure 18. The vanadium carbide precipitates act as pinning centers for the fluxoids. This pinning of the fluxoids leads to greatly enhanced values of F_p which can be seen in Figure 18. The effectiveness of the pinning centers in pinning the fluxoids is reflected quite clearly in the ability of the superconductor to carry transport currents in a lossless manner. Very weak pinning of the fluxoids, as represented by the pure, annealed specimen, leads to strong magnetic field dependence of the critical current density, J_c, as can be seen in Figure 19. In the case of the 0.3 atomic percent carbon specimen, aged one hour, the pinning centers are much more effective. The critical current density is relatively magnetic field independent, except close to H_{c2}, as can be seen in Figure 20. Figure 21 shows the critical current density as

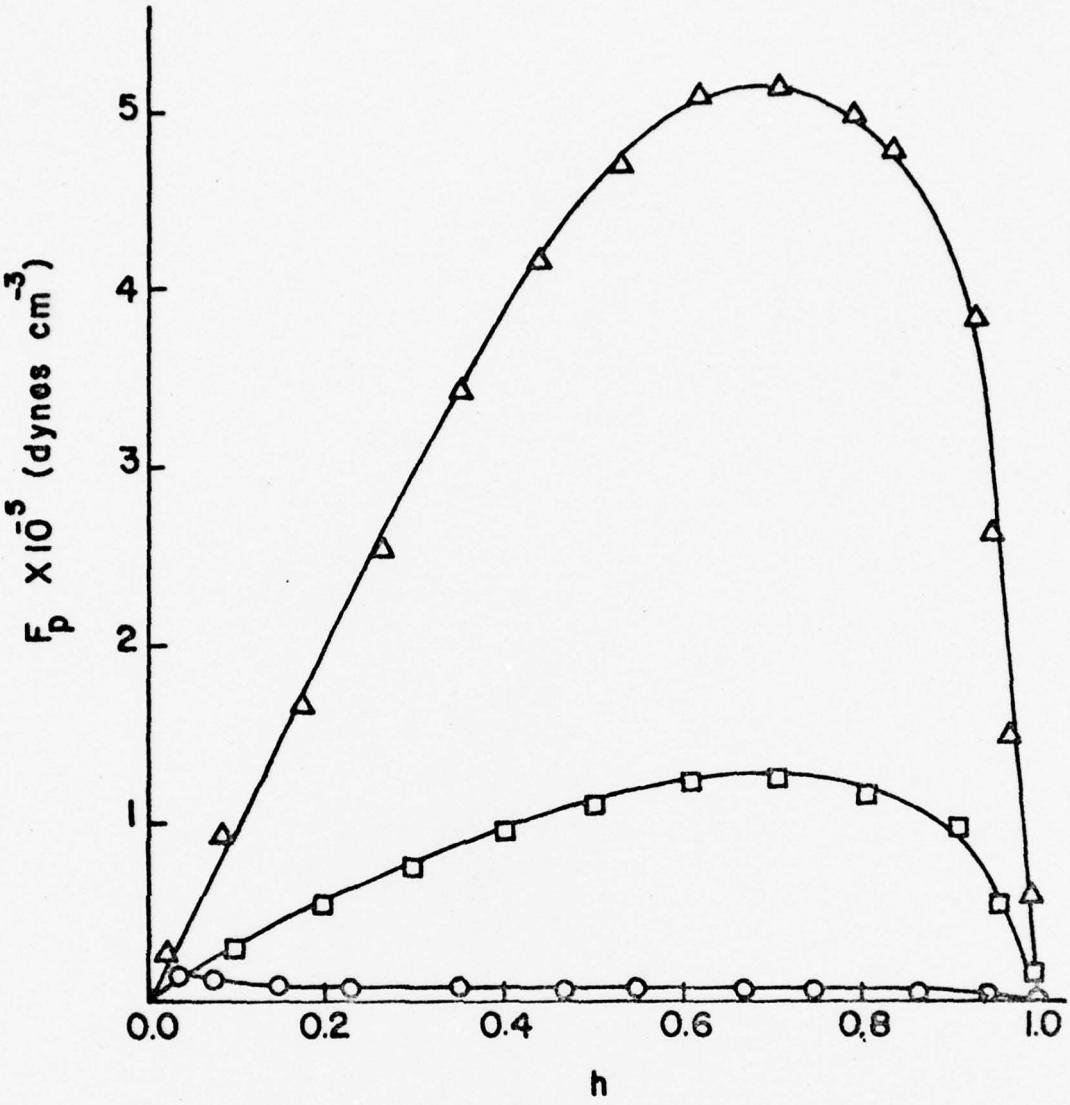


Figure 18. Macroscopic pinning force density as a function of reduced magnetic field. O - pure, annealed specimen, □ - the 0.3 atomic percent carbon specimen, aged one hour, and △ - the 0.4 atomic percent carbon specimen, aged zero hours. All data are for 4.00 K.

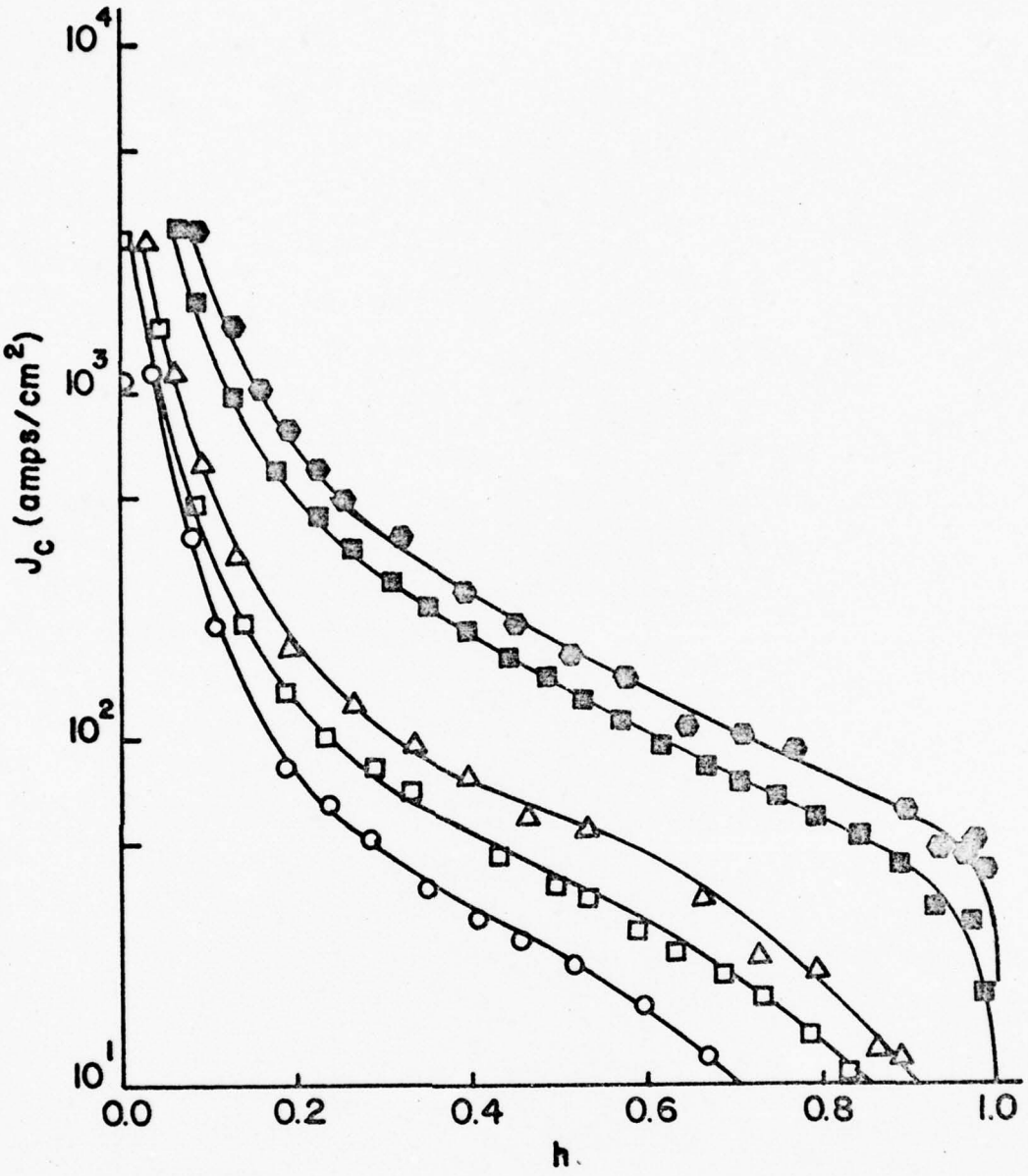


Figure 19. J_c vs. h for a pure, annealed specimen. ○ - 5.00 K, □ - 4.75 K, △ - 4.50 K, ▣ - 3.00 K, and ⬢ - 2.00 K.

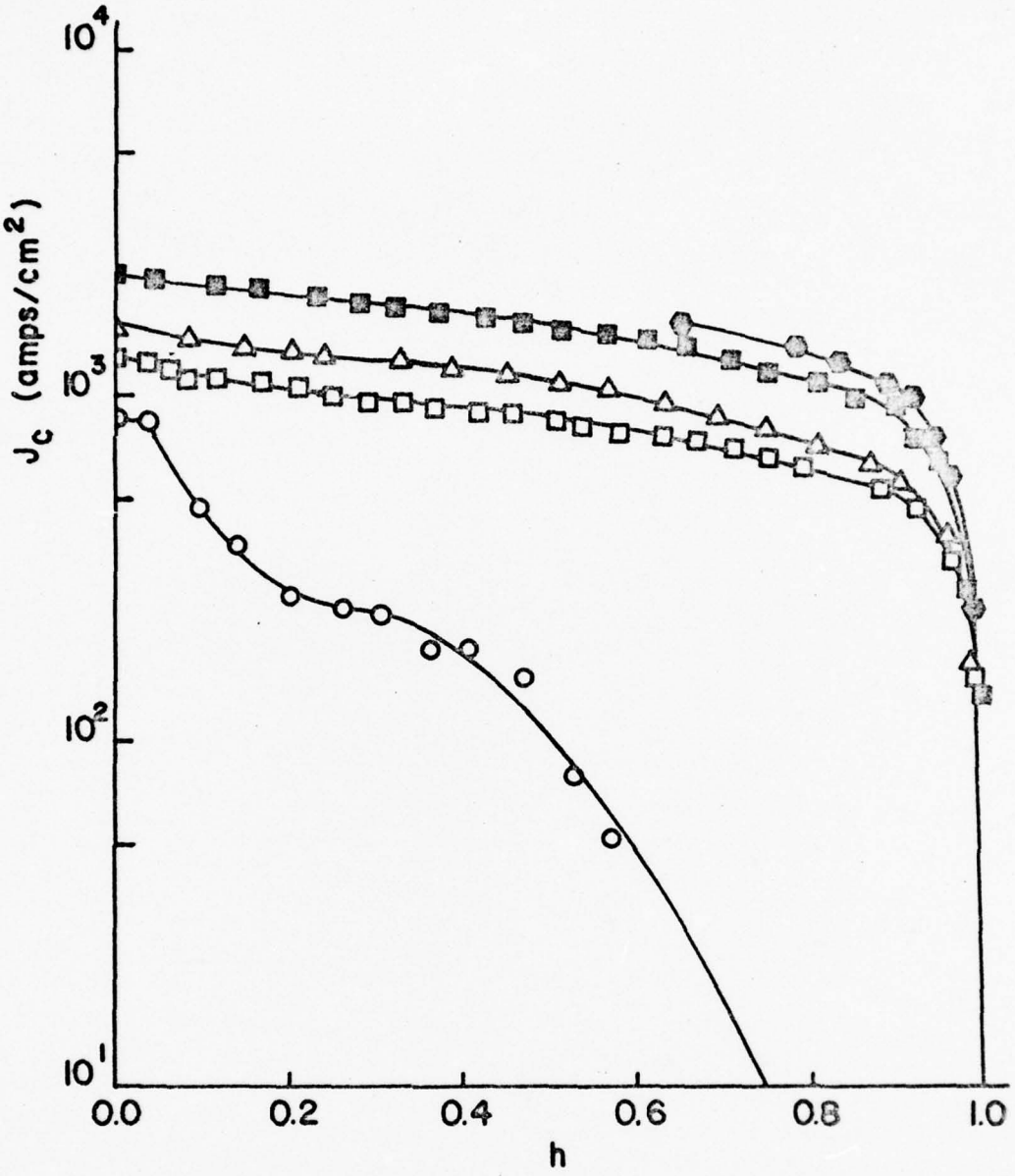


Figure 20. J_c vs. h for the 0.3 atomic percent carbon specimen, aged one hour. ○ - 5.00 K, □ - 4.75 K, △ - 4.50 K, ▣ - 3.50 K, and ⬢ - 2.00 K.

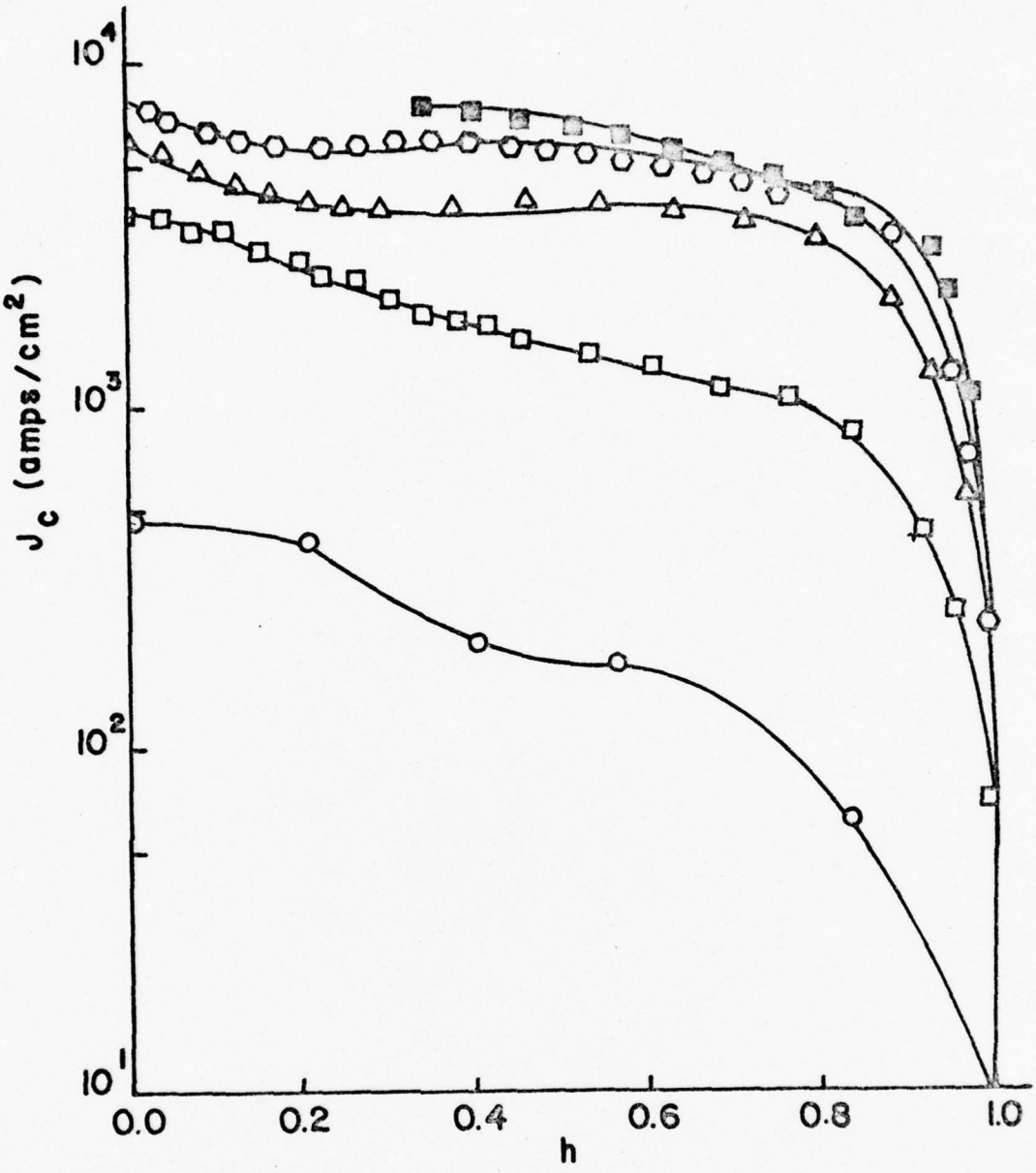


Figure 21. J_c vs. h for the 0.4 atomic percent carbon specimen, aged zero hours. ○ - 5.00 K, □ - 4.75 K, △ - 4.50 K, ⬡ - 4.00 K, and ▣ - 3.00 K.

a function of reduced magnetic field for the 0.4 atomic percent carbon specimen aged zero hours. This specimen has the largest macroscopic pinning force density at zero temperature. However, the critical current density is much more magnetic field dependent than the critical current densities for the 0.3 atomic percent carbon specimens.

The remaining specimens studied in this investigation give curves for F_p and J_c as a function of reduced magnetic field which lie between the limiting curves for F_p and J_c as a function of h for the annealed specimen and the 0.4 atomic percent carbon specimen discussed above.

Most of the specimens followed a scaling law of the form given by Equation (2.63), i.e.,

$$F_p = C_p H_{c2}^m(T)\ f(h) \quad . \tag{4.21}$$

The form factor is determined from the curve for the normalized macroscopic pinning force density as a function of the reduced magnetic field. Figure 22 is a plot of the normalized pinning force density, F_p/F_{pmax}, versus reduced magnetic field for the 0.3 atomic percent carbon specimen, aged one hour. The solid line is given by

$$f(h) = h(1 - h)^{\frac{1}{2}} \quad . \tag{4.22}$$

The different open and closed symbols are actual data points, the agreement of the data with Equation (4.22) is quite good except for the 5 K data. The macroscopic pinning force density is determined at eight different temperatures in the range 2 K to 5 K. For each temperature, the normalized pinning force density is calculated for twelve to fifty data points. Since the data for more than one

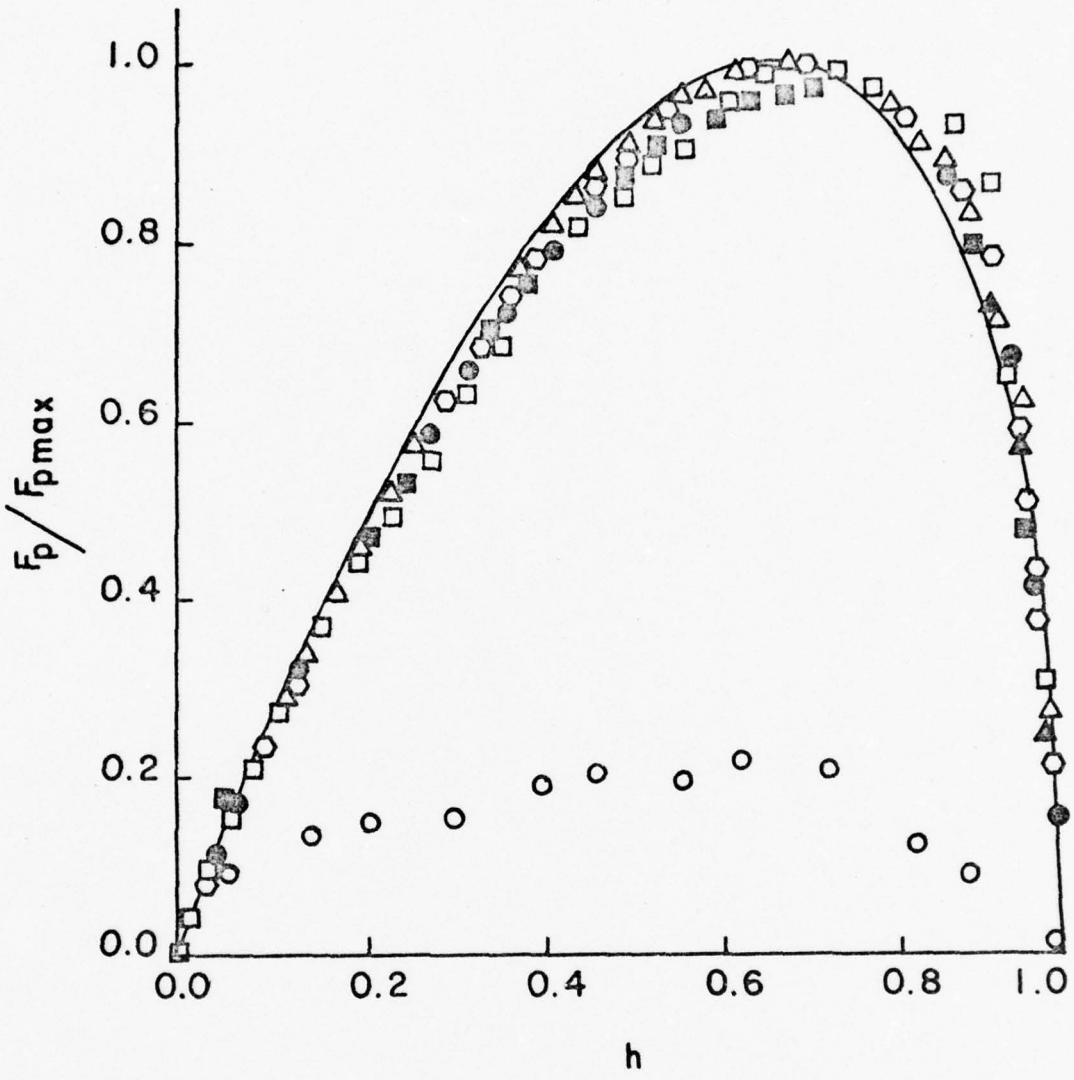


Figure 22. Normalized pinning force density, F_p/F_{pmax}, vs. reduced magnetic field, h, for the 0.3 atomic percent carbon specimen, aged one hour. ○ - 5.00 K, □ - 4.75 K, △ - 4.50 K, ⬡ - 4.00 K, ● - 3.50 K, ■ - 3.00 K, ▲ - 2.50 K, and ⬢ - 2.00 K.

temperature gives symbols which overlap only one symbol, representing an actual data point, is plotted in Figure 22. The exponent in the scaling law, m, is determined from the log-log plot of the maximum macroscopic pinning force density, F_{pmax}, as a function of the upper critical magnetic field, H_{c2}. m is the slope of the line in Figure 23, this plot is for the 0.3 atomic percent carbon specimen, aged one hour. The slope is calculated from a least-mean-squares fit to

$$\ln(F_{pmax}) = m \ln(H_{c2}) + C_1 \quad , \tag{4.23}$$

where C_1 is a constant for fixed h. The values of the exponents, for the specimens obeying the scaling law, vary from 1.1 to 1.8 with an average value of 3/2. F_{pmax} at T = 0 K is extrapolated from the log-log plot of the maximum pinning force density as a function of the upper critical magnetic field. Values of m, C_1, and $F_{pmax}(0)$ are listed in Table IV for the specimens used in this investigation.

The macroscopic pinning force density must be related to the microscopic pinning parameters. In order to apply Labush's point pinning theory, the number density of pinning centers must be less than some critical value n*, Equation (2.69), which is approximately 6×10^{12} particles/cm^3. The number density of pinning centers for the specimens used in this investigation range from 3.3×10^{15} particles/cm^3 to 4.2×10^{17} particles/cm^3; thus, Labush's theory is not applicable.

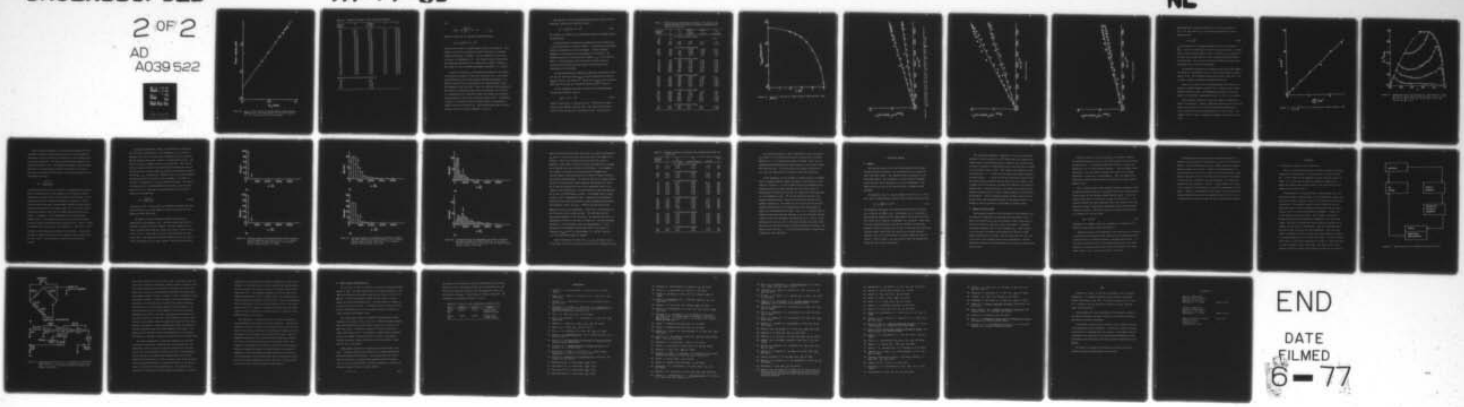
Kramer's theory based on the elastic energy stored in the fluxoid lattice, see page 38, leads to

$$F_p(h) = K_p H_{c2}^{5/2}(T)\, h^{\frac{1}{2}}(1 - h)^{-2} \qquad h < h_p$$

AD-A039 522 PENNSYLVANIA STATE UNIV UNIVERSITY PARK APPLIED RESE--ETC F/G 20/3
FLUXOID PINNING BY VANADIUM CARBIDE PRECIPITATES IN SUPERCONDUC--ETC(U)
MAR 77 A J MARKER

UNCLASSIFIED TM-77-81 NL

2 OF 2
AD
A039 522



END

DATE
FILMED
6-77

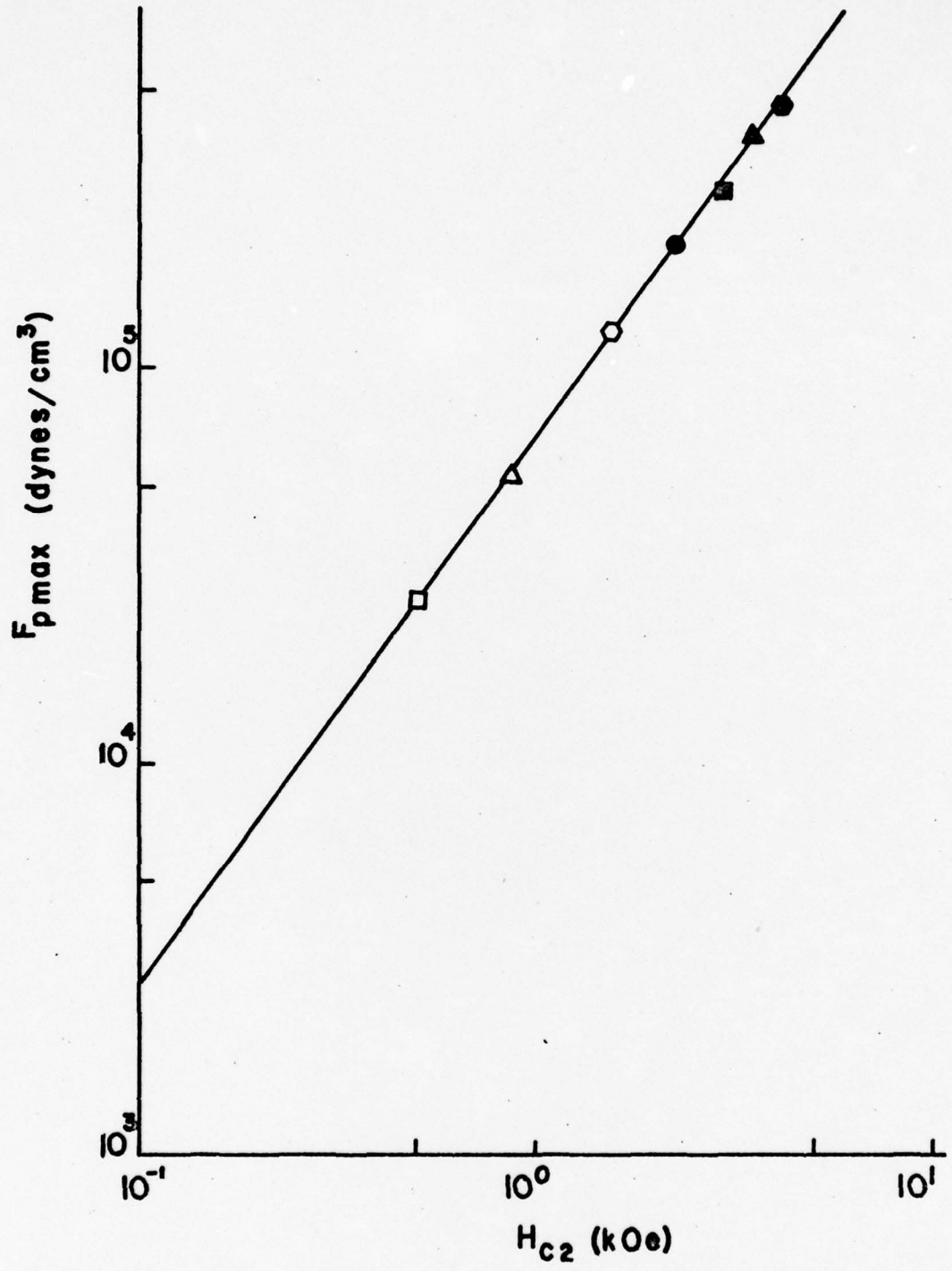


Figure 23. F_{pmax} vs. H_{c2} for the 0.3 atomic percent carbon specimen, aged one hour. The slope of the line gives the exponent ($m \sim 3/2$) used in the scaling law equation.

Table IV. Parameters relevant to the scaling law equation.

Specimen Number	C_p	F_{pmax} dynes/cm^3 $\times 10^5$	m	C_1
115	14.8	31.7	1.6	12.13
120	11.2	14.1	1.3	12.19
125	10.0	14.8	1.8	11.40
64	10.0	10.0	1.7	11.35
135	9.29	12.4	1.3	12.00
43	8.30	16.2	1.8	11.40
117	6.69	9.01	1.4	11.49
134	6.14	7.21	1.4	11.26
105	6.12	5.50	1.3	11.34
118	6.10	7.83	1.3	11.52
127	5.98	8.19	1.2	11.63
113	5.91	7.20	1.2	11.67
131	5.59	6.78	1.4	11.24
46	5.50	7.14	1.3	11.45
129	5.46	8.74	1.2	11.68
116	5.27	8.73	1.3	11.48
108	5.06	5.30	1.3	11.32
119	4.78	6.44	1.3	11.25
100	4.74	5.61	1.6	10.89
45	4.60	6.33	1.4	11.08
123	4.40	6.56	1.2	11.42
57	4.12	5.33	1.4	10.88
92	3.99	5.45	1.3	11.10
94	3.71	5.27	1.3	11.08
103	3.25	4.10	1.2	11.08
Specimens which do not obey the scaling law				
124		10.0		
98		5.31		
66		1.14		
97		0.37		
107		0.34		

and

$$F_s(h) = K_s \frac{H_{c2}^{5/2}(T)}{2\kappa^2} h(1 - h)^2 \qquad h > h_p \quad ,$$

whereas the data for the specimens investigated yield

$$F_p = C_p H_{c2}^{3/2}(T)\, h(1 - h)^{\frac{1}{2}}$$

over the entire range of reduced magnetic fields, see Figure 22. Thus, Kramer's theory fails to yield the correct form factor for vanadium carbide precipitates in vanadium. The two parameters in his theory, K_s and K_p, are independent of h. Also, Kramer's theory predicts that the temperature dependence of the scaling law is $H_{c2}^{5/2}(T)$, whereas in this study, we find a different temperature dependence, i.e., $H_{c2}^{3/2}(T)$.

In order to calculate F_p *from microscopic parameters,* the concept of an activation volume, V_p, was used, see Section II-D. This method of calculating F_p leads to the observed temperature dependence, i.e., $H_{c2}^{3/2}(T)$; however, the V_p is dependent on the reduced magnetic field, see Equations (2.89) and (2.92). Since the activation volume represents the volume of an effective pinning center interacting with a fluxoid, it is expected that the activation volume would change as the fluxoid lattice parameter changes with increasing magnetic field. A dependence of V_p on h is required to obtain agreement between our experimental results and the calculation of F_p. The available data cannot, however, shed any light on the actual dependence of V_p on h.

The specimens of this investigation that obey the scaling law have macroscopic pinning force densities given by

$$F_p = C_p H_{c2}^{3/2}(T)\, h(1 - h)^{\frac{1}{2}} \quad . \tag{4.24}$$

The constant, C_p, depends on the precipitate diameter and number density of precipitates.

The metallurgical microstructure parameters of the specimens used in this investigation are listed in Table V. The particles are measured using the transmission electron micrographs. From the measured diameters of the particles, the mean diameter is calculated. The standard deviation in the mean particle diameter, σ_a, is also listed in Table V. The mean surface area and the mean particle volume are calculated from the mean particle diameter and an appropriately correlated particle thickness.

The specimens which have temperature dependent form factors and do not obey the scaling law have $F_{pmax}(0)$ values obtained from a plot of $F_{pmax}(T)$ versus T, see Figure 24. The values of $F_{pmax}(0)$ for the specimens which do not obey the scaling law are also given in Table IV.

All the specimens, which obey the scaling law, have macroscopic pinning force densities given by

$$F_p(h) = K\, h(1 - h)^{\frac{1}{2}} \quad . \tag{4.25}$$

Figure 25 shows $F_p(h)$ as a function of $h(1 - h)^{\frac{1}{2}}$ for the 0.3 atomic percent carbon specimen, aged one hour. The slopes of the lines in Figure 25 give the value of K in Equation (4.25). The slopes are

Table V. Metallurgical microstructure parameters. The value of the various parameters describing the vanadium carbide precipitates are given here.

Specimen Number	a Å	σ_a Å	Surface Area $\times 10^6$ Å^2	Volume $\times 10^7$ Å^3	n_p $\times 10^{16}$/cm^3
		0.1 atomic percent carbon			
97	100				42.1
98					
100	975	949	2.98	5.18	1.11
103	2632	2022	17.5	43.9	0.333
		0.2 atomic percent carbon			
107	150		0.039	0.015	30.4
105	622	248	0.741	0.700	6.47
108	618	442	0.945	1.10	4.45
113	897	479	1.69	2.11	2.54
		0.3 atomic percent carbon			
57	665	532	1.18	1.54	4.94
94	951	548	1.96	2.55	4.44
43	847	584	1.72	2.31	3.79
92	1116	580	2.57	3.53	2.30
45	1260	644	3.30	4.70	1.70
46	1622	903	5.60	9.50	0.90
64	1838	1105	7.40	13.8	0.40
		0.4 atomic percent carbon			
115	513	324	0.607	0.663	14.1
125	1387	884	4.38	7.42	1.31
124	2062	1488	10.4	22.4	0.538
123	965	689	2.28	3.26	3.02
135	1374	1382	6.11	12.5	0.934
118	1528	1151	5.89	11.1	1.09
		0.5 atomic percent carbon			
116	1009	735	2.53	3.82	3.02
131	1694	1256	7.16	14.4	1.04
127	1563	1196	6.24	12.3	1.01
134	2543	2144	17.7	44.4	0.345
129	2218	1581	11.9	26.6	0.531
119	2454	1813	14.9	35.5	0.413
		0.6 atomic percent carbon			
117	2345	1557	12.9	28.4	0.529
120	2511	1408	13.3	28.4	0.505

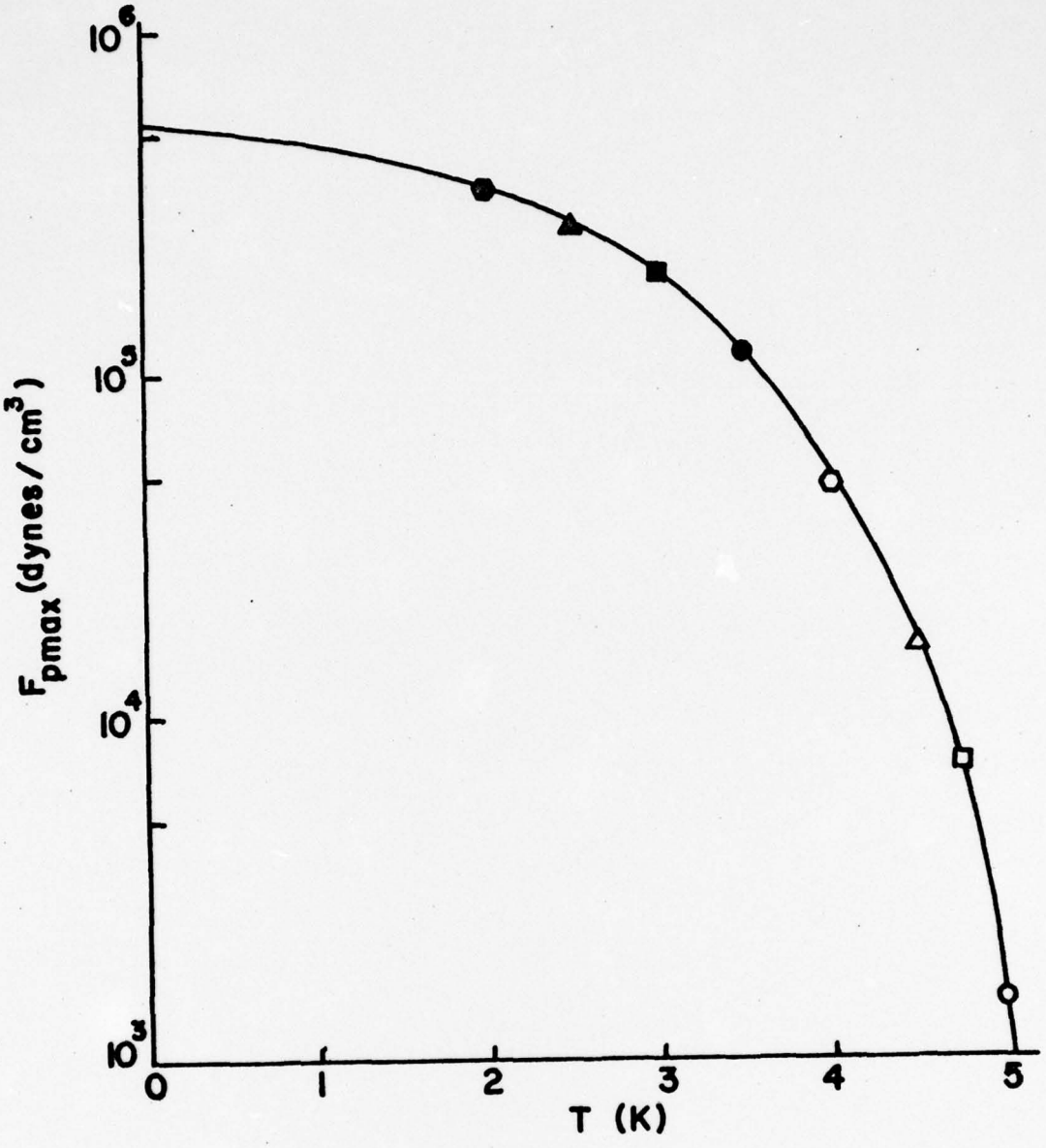


Figure 24. F_{pmax} vs. T for the 0.1 atomic percent carbon specimen, aged one hour.

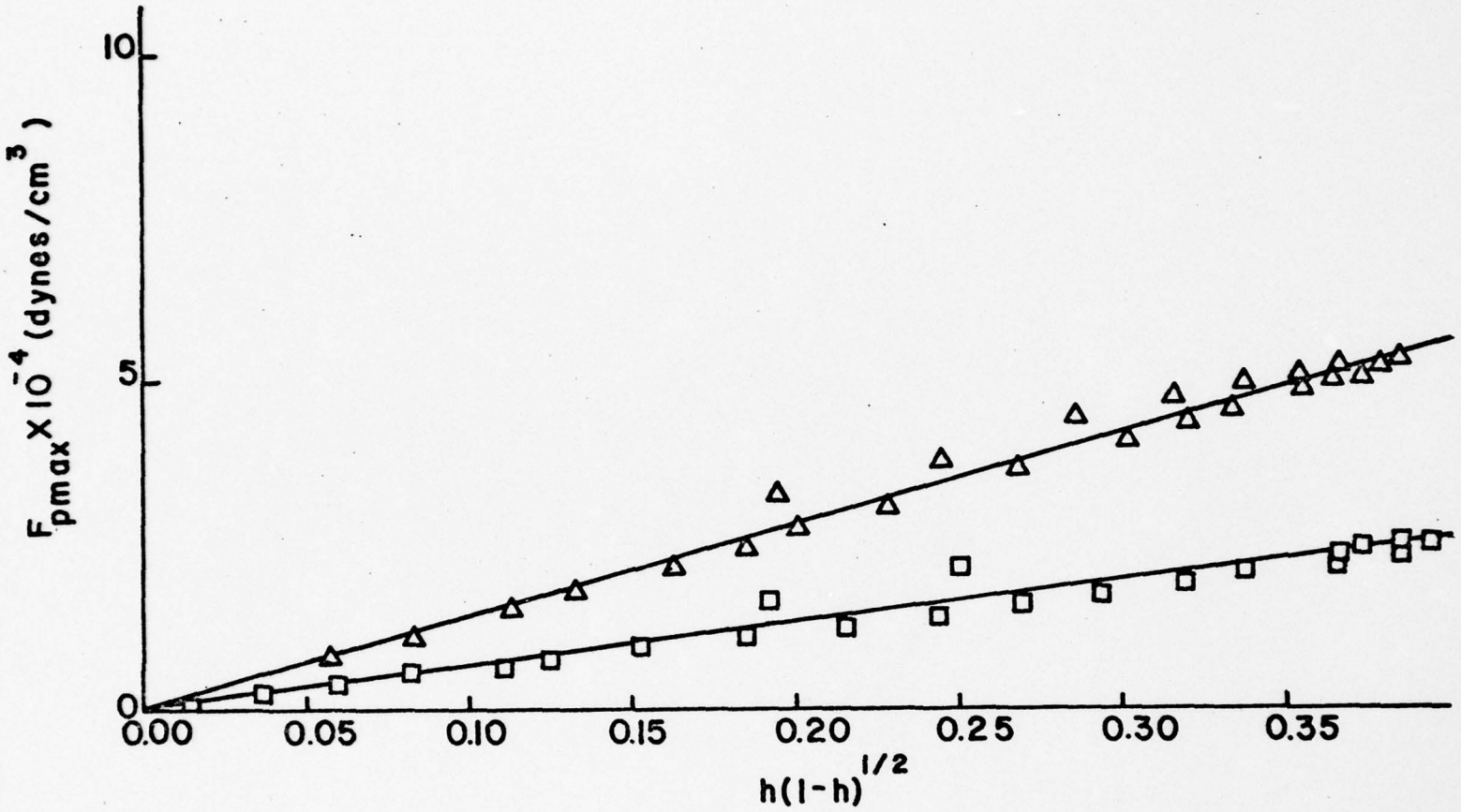


Figure 25. F_p as a function of $h(1-h)^{1/2}$ for the 0.3 atomic percent carbon specimen, aged one hour. □ - 4.75 K, △ - 4.50 K, ⬡ - 4.00 K, ◍ - 3.50 K, ▲ - 2.50 K, ⬢ - 2.00 K.

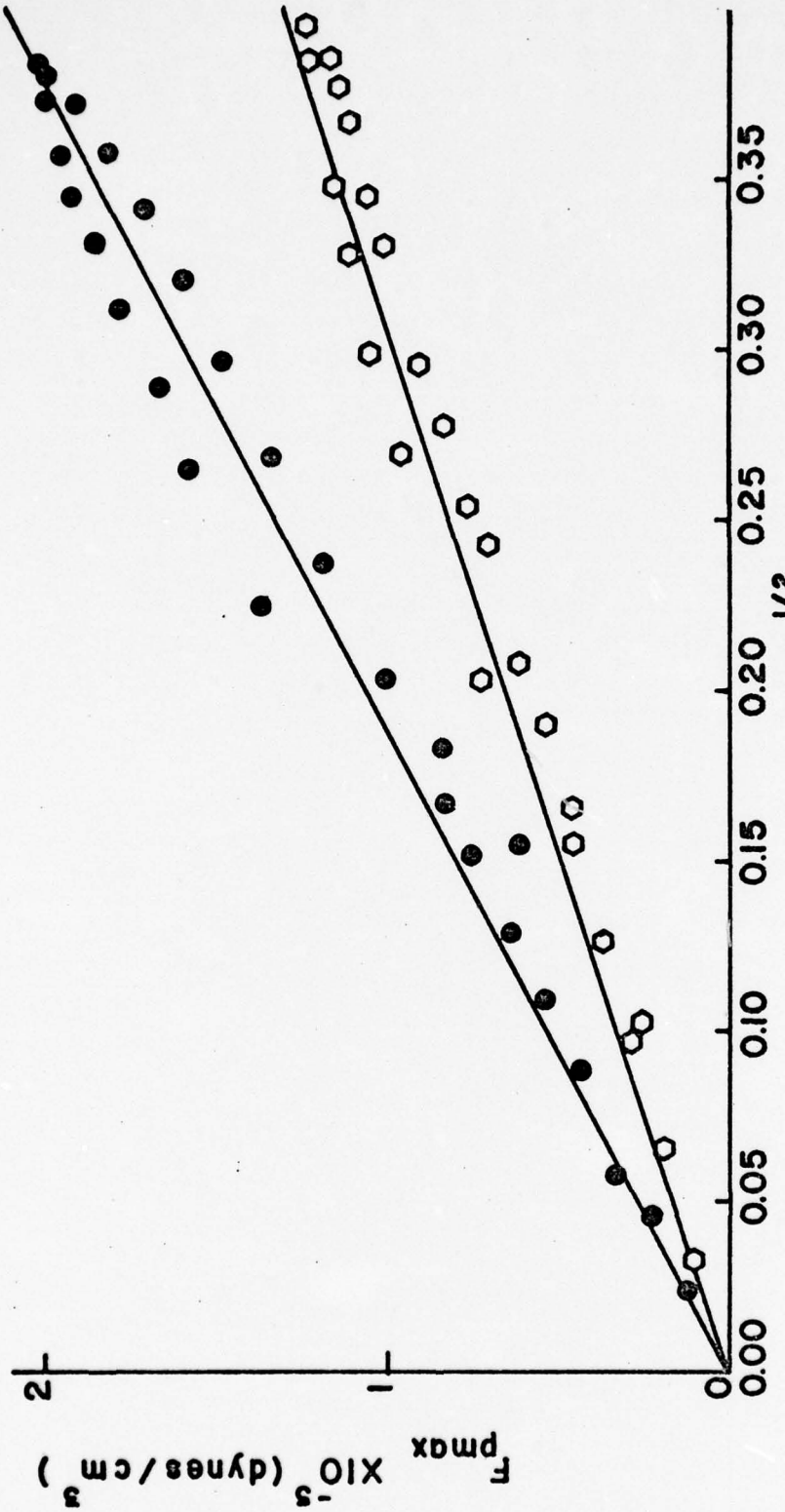


Figure 25 (continued)

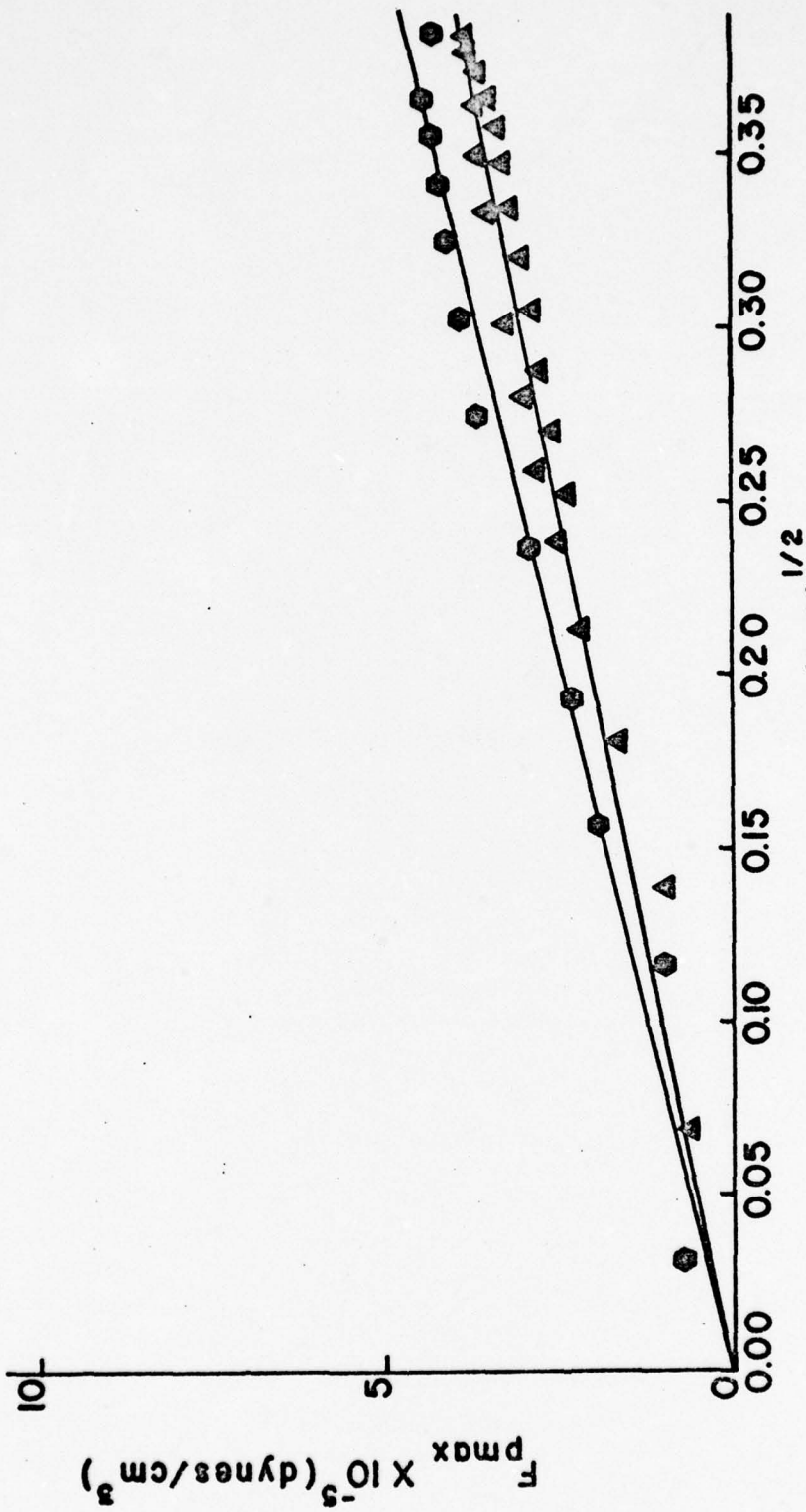


Figure 25 (continued)

determined from a least-mean-squares fit of F_p as a function of $h(1 - h)^{\frac{1}{2}}$. The value of C_p in the scaling law Equation (2.24) is determined from

$$K = C_p H_{c2}^{3/2} \quad . \tag{4.26}$$

C_p is determined by a least-mean-squares fit of K as a function of $H_{c2}^{3/2}$. A plot of K versus $H_{c2}^{3/2}$ is given in Figure 26 for the 0.3 atomic percent carbon specimen, aged one hour. The constant, C_p, depends on the size and the number density of the vanadium carbide precipitates in the specimen. The C_p values are listed in Table IV for the specimens which obey the scaling law equation.

The specimens which obey the scaling law over most of the temperature range are represented by the 0.3 atomic percent carbon specimen, aged one hour. The normalized pinning force density curve for T = 5K in Figure 22 shows a temperature dependent form factor.

Figure 27 is a plot of the normalized pinning force density as a function of reduced magnetic field for the 0.3 atomic percent carbon specimen, aged zero hours. The temperature dependence of the form factor at the different temperatures between 2 K and 5 K is apparent.

This temperature dependence of the form factor is observed for most of the specimens. However, temperature dependent form factors are usually only observed at the highest experimental temperatures of 4.75 K and/or 5.0 K for the specimens which are said to scale. For example, Figure 22 shows a temperature dependent form factor at only 5.0 K.

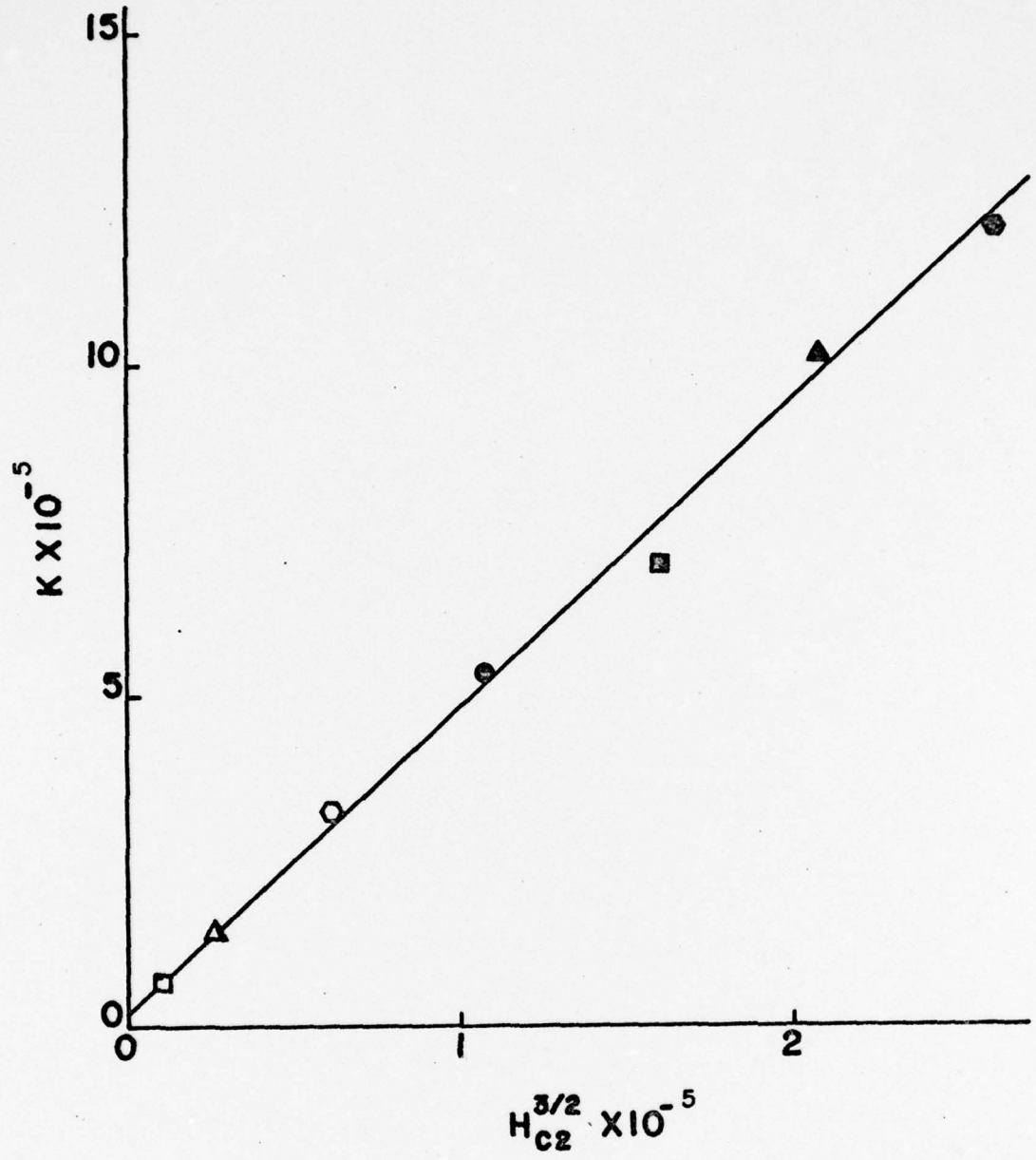


Figure 26. K vs. $H_{c2}^{3/2}$ for the 0.3 atomic percent carbon specimen, aged one hour.

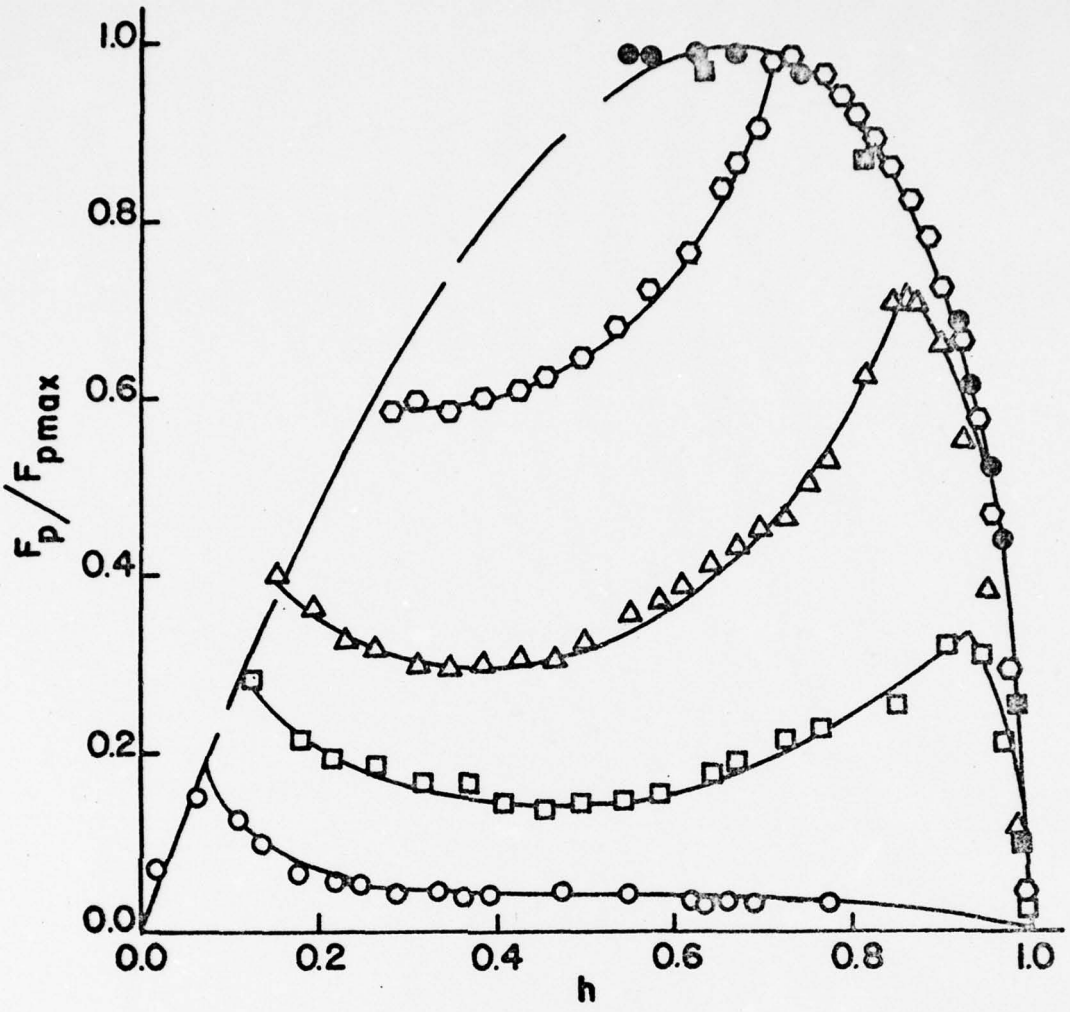


Figure 27. Normalized pinning force density vs. reduced magnetic field for the 0.3 atomic percent carbon specimen, aged zero hours. ○ - 5.00 K, □ - 4.75 K, △ - 4.50 K, ⬡ - 4.14 K, ◍ - 3.50 K, and ◙ - 3.00 K.

The temperature dependence of the form factor suggests that some temperature dependent superconducting parameter is being matched to some property of the specimen's microstructure at low temperatures but not at high temperatures. An obvious superconducting parameter that could be important is $\xi(T)$, the temperature dependent coherence length. Twice $\xi(T)$ is a length used to describe the diameter of a fluxoid. Thus at high temperatures fluxoids have a much larger diameter than at low temperatures since

$$\xi(T) = \sqrt{\frac{\phi_0}{2\pi H_{c2}(T)}} \quad .$$

One should note, however that the density of superconducting electrons does not abruptly change at the boundary of the fluxoid but changes continuously, reaching zero at the very center of the fluxoid. If the pinning centers in the specimen have diameters comparable to $2\xi(T_s)$, one would expect that when a fluxoid passes through the normal pinning center a maximum reduction of energy would occur. For pinning centers significantly smaller than $2\xi(T)$ the energy reduction would be much smaller. In addition, if the fluxoid must bend to pass through a pinning center, the bending energy increase must be balanced against the energy saved by passage through the pinning center. Hence, it might be expected that pinning centers with diameters, a, such that $a \gtrsim 2\xi(T)$ would be the most important contributers to the pinning. Furthermore, it might be expected that some critical number of such pinning centers per unit length of fluxoid might be required to achieve optimum pinning.

The present experimental results can be shown to be consistent with the ideas presented above. The temperature, T_s, at which the specimen first obeys the scaling law is determined for each specimen. All the specimens that scale, scale at all temperatures below T_s. The value of $2\xi(T_s)$ is computed for each of the specimens. The value of $2\xi(T_s)$ is located on the particle distribution histograms for each of the specimens and the total number of particles with diameters greater than $2\xi(T_s)$, n_{p2}, is determined. Figures 28, 29, and 30 are histograms for specimens that have received no heat treatment. The number of fluxoids is determined at $0.7\ H_{c_2}(T_s)$ for each specimen. This value of the magnetic field is used because the peak in the F_p versus h plots occurs at h = 0.7. The number of pinning centers per cm length of fluxoid is calculated from

$$N_p = \frac{n_{p2}\ \phi_0}{0.7\ H_c\ (T_s)} \quad . \tag{4.29}$$

In Equation (4.29), $0.7\ H_{c_2}(T_s)/\phi_0$ is the number of fluxoids per centimeter squared and n_{p2} is the number of pinning centers per cm^3 with diameters greater than $2\xi(T_s)$.

The number of pinning centers/cm length of fluxoid, N_p, is determined for each specimen at T_s. The exact value of N_p-critical is difficult to obtain for several reasons: First the temperature at which a specimen first obeys the scaling law is known, at best, only to 0.25 K or 0.5 K. Thus, there is an error associated with the value $2\xi(T_s)$ used. This error may be large for higher values of T_s since at higher temperatures $\xi(T)$ increases rapidly. Secondly, the histograms

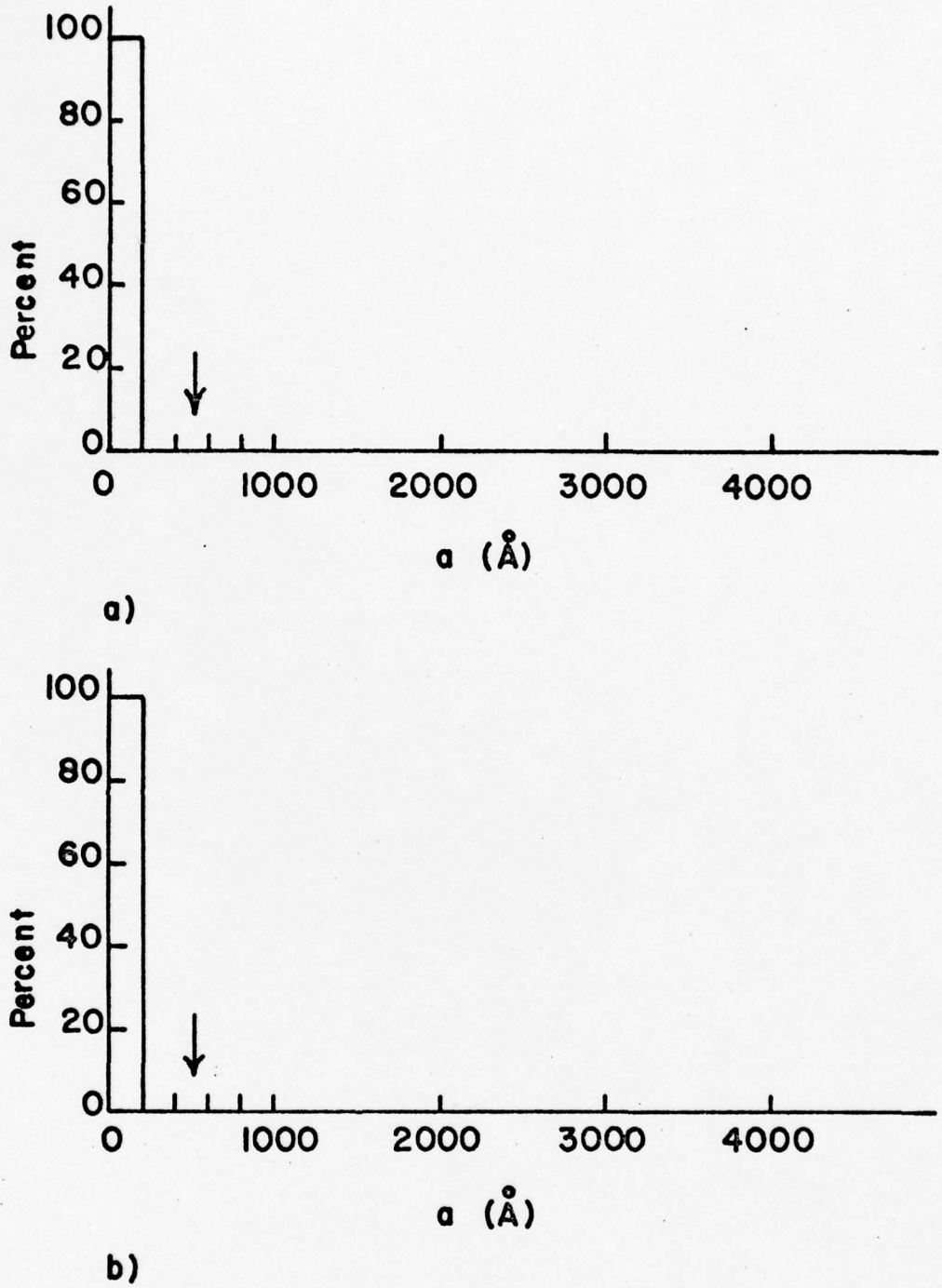


Figure 28. Histogram showing the distribution of particle diameters. The arrow indicates the value of $2\xi(0)$. a) 0.1 atomic percent carbon specimen, zero hours. b) 0.2 atomic percent carbon specimen, zero hours.

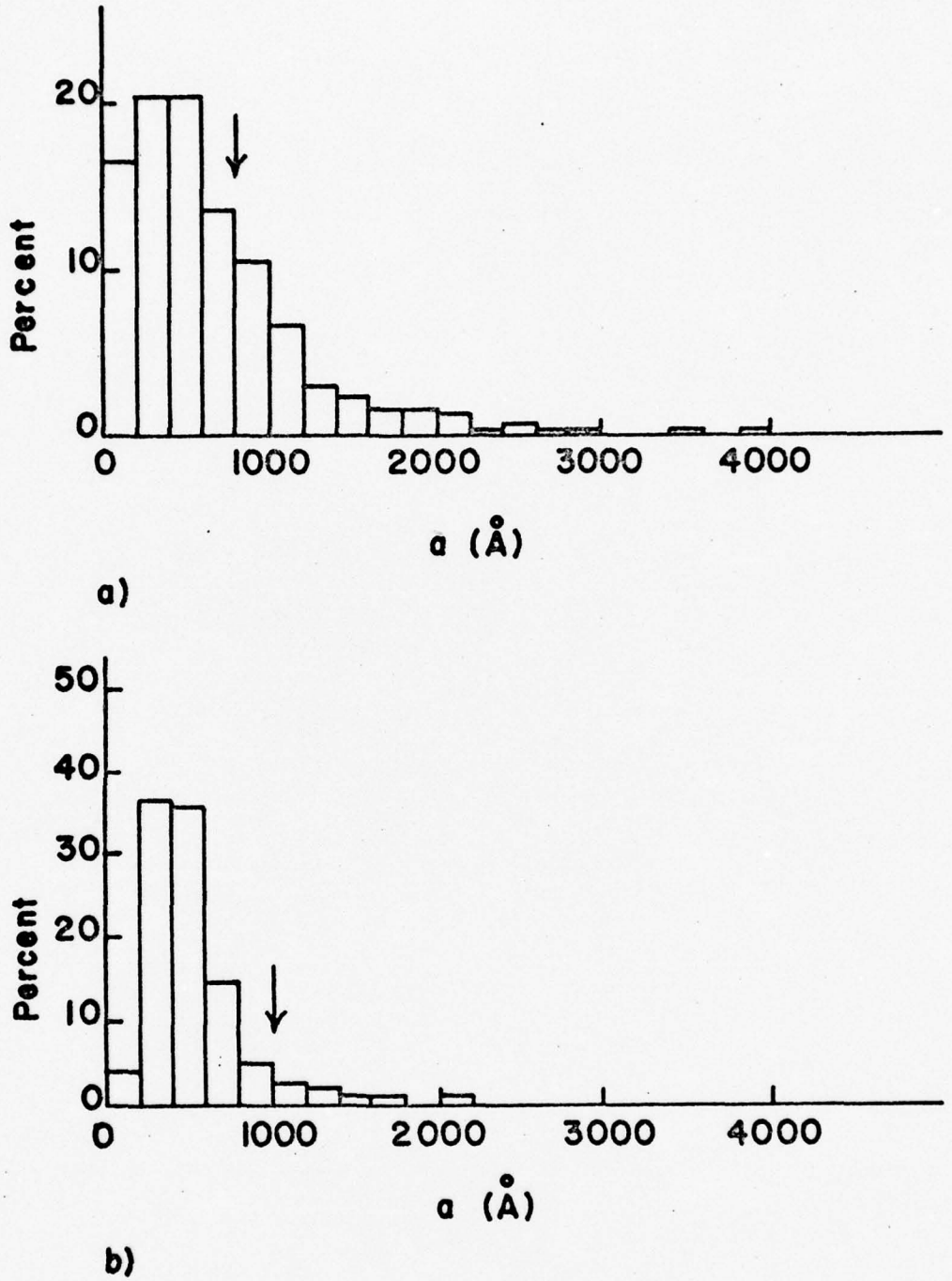


Figure 29. Histogram showing the distribution of particle diameters. The arrow indicates the value of $2\xi(T_S)$. a) 0.3 atomic percent carbon specimen, zero hours. b) 0.4 atomic percent carbon specimen, zero hours.

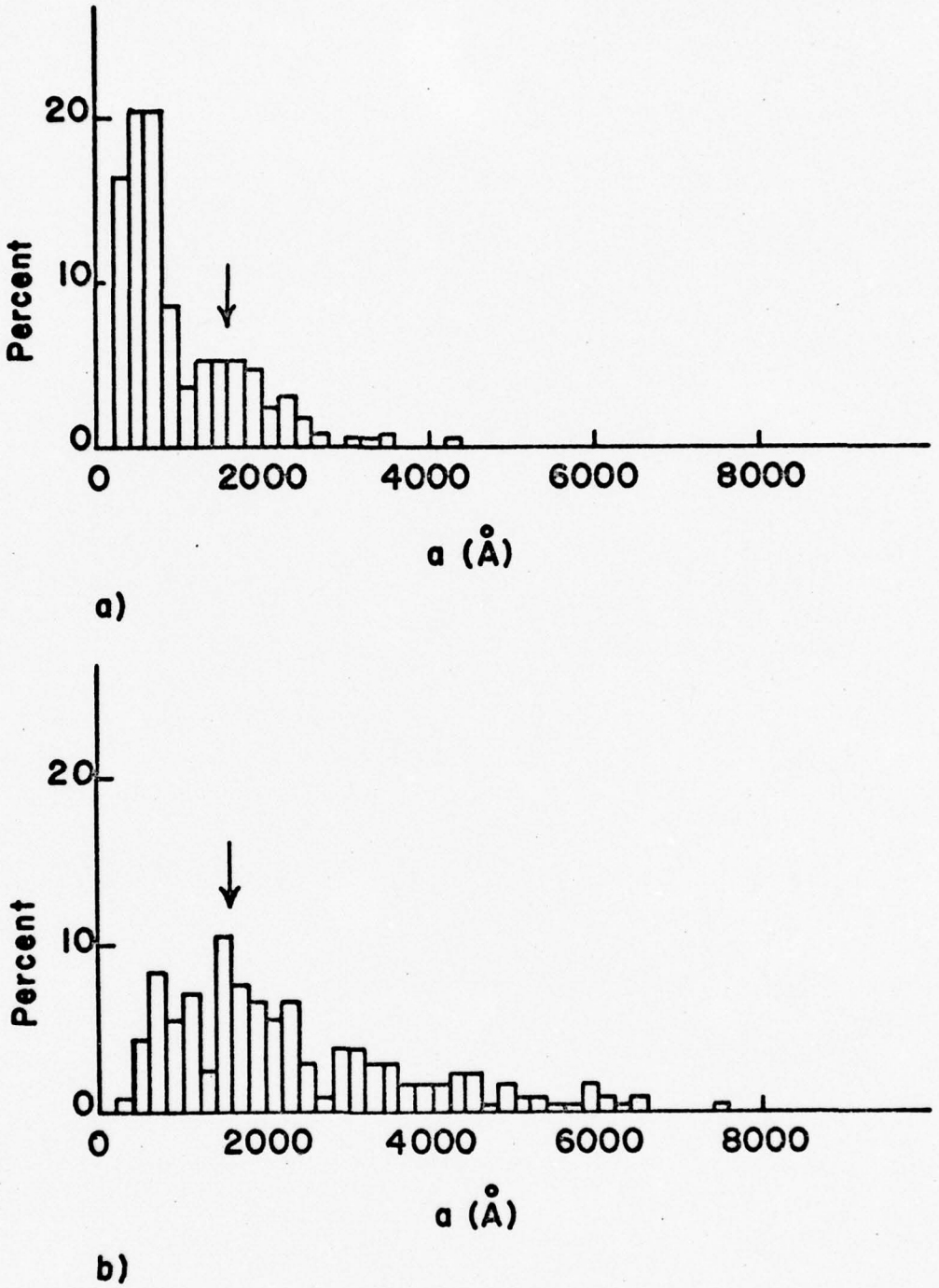


Figure 30. Histogram showing the distribution of particle diameters. The arrow indicates the value of $2\xi(T_S)$. a) 0.5 atomic percent carbon specimen, zero hours. b) 0.6 atomic percent carbon specimen, zero hours.

have an interval of 200 Å width, thus there is an error in determining n_{p2} since it is very likely that $2\xi(T_s)$ may come in the middle of an interval. Third, the criterion that the particle has to have a diameter $\geq 2\xi(T_s)$ leads to deleting from n_{p2} particles which, although not of optimum size, may contribute to the pinning. As an example of how to apply the concepts of a critical particle diameter and a critical number of pinning centers per cm length of fluxoid, consider the zero hour aged specimens. In Figure 28 both the 0.1 atomic percent and the 0.2 atomic percent carbon specimens experimentally are shown not to obey the scaling law at any of the temperatures used in the course of this investigation. All the particles in these two specimens are in the 0 to 200 Å diameter interval. The minimum value of $2\xi(T_s)$ is $2\xi(0)$, this is approximately 500 Å. Looking at the histograms in Figure 28 one will note that neither of these specimens have particles with diameters $\geq 2\xi(0)$, thus $N_p = 0$ and the specimen would not be expected to scale at any temperature. Figure 30a is the histogram for the 0.5 atomic percent carbon specimen. This specimen obeys the scaling law equation at 4.75 K and below. The value of $2\xi(4.75\ K)$ is approximately 1400 Å, see the arrow in Figure 30a. From the histogram and Table V, one can determine there are approximately 6.2×10^{15} particles/cm^3 with diameters greater than 1400 Å. The number of fluxoids at $F_{pmax}(4.75\ K)$ is approximately 2.6×10^9/cm^2, thus $N_p = 2.4 \times 10^6$ particles/cm length of fluxoid.

Table VI tabulates the values of T_s, n_{p2}, N_p, and $2\xi(T_s)$ for all the specimens that obey the scaling law for any of the temperatures used.

Table VI. Critical parameters associated with specimens which obey the scaling law.

Specimen Number	T_s K	n_{p2} $\times 10^{15}/cm^3$	n_p $\times 10^6$/cm fluxoid	n $\times 10^9/cm^2$	$\xi(T_s)$ Å
		0.1 atomic percent carbon			
100	4.50	2.54	1.53	1.66	630
103	4.75	2.22	1.26	1.77	750
		0.2 atomic percent carbon			
105	4.50	1.33	0.33	4.02	600
108	4.75	1.78	0.71	2.50	780
113	4.50	5.30	1.26	4.20	600
		0.3 atomic percent carbon			
57	3.50	9.36	0.85	11.0	400
94	4.00	18.9	2.52	7.50	460
43	4.75	4.14	1.48	2.00	800
92	4.75	4.68	1.87	2.50	810
45	4.75	4.77	2.07	1.77	800
46	4.50	5.48	1.80	3.04	600
64	4.50	2.86	1.28	3.03	600
		0.4 atomic percent carbon			
115	4.50	3.91	0.91	4.30	610
125	4.00	6.65	0.94	7.10	480
124	3.50	4.67	0.47	10.0	400
123	4.00	12.1	1.58	7.65	450
135	4.00	4.58	0.62	7.40	470
118	4.75	3.98	1.46	2.72	770
		0.5 atomic percent carbon			
116	4.75	6.22	2.37	2.62	760
131	5.00	2.18	2.26	0.97	1200
127	4.00	5.40	0.71	7.65	460
134	4.50	2.12	0.49	4.30	460
129	4.00	4.13	0.52	8.00	450
119	4.75	2.47	0.90	2.75	780
		0.6 atomic percent carbon			
117	4.75	3.23	1.20	2.70	740
120	4.50	4.15	0.98	4.25	610

The interesting result is that, independently of T_s, the value of N_p is about 1.3×10^6 particles/cm length of fluxoid with a standard deviation of 7×10^5 particles/cm length of fluxoid. Hence, for the vanadium-vanadium carbide system investigated, one can say with reasonable certainty that $\sim 10^6$ pinning centers/cm length of fluxoid and $a \gtrsim 2\ (T_s)$ are required for the specimen to obey the scaling law.

As the temperature of the specimen is reduced $H_{c2}(T)$ is increased, $2\xi(T)$ is decreased and the number of fluxoids to be pinned at a given value of h increases. In view of these facts and the immediately preceding discussion, one might conclude that with certain kinds of distributions of pinning centers that the scaling law could break down at a low temperature if $N_p \sim 10^6$ was not maintained because of the increased fluxoid density. However, this was never observed in the present investigation. The reason for this lies in the fact that the vanadium carbide particle size distributions were always peaked at values of a considerably below $2\xi(T_s)$. Hence, as T is reduced $2\xi(T)$ is reduced and more particles are available to pin the additional fluxoids. A check of this idea was made by calculating N_p for T = 3.00 K for all specimens that scale at 3.00 K. The result was that there were always more than 10^6 particles/cm length of fluxoid available for pinning. The average result was that $\sim 1.2 \times 10^6$ particles/cm length of fluxoid were available at this temperature.

V. CONCLUDING REMARKS

A. Summary

The pinning centers used in this investigation are disc shaped vanadium carbide precipitates. The precipitates have a thickness of only a few atomic layers. The vanadium carbide precipitates on the {310} habit planes. The precipitate is coherent with the vanadium lattice for most of the specimens used in this investigation. The number density and size of the pinning centers is changed by heat treatment.

The specimens have low κ values ranging from 1.56 to 2.24. These low κ Type II superconducting specimens obey a scaling law of the form

$$F_p = C_p H_{c2}^{\frac{3}{2}}(T)\ h(1-h)^{\frac{1}{2}} \quad . \tag{5.1}$$

The temperature dependence of the macroscopic pinning force density, F_p, is given by the $H_{c2}^{\frac{3}{2}}(T)$ term. The constant, C_p, is a function of the precipitate diameter and the number density of the pinning centers. The scaling law is obeyed at a temperature, T_s, and below. There seems to be two important criteria which must be fulfilled in order for a specimen to obey the scaling law: The first is that particles which have diameters greater than $2\xi(T_s)$ are likely to be the most important. Secondly, there is a critical number of pinning centers/cm length of fluxoid. If N_p is greater than this critical value the specimen will likely obey the scaling law equation.

The temperature dependence in Equation (5.1) and the form factor observed for these specimens, $h(1-h)^{\frac{1}{2}}$, differ from those predicted by either Labusch's point pinning theory or Kramer's line pinning theory. In order to calculate the macroscopic pinning force density the concept of an activation volume is used. This volume is the effective volume of an effective pinning center for each fluxoid which would accomplish the same pinning as the sum of all the real individual pinning centers. The fluxoid interacts with the pinning centers in this volume in such a manner that the interaction is between the fluxoid and the effective pinning center. From this analysis, one obtains the distance between effective pinning centers in terms of reduced magnetic field and specimen parameters. Since the distance between effective pinning centers is much larger than the distance between actual pinning centers, the fluxoid is actually pinned by a great number of pinning centers.

B. Comments on Future Work

Two important parameters in the discussion of superconductors are the transition temperature and the upper critical magnetic field. A method for determining H_{c2} for zero transport current would provide a check on the values of H_{c2} used in this investigation. Ultrasonic attenuation techniques may be used to determine H_{c2}. Early attempts to use ultrasonic techniques proved unsuccessful because reliable acoustic bonds could not be made. Also the electronic mean free path is too short in the specimens used in this investigation. However, ultrasonic attenuation techniques should not be ruled out automatically for the future.

During the course of this investigation, the magnetic induction is considered numerically equal to the applied magnetic field intensity, see Section II-B. An interesting experiment would be to measure the magnetization of the superconducting specimens. From the magnetization measurements, one could readily determine how closely the specimens approximate an ideal Type II superconductor. Also, the magnetization measurements provide another method for determining the upper critical magnetic field.

The 0.3 atomic percent carbon specimens provide a convenient group of superconducting specimens to investigate because they show moderately strong pinning for the vanadium carbide-vanadium system. This atomic percent carbon would be interesting to study as a function of κ. By alloying vanadium with some appropriate metal, the electronic mean free path can be greatly reduced while the pinning centers remain vanadium carbide precipitates. This would allow one to observe the form factor as a function of κ and see if the

$$f(h) = h(1-h)^{\frac{1}{2}} \tag{5.2}$$

dependence is a property of the low κ vanadium, or a property of the platelet shaped vanadium carbide precipitates.

Another possibility for determining if the form factor is a property of the matrix or the pinning center would be to use vanadium foil with pinning centers of a different geometry, say spherical particles. If the sperical particles prove to be strong pinning centers, the number density of the pinning centers may be able to be reduced to the point where Labusch's point pinning theory may be applicable.

A third method for investigating the form factor would be to study the pinning properties of vanadium as a function of dislocation density. The dislocation density can be readily changed by applying different amounts of cold work. However, the characterization of the dislocations would not be as clear cut as for precipitates. Measurements were made on an as received piece of vanadium. The pinning in this specimen is primarily due to dislocations. The form factor observed for this specimen is $h(1-h)^{\frac{1}{2}}$. A more complete set of data on the pinning due to dislocations is needed to substantiate the form factor. However, the preliminary result suggest that the form factor observed during the course of this experiment may be due to the low K vanadium matrix and not the specific type of pinning center present.

APPENDICES

A. Temperature Regulation of the Vacuum Can

Since the transition temperature of vanadium is above the critical temperature of liquid helium, the specimen block is inside a vacuum can. A block diagram of the temperature control apparatus appears in Figure 31. An excellent discussion of temperature regulation by Forgan (83) provides many concepts useful in the construction of the temperature regulation circuit.

A WaveTek Model 112 oscillator serves a dual purpose; first, the oscillator provides a 1000 Hz signal to the ac bridge and, second, the oscillator provides a reference signal to the Keithley Model 840 lock-in amplifier. The oscillator signal to the ac bridge has to be of small amplitude to insure a minimum of self heating of the 56Ω carbon resistor, which is used as the regulating thermometer. Figure 32a is the schematic for the ac bridge. The ac bridge is basically a Wheatstone bridge with the regulating thermometer as one leg of the bridge. By using an ac bridge and lock-in amplifier, problems due to thermal emfs and noise are reduced (84). When the bridge unbalances, the error signal is sent to the lock-in amplifier. Here, the error signal is amplified 10^4 times and phase sensitive detected to produce a dc output proportional to the input error signal. The lock-in amplifier's phase is adjusted by unbalancing the bridge in a known direction in order to produce a large error signal. The phase of the lock-in amplifier reference channel is then adjusted to maximize the detected

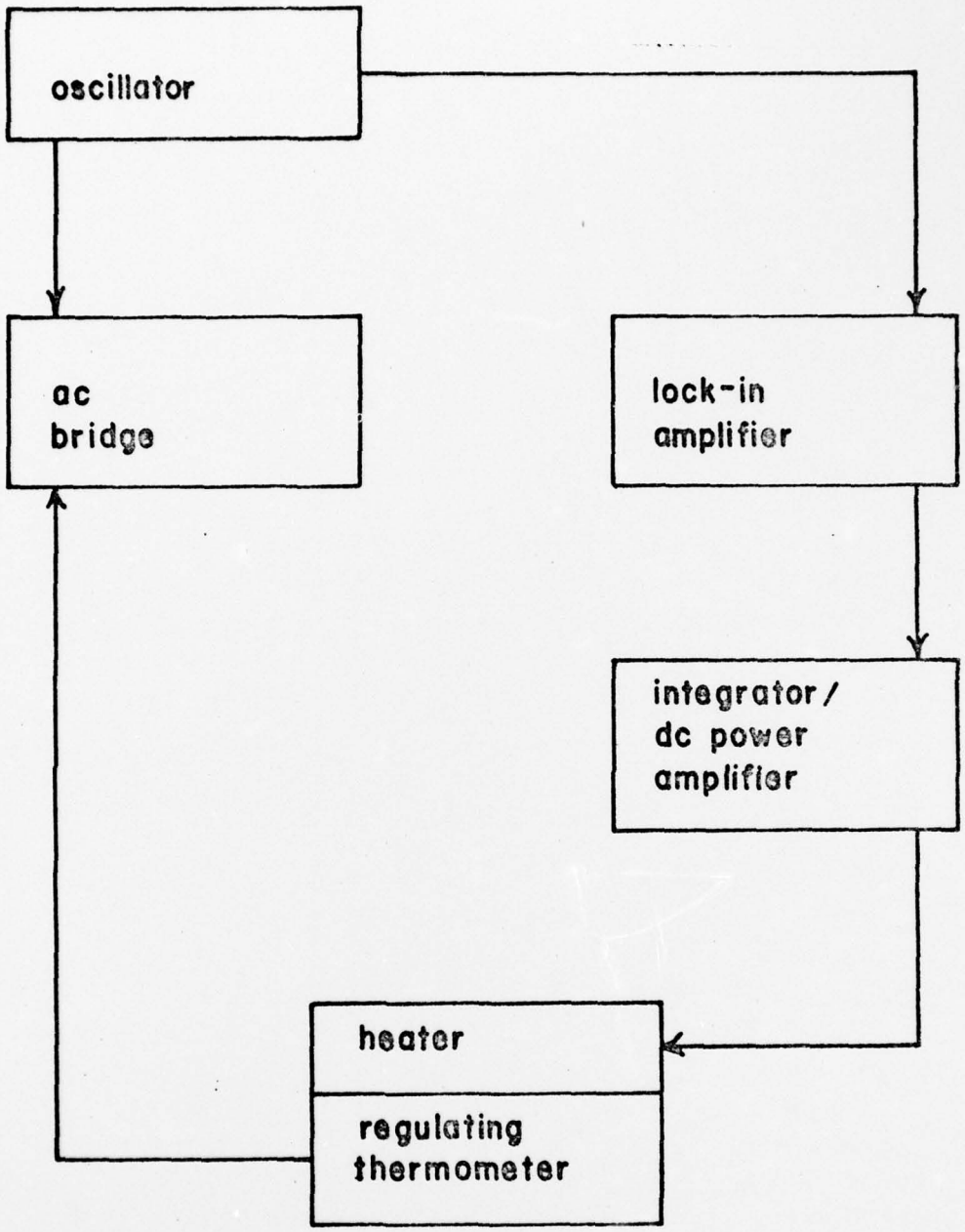


Figure 31. Block diagram of the temperature regulation circuit.

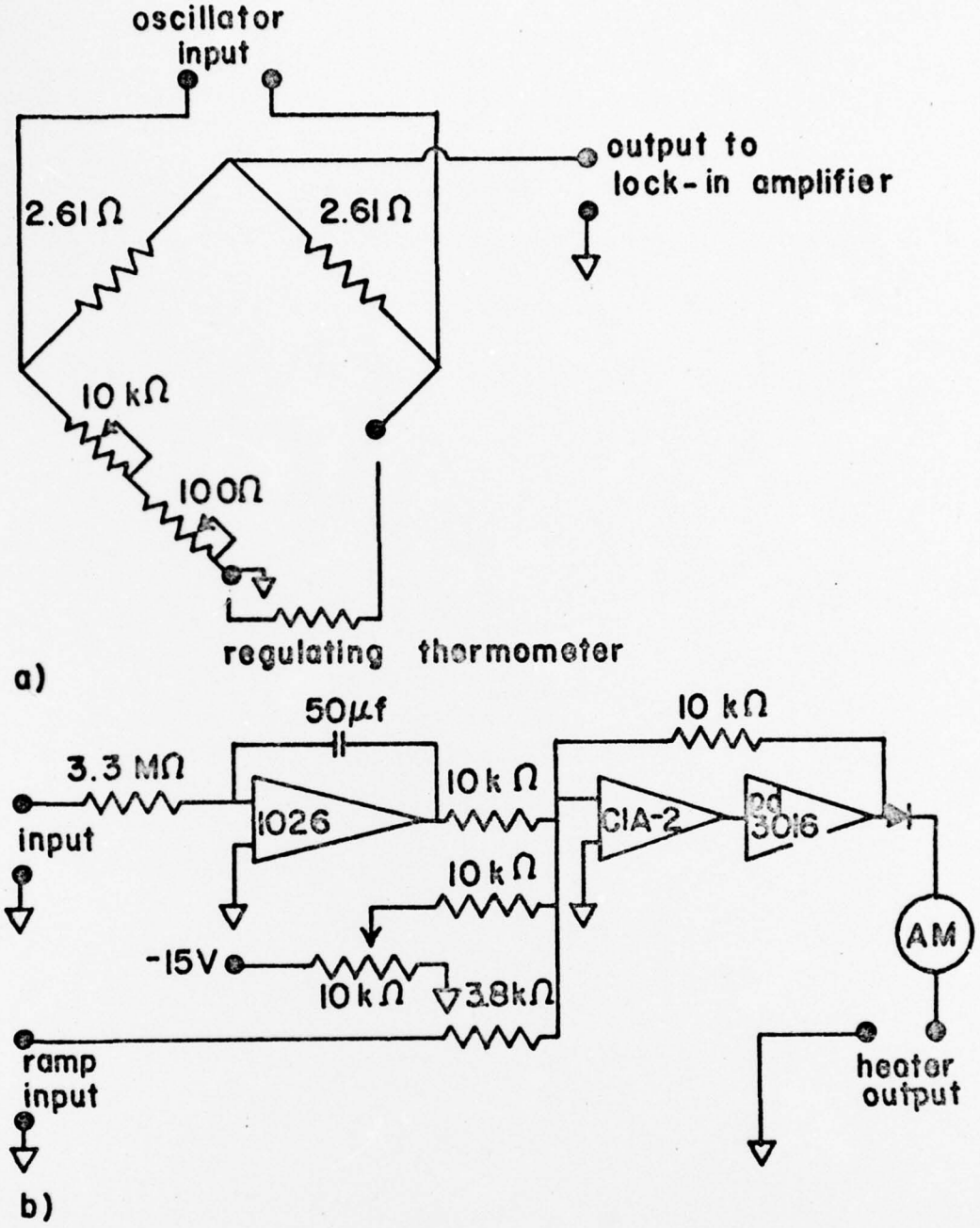


Figure 32. Temperature control circuit. a) ac bridge. b) integrator/ power amplifier. Note all the variable resistors are ten turn potentiometers. The fixed resistors are either wire wound or metal film.

error signal, and to give it the correct sign. This insures that the error signal produced by the bridge, operating around its balance point, is not only proportional to the amount of unbalance, but also of the proper sign. The sign of the detected (rectified) error signal determines whether heating (+ sign) or cooling (- sign) is required to return the bridge to balance. The time constant of the lock-in amplifier is typically 3 or 10 milliseconds. The short time constant allows the lock-in amplifier to follow rapid changes in the error signal. The rectified signal from the lock-in amplifier is sent to an electronic integrator which smooths the signal, and provides the necessary time lag in the circuit, see Figure 32b. The integrator, which has a time constant of 165 seconds, sums and averages the signal from the lock-in amplifier and supplies a slowly varying signal to the power amplifier. The power amplifier drives the current supplied to the heater. The maximum current available from the power amplifier is 100 milliamps. The heater is a 40Ω piece of Nicrome wire epoxied to the specimen block.

The desired temperature is obtained by adjusting the resistance in one arm of the bridge. The bridge will then be unbalanced. The temperature control circuit will cause the specimen block to either heat or cool until the bridge is balanced once more. The temperature control circuit, then, maintains the bridge balance by constantly adjusting the heater power to insure a constant value of the resistance of the regulating thermometer. The actual temperature of the specimen block is read from the recording thermometer. This alleviates the necessity of calibrating the carbon regulating thermometer. The major

difficulty with calibrating the regulating thermometer is that the resistance of the carbon resistor is cycle dependent and the thermometer must be calibrated each time the resistor is cooled to liquid helium temperature (85). The recording thermometer can not be used as the regulating thermometer for the ac bridge because the germanium resistance thermometers are magnetic field dependent. Thus, the temperature of the system must be set in zero applied magnetic field. The carbon resistor which is not magnetic field dependent allows the temperature control circuit to maintain the desired temperature regardless of the external magnetic field present.

The temperature, as determined from the recording thermometer, is not dependent on the liquid helium bath temperature. Although the temperature difference between the liquid helium bath and the specimen block is not critical, the smaller the temperature difference the less the amount of power dissipated in the liquid helium bath. For best temperature regulation, the liquid helium bath temperature should be 0.5 K below the operating temperature of the specimen block. The pressure in the vacuum can is adjusted so that 8 to 12 mA through the heater are required to maintain the specimen block at the desired temperature. With this amount of helium transfer gas in the vacuum can the temperature of the specimen block may be maintained to within 50 mK of the desired temperature during a data run, as long as there is less than 5 mW of power dissipated in the specimen.

B. Magnet Systems and Calibrations

In the course of this investigation, one of the two following magnet systems is used. The first magnet system is an American Magnetics, Inc. (AMI) multifilamentary NbTi superconducting coil rated at 10 kOe at 40 amperes. A Hewlett-Packard Model 6228A dc power supply is used to operate this AMI superconducting coil. The power supply is capable of an output of 30 A at 40 volts. A 0.02497Ω resistor is placed in series with the superconducting coil and the voltage across the resistor is used to determine the magnetic field.

The second magnet system is an AMI multifilamentary NbTi superconducting coil rated at 75 kOe at 79.2 A. A Didcot Instrument Company, Ltd., Model DPSA/100/4.5/1 power supply provides the current for the AMI 75 kOe system. An internal resistor of 10 mΩ was provided for output current monitoring. This resistor is replaced with an external resistor of 0.2649Ω in series with the 75 kOe coil. The external resistor allows more current sensitivity at the low magnetic fields used for this investigation.

Both magnetic systems are calibrated using the NMR proton resonance. The NMR frequencies are measured with a Hewlett-Packard Model 524L counter/model 5253B converter. The voltage across the current sense resistor which is related to the magnetic field is monitored with a five place Keithley Model 190 digital multimeter. All data are least-mean-squares fitted to a linear relation

$$H = aV + b \quad . \tag{B.1}$$

The values of a and b depend on whether the magnetic field is being swept up or down. The magnetic fields set at the beginning of each data run are dialed up from zero, thus the appropriate values of a and b are for up-sweeps. These values are listed in Table VII. The uncertainty in the magnetic field is ± 0.2 Oe.

Table VII. Values of a and b Appearing in Equation (B.1).

Coil	a(kOe/V)	b(kOe)	Remarks
10 kOe AMI	10.591	0.004	Voltage across 0.02497Ω resistor
75 kOe AMI	3.6027	-0.0007	Voltage across 0.2649Ω resistor

BIBLIOGRAPHY

1. Narlika, A. V., and Dew-Hughes, D.; Phys. Stat. Sol., 6, 383 (1964).

2. Mathur, M. P., Ashken, M., and Deis, D. W.; J. Appl. Phys., 45, 3627 (1974).

3. Thompson, S. J., and Flewitt, P. E. J.; J. Less-Common Metals, 40, 269 (1975).

4. Freyhardt, H. C., Taylor, A., and Loomis, B. A.; Applications of Ion Beams to Metals (S. T. Picraux, E. P. FerNisse, and F. L. Vook, ed.) Plenum Press, New York (1974).

5. Bean, C. P.; Phys. Rev. Lett., 8, 250 (1962).

6. Kim, Y. B., Hempstead, C. F., and Strnad, A. R.; Phys. Rev., 131, 2486 (1963).

7. Yamafuji, K., and Irie, F.; Phys. Lett., 25A, 387 (1967).

8. Webb, W. W.; J. Appl. Phys., 42, 107 (1971).

9. Fietz, W. A., and Webb, W. W.; Phys. Rev., 178, 657 (1969).

10. Lynton, E. A.; Superconductivity, 3rd ed., Barnes and Noble, Inc., New York (1969).

11. Kuper, C. G.; An Introduction to the Theory of Superconductivity, Clarendon Press, Oxford (1968).

12. de Gennes, P. G.; Superconductivity of Metals and Alloys, W. A. Benjamin, Inc., New York (1966).

13. Saint-James, D. Sarma, G., and Thomas, E. J.; Type II Superconductivity, Pergamon Press, New York (1969).

14. Tinkham, M.; Introduction to Superconductivity, McGraw-Hill Book Company, New York (1975).

15. Kamerlingh Onnes, H.; Leiden Comm., 120b, (1911).

16. Kamerlingh Onnes, H.; Leiden Comm., 122b, (1911).

17. Kamerlingh Onnes, H.; Leiden Comm., 124c, (1911).

18. Kamerlingh Onnes, H.; Leiden Comm., 134, (1913).

19. Meissner, W., and Ochsenfeld, R.; Naturwiss, 21, 787 (1933).

20. Gorter, C. J., and Casimir, H.; Physica, 1, 306 (1934).

21. London, F. and London, H.; Proc. Roy. Soc. (London), A149, 71 (1935).

22. London, F.; Superfluids, Vol. I, John Wiley and Sons, Inc., New York (1950).

23. Pippard, A. B.; Proc. Roy. Soc. (London), A216, 547 (1953).

24. Faber, T. E., and Pippard, A. B.; Proc. Roy. Soc. (London), A231, 336 (1955).

25. Ginzburg, V. L., and Landau, L. D.; Zh. Eksperim. i Teor. Fiz., 20, 1064 (1950). A complete English translation is available in Men of Physics: L. D. Landau, Vol. I, (d. terHaar, ed.), Pergamon Press, New York (1965).

26. Seeger, A.; Comments Solid State Phys., 3, 97 (1970).

27. Seeger, A.; Comments Solid State Phys., 1, 56 (1968).

28. Bardeen, J., Cooper, L. N., and Schrieffer, J. R.; Phys. Rev., 108, 1175 (1957).

29. Gor'kov, L. P.; Zh. Eksperim. i Teor. Fiz., 36, 1918 (1959), Soviet Phys. - JETP, 9, 1364 (1959).

30. Abrikosov, A. A.; Soviet Phys. - JETP, 5, 1174 (1957).

31. Trauble, H., and Essman, U.; Phys. Stat. Sol., 18, 813 (1966).

32. Krageloh, U.; Phys. Lett., 28A, 657 (1969).

33. Krageloh, U., Kumpf, U., and Seeger, A.; Proceedings of the Twelfth International Conference on Low Temp. Phys., Kyoto (1970).

34. Essman, U.; Physica (Net.), 55, 83 (1971).

35. Seeger, A.; Comments Solid State Phys., 1, 134 (1968).

36. Livingston, J. D., and Schadler, H. W.; Prog. Mater. Sci., 12, 183 (1964).

37. Huebener, R. P., and Clem, J. R.; Rev. Mod. Phys., 46, 409 (1974).

38. Fetter, A. L., and Hohenberg, P. C.; Superconductivity, (R. D. Parks, ed.), Dekker, New York (1969), Ch. 14.

39. Kim, Y. B., and Stephen, M. J.; Superconductivity, (R. D. Parks, ed.), Dekker, New York (1969), Ch. 19.

40. Tsubakihara, H., Okada, T., and Suita, T.; Phys. Stat. Sol. (a), 20, K103 (1973).

41. Friedel, J., de Gennes, P. G., and Matricon, J.; Appl. Phys. Lett., 2, 119 (1963).

42. Campbell, A. M., and Evetts, J. E.; Critical Currents in Superconductors, Barnes and Noble Books, New York (1972).

43. Kim, Y. B., Hempstead, C. F., and Strnad, A. R.; Phys. Rev. Lett., 12, 145 (1964).

44. Kim, Y. B., Hempstead, C. F., and Strnad, A. R.; Rev. Mod. Phys., 36, 43 (1964).

45. Kim, Y. B., Hempstead, C. F., and Strnad, A. R.; Phys. Rev., 139, A1163 (1965).

46. Schelten, J., Ullmaier, H., and Lippmann, G.; Phys. Rev. B, 12, 1772 (1975).

47. Bardeen, John, and Stephen, M. J.; Phys. Rev., 140, A1197 (1965).

48. Anderson, P. W.; Phys. Rev. Lett., 9, 309 (1962).

49. Anderson, P. W., and Kim, Y. B.; Rev. Mod. Phys., 36, 39 (1964).

50. Bardeen, John, and Sherman, Richard D.; Phys. Rev. B, 12, 2634 (1975).

51. Willis,J. S., Schenck, J. F., and Shaw, R. W.; Appl. Phys. Lett., 10, 101 (1967).

52. Beasley, M. R., Labusch, R., and Webb, W. W.; Phys. Rev., 181, 682 (1969).

53. Sernetz, Friedrich; J. of Low Temp. Phys., 24, 85 (1976).

54. Campbell, A. M., Evetts, J. E., and Dew-Hughes, D.; Phil. Mag. 18, 313 (1968).

55. Dew-Hughes, D.; Phil. Mag., 30, 293 (1974).

56. Schuyler, III, Roy Lewis; Ph. D. Thesis (1975), The Pennsylvania State University, entitled "The Preparation and Characterization of Carbide Containing Samples to Study Vortex Pinning in Superconducting Vanadium."

57. Antesberger, G., and Ullmaier, H.; Phil. Mag., 29, 1101 (1974).

58. Labusch, R.; Crystal Lattice Defects, 1, 1 (1969).

59. Labusch, R.; Phys. Stat. Sol., 32, 439 (1969).

60. Takacs, S.; Czech. J. Phys., B25, 1155 (1975).

61. Kramer, E. J.; J. Appl. Phys., 44, 1360 (1973).

62. Kramer, E. J.; Electronic Materials, 4, 839 (1975).

63. Khanra, B. C.; Phys. Stat. Sol. (b), 72, 303 (1975).

64. Timms, W. E. and Walmsley, D. G.; Phys. Stat. Sol. (b), 71, 741 (1975).

65. Scanlon, R. M. W., Feitz, W. A., and Koch, E. F.; J. Appl. Phys., 46, 2244 (1975).

66. Reed-Hill, Robert E.; Physical Metallurgy Principles, D. Van Nostrand Company, Inc., Princeton, New Jersey (1964).

67. Thomas, Gareth; Transmission Electron Microscopy of Metals, John Wiley and Sons, Inc., New York (1962).

68. Balain, K. S., and Bergeron, C. J.; Rev. Sci. Instr., 30, 1058 (1959).

69. Duffy, R. J., and Meissner, Hans; Phys. Rev., 147, 248 (1966).

70. Shmidt, V. V.; Soviet Phys. - JETP, 18, 1368 (1964).

71. Heaton, J. W., and Rose-Innes, A. C.; Cryogenics, 4, 85 (1964).

72. Campbell, A. M., Evetts, J. E., and Dew-Hughes, D.; Phil. Mag., 10, 333 (1964).

73. Steingart, Marvin, Putz, Antide G., and Kramer, Edward J.; J. Appl. Phys., 44, 5580 (1973).

74. Campbell, A. M.; J. Phys. C, 4, 3186 (1971).

75. Montgomery, D. B., and Sampson, W.; Appl. Phys. Lett., 6, 108 (1965).

76. Kirschenbaum, J.; Phys. Rev. (B), 12, 3690 (1975).

77. Waynert, J. A., Salvo, Jr., H., and Levy, M.; Phys. Rev. (B), 10, 1859 (1974).

78. Radebaugh, R., and Keesom, P. H.; Phys. Rev., 149, 217 (1966).

79. Goodman, B. B.; IBM J. Res. Develop., 6, 63 (1962).

80. Radebaugh, R., and Keesom, P. H.; Phys. Rev., 149, 209 (1966).

81. Meaden, G. T.; Electric Resistance of Metals, Plenum Press, New York (1965).

82. Weast, Robert C. (ed.); Handbook of Chemistry and Physics, The Chemical Rubber Co., Cleveland, Ohio (1970).

83. Forgan, E. M.; Cryogenics, 14, 207 (1974).

84. White, G. K.; Experimental Techniques in Low Temperature Physics, Clarendon Press, Oxford, England (1968).

85. Rose-Innes, A. C.; Low Temperature Techniques, D. Van Nostrand Company, Inc., Princeton, New Jersey (1964).

VITA

Alexander J. Marker, III was born 3 September, 1947 in Scranton, Pennsylvania. He graduated from North Pocono Jointure High School, Moscow, Pennsylvania, June, 1965. Mr. Marker received his B. S. and M. S. in Physics from the University of Scranton in June, 1969 and June, 1970 respectively.

From September 1970 until September, 1972 Mr. Marker was Head of the Science Department and Physics teacher at South Scranton Catholic High School, Scranton, Pennsylvania.

In September, 1972 Mr. Marker entered the Ph.D. program in Physics at The Pennsylvania State University. He served as a graduate teaching assistant and as a graduate research assistant. His graduate research assistantship was supported by the Applied Research Laboratory of The Pennsylvania State University under contract with the Naval Sea Systems Command.

Mr. Marker is a member of the American Association of Physics teachers and Sigma Pi Sigma Physics honor society.

DISTRIBUTION

Commander (NSEA 09G32)
Naval Sea Systems Command
Department of the Navy
Washington, D. C. 20362 — Copies 1 and 2

Commander (NSEA 0342)
Naval Sea Systems Command
Department of the Navy
Washington, D. C. 20362 — Copies 3 and 4

Defense Documentation Center
5010 Duke Street
Cameron Station
Alexandria, VA 22314 — Copies 5-16